NEANDC (E) - 202 U Vol. V
INDC (Ger) - 21/L + Special

PROGRESS REPORT ON NUCLEAR DATA RESEARCH IN THE FEDERAL REPUBLIC OF GERMANY

for the Period April 1, 1978 to March 31, 1979

June 1979

Edited by
S.M. Qaim
Institut für Chemie (1): Nuklearchemie
Kernforschungsanlage Jülich GmbH

NEANDC (E) - 202 U Vol. V
INDC (Ger) - 21/L + Special

PROGRESS REPORT ON NUCLEAR DATA RESEARCH IN THE FEDERAL REPUBLIC OF GERMANY

for the Period April 1, 1978 to March 31, 1979

June 1979

Edited by
S.M. Qaim
Institut für Chemie (1): Nuklearchemie
Kernforschungsanlage Jülich GmbH

F O R E W O R D

This report has been prepared to promote exchange of nuclear data research information between the Federal Republic of Germany and the other member states of NEA and IAEA. It is a compendium of progress reports from KFZ Karlsruhe, KFA Jülich, the Universities of Hamburg, Köln, Mainz, Marburg, Stuttgart and München, as well as from PTB Braunschweig and FIZ Karlsruhe.

Each contribution is presented under the laboratory heading where the work was done. If the work is relevant to requests in the World Request List for Nuclear Data, WRENDA 76/77 (INDC(SEC)-55/URSF), the corresponding request numbers have been listed after the title and authors' names of the respective contribution.

Acknowledgement is made to the Board of Directors of KFA Jülich for a financial grant to publish this report. The CINDA type index has been prepared by Dr. H.Behrens and Mr. G. Schust of FIZ Karlsruhe.

Jülich, June 1979 S.M. Qaim

C O N T E N T S

Page

INSTITUT FÜR ANGEWANDTE KERNPHYSIK
KERNFORSCHUNGSZENTRUM KARLSRUHE

1. Isochronous Cyclotron 1

1.1 High Precision Time-of-Flight Measurements of Neutron Resonance Energies in Carbon and Oxygen between 3 and 30 MeV 1

S. Cierjacks, F. Hinterberger, G. Schmalz , D. Erbe, P. v.Rossen, B. Leugers

1.2 Neutron-Induced Fission Cross Sections of ^{239}Pu, ^{240}Pu and ^{235}U between 0.5 and 30 MeV Part I. Measurement of Fission Cross-Section Ratios ^{239}Pu:^{235}U and ^{240}Pu:^{235}U 1

K. Kari, S. Cierjacks

1.3 Neutron-Induced Fission Cross Sections of ^{239}Pu, ^{240}Pu and ^{235}U between 0.5 and 20 MeV Part II. Measurement of Absolute Fission Cross Sections of ^{239}Pu, ^{240}Pu and ^{235}U 2

S. Cierjacks, K. Kari

2. 3 MV Van de Graaff-Accelerator 3

2.1 Structural Materials 3

2.1.1 Determination of the Capture Width of the 27.7 keV s - Wave Resonance in ^{56}Fe 3

K. Wisshak, F. Käppeler

2.1.2 The Capture Cross Section of ^{58}Fe between 5 and 400 keV Neutron Energy 6

F. Käppeler, L.D. Hong

		Page
2.1.3	Investigation of the Validity of the Valence Model for Neutron Capture in the Mass Range $40 < A < 70$ H. Beer	8
2.2	Fission Products	10
2.2.1	Capture Cross-Section Measurements on the Stable Krypton Isotopes B. Leugers, F. Käppeler	10
2.2.2	Measurement of the keV Neutron Capture Cross Sections of ^{138}Ba, $^{140,142}Ce$, $^{175,176}Lu$ and ^{181}Ta with the Activation Method H. Beer	12
2.3	Actinide Cross Sections	15
2.3.1	Neutron Capture Cross Sections of ^{241}Am in the Energy Range from 10 to 250 keV K. Wisshak, F. Käppeler	15
2.3.2	The Subthreshold Fission Cross Section of ^{241}Am in the Energy Range from 10 - 250 keV W. Hage, F. Käppeler, K. Wisshak	17
2.3.3	The Distribution of Fragment Mass and Fragment Kinetic Energy from Fast Neutron Induced Fission of ^{237}Np A.A. Naqvi, F. Käppeler, R. Müller, F. Gönnenwein	18
2.3.4	Neutron Total Cross Sections for ^{240}Pu and ^{242}Pu in the Energy Range from 10 to 375 keV F. Käppeler, L.D. Hong, H. Beer	21

Page

2.4 Standards 24

2.4.1 Resonance Analysis of the ^{10}B Total Cross Section in the Energy Range from 90 to 420 keV 24

H. Beer

INSTITUT FÜR KERNPHYSIK
KERNFORSCHUNGSZENTRUM KARLSRUHE

1. Isochronous Cyclotron 26

1.1 High Precision Measurement of the Total Neutron Cross Section of the Helium Isotopes 26

B. Haesner, H.O. Klages, H. Dobiasch, W. Heeringa, B. Zeitnitz, D. Erbe, F. Käppeler, B. Leugers, G. Schmalz

1.2 Total Neutron Cross Sections of the Stable Hydrogen Isotopes 27

H. Bente, P. Schwarz, H.O. Klages, H. Dobiasch, D. Erbe, B. Haesner, L. Husson, G. Schmalz, J. Wilczynski, B. Zeitnitz

1.3 The Total Neutron Cross Section of ^{20}Ne and T = 3/2 States in ^{21}Ne 27

H. Abdel-Wahab, H.O. Klages, D. Eversheim, F. Hinterberger

INSTITUT FÜR NEUTRONENPHYSIK UND REAKTORTECHNIK
KERNFORSCHUNGSZENTRUM KARLSRUHE

1. Nuclear Data Evaluation 29

1.1 Clarification of ^{241}Am Thermal Cross-Section Discrepancies 29

B. Goel

Page

1.2 Comparative Study of Neutron Strength Functions for Actinides 31

F.H. Fröhner, U. Fischer, H. Jahn

1.3 Absolute Values of Inelastic Neutron Scattering Cross Sections Calculated with Account of the Pre-equilibrium Mechanism 37

H. Jahn

1.4 Inelastic Neutron Scattering Calculations including the Pre-equilibrium and Direct Components using Optical Model Fit Parameters only 37

H. Jahn

1.5 Review of Applied Neutron Resonance Theory 38

F.H. Fröhner

INSTITUT FÜR CHEMIE (1): NUKLEARCHEMIE
KERNFORSCHUNGSANLAGE JÜLICH

1. Neutron Data 39

1.1 Investigation of (n, ^{3}He) Reactions 39

S.M. Qaim, G. Stöcklin, R. Wölfle, C.H. Wu

1.2 Cross-Section Measurements on Hydrogen and Helium Producing Reactions 39

S.M. Qaim, G. Stöcklin, R. Wölfle

1.3 Evaluation, Systematics and Review of Fast Neutron Induced Reaction Cross-Section Data 41

S.M. Qaim

2. Charged Particle Data for Radioisotope Production 42

2.1 Cross-Section Data for the Production of Organic Radioisotopes 42

Z.B. Alfassi, S.M. Qaim, G. Stöcklin, R. Weinreich

Page

2.2 Excitation Functions for the Production of Inorganic Radioisotopes 43

S.M. Qaim, R. Weinreich

2.3 Cross Sections for the Production of Rare Gases 43

J. Knieper, R. Weinreich

2.4 Survey of Charged Particle Data for Radioisotope Production 43

S.M. Qaim, G. Stöcklin, R. Weinreich

INSTITUT FÜR KERNPHYSIK: EXPERIMENTELLE KERNPHYSIK II
KERNFORSCHUNGSANLAGE JÜLICH

1. Slow Neutron Induced Nuclear Reactions 45

1.1 Cross Section of the Reaction $^{16}O(n,\gamma)^{17}O$ 45

N. Wüst, H. Seyfarth, L. Aldea

1.2 Partial Cross Sections of the Reactions $^{123}Te(n,\alpha)^{120}Sn$, $^{143}Nd(n,\alpha)^{140}Ce$, $^{123}Te(n,\gamma\alpha)^{120}Sn$ and $^{143}Nd(n,\gamma\alpha)^{140}Ce$ 45

L. Aldea, H. Seyfarth, N. Wüst

ZENTRALABTEILUNG FÜR CHEMISCHE ANALYSEN
KERNFORSCHUNGSANLAGE JÜLICH

Gamma-Ray Data Compilations for Applied Gamma-Ray Spectrometry 48

G. Erdtmann, W. Soyka

I. INSTITUT FÜR EXPERIMENTALPHYSIK
UNIVERSITÄT HAMBURG

1. Study of the $(\alpha,\times n)$-Reactions on ^{59}Co and ^{60}Ni 59

A. Alevra, H.H. Bissem, R. Langkau, P. Plischke, W. Scobel

Page

2. Continuous Spectra of Light Particles from $p+^{58,60,61,62,63}Ni$ and $p+^{63,65}Cu$ at E_p = 27 MeV — 62

J. Friese, H.H. Bissem, H.J. Langanke, W. Scobel, R. Wien

3. Measurement of Neutrons Emitted in Fission of $^{235,236,238}U$ by Protons — 65

P. Plischke, H. Krause, R. Langkau, W. Scobel

INSTITUT FÜR KERNCHEMIE
UNIVERSITÄT ZU KÖLN

1. Integral Excitation Functions for p-Induced Reactions — 68

R. Michel, G. Brinkmann, W. Herr

1.1 P-Induced Reactions on Ti, V, Fe, Co and Ni for p-Energies between 2 and 17 MeV — 68

1.2 Redetermination of the Excitation Function for the Reaction $^{27}Al(p,3p3n)^{22}Na$ — 70

1.3 Excitation Functions for the Production of ^{54}Mn, $^{52m+g}Mn$ and ^{51}Cr from Manganese with Proton Energies up to 45 MeV — 72

INSTITUT FÜR KERNCHEMIE
JOHANNES GUTENBERG-UNIVERSITÄT MAINZ

1. Some Decay Properties and Yields in Fission Product Chains 131, 133 and 135 — 74

H. Braun, T. Izak-Biran, Z. Alfassi, W. Lauppe, H.O. Denschlag

Page

2. Spectroscopy of Beta Delayed Neutrons in Coincidence with Gamma-Rays Depopulating Excited States in the Final Nucleus 76

H. Ohm, A. Schröder, W. Rudolph, K. Sümmerer, U. Tharun, K.D. Wünsch, G. Jung, K.-L. Kratz

REAKTORSTATION GARCHING, FACHBEREICH PHYSIK
TECHNISCHE UNIVERSITÄT MÜNCHEN

1. Coherent Neutron Scattering Lengths 81

1.1 Neutron Refractometer 81

L. Koester, W. Waschkowski, H. Reiner

1.2 Christiansen Filter Technique 81

L. Koester, K. Knopf

2. Neutron Cross Sections 82

L. Koester, W. Waschkowski, P. Hurst

PHYSIKALISCH-TECHNISCHE BUNDESANSTALT (PTB)
BRAUNSCHWEIG

1. Radionuclide Data 84

1.1 Gamma-Ray Emission Probabilities 84

K. Debertin, W. Peßara, U. Schötzig, K.F. Walz

1.2 Half-lives 84

K.F. Walz, K. Debertin, U. Schötzig

2. Fission Yields 86

2.1 Fission Product Yields in ^{238}U Fission by ^{252}Cf-Neutrons 86

K. Debertin

Page

3. Neutron Cross Sections and Californium-252 Data 86

3.1 Covariance Matrix of Average Cross Sections Measured in the Neutron Field of Cf-252 86

W. Mannhart

3.2 Sensitivity Coefficients of Cf-252 Spectrum Averaged Cross Sections 88

W. Mannhart

3.3 Half-life of Californium-252 91

W.G. Alberts, W. Mannhart, M. Matzke

4. Variable Energy Cyclotron 91

A New High-Precision Fast Neutron Time-of-Flight Facility 91

H.J. Brede, G. Dietze, R. Jahr, H. Klein, D. Schlegel-Bickmann, H. Schölermann, B.Siebert

INSTITUT FÜR KERNENERGETIK UND ENERGIESYSTEME
UNIVERSITÄT STUTTGART

1. Study of Nuclear Data Requirements for the Application of Fast Neutrons in Radiation Therapy 94

G. Pfister, G. Hehn, H.P. Friedlein, M. Mattes

1.1 Calculations for Neutron Generators used in Cancer Treatment 94

1.2 The IKE Cross Section Sensitivity and Uncertainty Analysis Code System 94

1.3 Nuclear Data Requirements in Radiation Treatment Planning 96

Page

INSTITUT FÜR KERNCHEMIE
PHILIPPS-UNIVERSITÄT MARBURG

1. Gamma-Ray Catalog 98

U. Reus, W. Westmeier, I. Warnecke

2. Alpha-Energy Table 98

W. Westmeier, R.A. Esterlund

FACHINFORMATIONSZENTRUM ENERGIE, PHYSIK, MATHEMATIK
KARLSRUHE

Status Report 99

H. Behrens, J.W. Tepel

APPENDIX I Addresses of Contributing Laboratories 101
APPENDIX II CINDA Type Index 105

INSTITUT FÜR ANGEWANDTE KERNPHYSIK
KERNFORSCHUNGSZENTRUM KARLSRUHE

1. Isochronous Cyclotron

1.1 High Precision Time-of-Flight Measurements of Neutron Resonance Energies in Carbon and Oxygen between 3 and 30 MeV*

S.Cierjacks+, F. Hinterberger++, G. Schmalz, D. Erbe,
P. v.Rossen++, B. Leugers

An essentially improved time-of-flight device has been set up at the Karlsruhe isochronous cyclotron. Transmission measurements on carbon and oxygen in the energy range from 3 to 30 MeV with a spectrometer resolution of 5.5 psec/m allowed to determine neutron resonance energies of some narrow resonances with an accuracy of 1.2×10^{-5}. The present results are in many cases by more than two orders of magnitude more accurate than previously published values. Above 10 MeV, measured excitation energies of various T = 3/2 states in ^{17}O have an order of magnitude higher accuracy than the most precise determinations from charged particle reactions. Resonance energies of narrow neutron resonances were obtained and two sets of data suitable as high precision energy standards are proposed. For the $^{16}O+n$ system, energies and total widths of five T = 3/2 states in the range $7 \leq E_n \leq 11$ MeV were determined.

1.2 Neutron-Induced Fission Cross Sections of ^{239}Pu, ^{240}Pu and ^{235}U between 0.5 and 30 MeV Part I. Measurement of Fission Cross-Section Ratios ^{239}Pu:^{235}U and ^{240}Pu:^{235}U**

K. Kari+++, S. Cierjacks+

The fission cross-section ratios ^{239}Pu:^{235}U and ^{240}Pu:^{235}U were determined in the energy range between 0.5 and 20 MeV using gas scintillation counters and the time-of-flight technique at the Karlsruhe isochronous

---

* Submitted to Nucl . Instr. Methods for publication

\+ Now at Institut für Kernphysik, Kernforschungszentrum Karlsruhe und Universität Karlsruhe

++ Institut für Strahlen- und Kernphysik, Universität Bonn

** To be submitted to Nucl. Sci. Eng. for publication

+++ Now at Siemens-Entwicklungslaboratorium, München

cyclotron. Fission events were measured requiring fast coincidences from both fission fragments. The high neutron flux available at the 12 m flight path allowed to measure the ratios with statistical accuracies between 0.2 and 1% with a spectrometer resolution of 0.3 nsec/m. Total uncertainties of measured ratios range between 2.1 and 2.3% for ^{239}Pu:^{235}U and between 2.5 and 2.7% for ^{240}Pu:^{235}U. The present cross-section ratio determinations deviate in some energy intervals significantly from those presently recommended for fast reactor calculations.

1.3 Neutron-Induced Fission Cross Sections of ^{239}Pu, ^{240}Pu and ^{235}U between 0.5 and 20 MeV Part II. Measurements of Absolute Fission Cross Sections of ^{239}Pu, ^{240}Pu and ^{235}U

S. Cierjacks[+] , K. Kari[++]

Absolute fission cross sections of ^{239}Pu, ^{240}Pu and ^{235}U were measured simultaneously with fission cross-section ratios described in Part I using the same fission device. Absolute neutron fluxes between 0.5 and 20 MeV were determined by means of a telescope-like proton recoil device employing solid radiators and gas scintillation counting. For ^{235}U two different sets of data were obtained from samples of 0.4 and 0.8 mg/cm^2 areal densities. Absolute fission cross sections for the three isotopes were measured with a total uncertainty of 2.0 - 2.5% for ^{239}Pu and ^{235}U and of 2.2 - 2.7% for ^{240}Pu.

[+] Now at Institut für Kernphysik, Kernforschungszentrum Karlsruhe und Universität Karlsruhe

[++] Now at Siemens-Entwicklungslaboratorium, München

2. 3 MV Van de Graaff-Accelerator

2.1 Structural Materials

2.1.1 Determination of the Capture Width of the 27.7 keV s-Wave Resonance in ^{56}Fe

K. Wisshak, F. Käppeler

(Relevant to request numbers: 692101, 692102, 692103, 692104, 712024, 714005, 741040, 742032, 753036, 741046)

Many s-wave resonances of structural materials in the keV range are characterized by large ratios of typically 10^3 for the neutron to capture width. In these cases the experimental determination of the respective capture widths is complicated for the following reasons:

1) A rather large sample thickness is required to observe capture events with sufficient intensity. Therefore, sizeable corrections for multiple scattering and self-shielding effects have to be applied.
2) The high flux of neutrons scattered in the resonance may be captured with some probability in the sample canning, the detector or in surrounding materials. If, as it was the case in almost all experiments performed so far, the flight path of the scattered neutrons is very short compared to the primary flight path between neutron source and sample, there originates a background which falls within the area of the capture resonance.

For both these corrections detailed Monte-Carlo calculations are necessary which are very difficult, especially for the second point.

In the present investigation of the 27.7 keV resonance in ^{56}Fe which was stimulated by recent results of Moxon et al [1] the above difficulties have been avoided by a set-up which is completely different from those of previous measurements. A fast pulsed Van de Graaff-accelerator and the $^7Li(p,n)^-$reaction were used for neutron production. The proton energy was adjusted slightly above the reaction threshold in order to obtain a continuous neutron spectrum in the energy range from 10 to 60 keV. The neutrons are kinematically collimated into a cone with an opening angle of $\sim$ 40 deg in the forward direction. The neutron flight path from the target to the sample was only 8 cm whereas the distance between the sample and

the Moxon-Rae detector for the registration of the capture gamma-rays was 16 cm. The main advantages of this arrangement are the following:

1) The high neutron flux obtained with the sample so close to the target allowed to use very thin samples. Enriched metallic ^{56}Fe disks with thicknesses down to 0.15 mm (1.4×10^{-3} atoms/barn) have been used in our measurements. Compared to previous experiments [1-4] our sample was thinner by a factor of 3 to 7, resulting in a considerable reduction of the multiple scattering and self-shielding correction.
2) The distance between sample and detector is a factor of two larger than the flight path of the primary neutrons. In addition, the immediate surrounding of the sample to a distance of at least 8 cm in all directions was completely free of any material. Consequently, events due to capture of neutrons scattered by the sample appear with such a long delay compared to prompt capture events in the sample that they are clearly discriminated in the time-of-flight spectrum and do not contribute to the 27.7 keV resonance.
3) The limited energy range of the neutron spectrum (10 to 60 keV) guarantees that no other s-wave resonance of ^{56}Fe contributes to the experimental background.
4) The excellent timing properties of accelerator and detector allow for an overall time resolution of 1.2 ns. Thus the flight path of 8 cm is sufficient to separate unambiguously the 27.7 keV resonance in ^{56}Fe from the neighbouring p-wave resonances.

In Fig. 1 an experimental time-of-flight spectrum is shown which was obtained with a 0.3 mm thick sample (2.6×10^{-3} atoms/barn). The spectrum demonstrates that statistics, effect-to-background ratio and energy resolution are sufficient for proper data analysis. A preliminary evaluation indicates a capture width which is significantly lower than most of the values reported earlier.

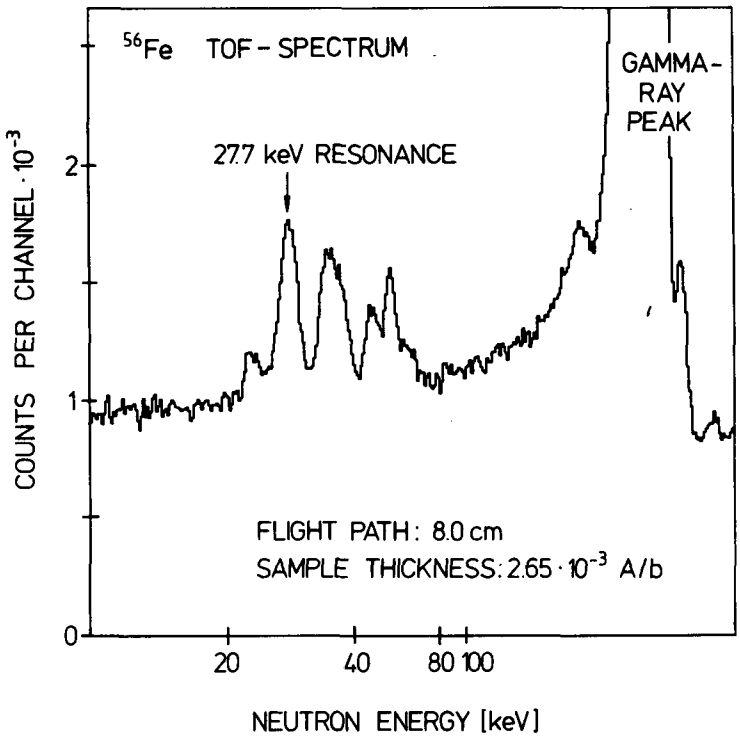

Fig. 1 Experimental time-of-flight spectrum of neutron capture events in ^{56}Fe taken with a continuous neutron spectrum in the energy range from 10 to 60 keV and with a flight path of only 8 cm.

References

[1] D.B. Gayther, B.W. Thomas, B. Thom, M.C. Moxon, Proc. of a Specialist Meeting on Neutron Data of Structural Materials for Fast Reactors, CBNM Geel (December 1977) p. 547

[2] F.H. Fröhner, Proc. of a Specialist Meeting on Neutron Data of Structural Materials for Fast Reactors, CBNM Geel (December 1977) p. 138; A. Ernst, F.H. Fröhner, D. Kompe, Proc. of an Int. Conf. on Nuclear Data for Reactors, Helsinki, 1970, Vol. 1, p. 619 (IAEA, Vienna 1970)

[3] B.J. Allen, A.R. de L. Musgrove, Proc. of a Specialist Meeting on Neutron Data of Structural Materials for Fast Reactors, CBNM Geel (December 1977) p. 447

[4] R.W. Hockenbury, Z.M. Bertolome, J.R. Tatarczuk, W.R. Moyer, R.C. Block, Phys. Rev. 178 (1969) 1746

2.1.2 The Capture Cross Section of ^{58}Fe between 5 and 400 keV Neutron Energy

F. Käppeler, L.D. Hong

(Relevant to request numbers: 691104, 762179)

In the preceding progress report [1] we described the first measurement of the capture cross section of ^{58}Fe in the neutron energy range from 10 to 200 keV. However, the results showed rather large statistical uncertainties and therefore the measurement was repeated with an improved experimental set-up. Instead of the 800 ℓ liquid scintillator tank a C_6D_6-detector was used, as it is described in contribution 2.3.1 of this report. The main advantage was that with this fast detector system the same time resolution of 1.5 ns/m could be obtained at a three times shorter flight path of 60 cm and therefore the sensitivity was considerably better. Moreover, in the second measurement a sample with a higher enrichment of 73 % was made available by the US loan pool. As a result, we were able to extend the investigated neutron energy range to the region between 5 and 400 keV and to accumulate data with good statistical accuracy.

As this measurement on ^{58}Fe was the first one we performed with the C_6D_6-detector system, a variety of different runs were made with different samples and different neutron spectra in order to investigate carefully the background problems, especially in view of the neutron sensitivity of this detector.

It turned out that we could benefit from the same effect of discriminating prompt capture gamma rays and scattered neutrons by their respective time-of-flight from the sample to the detector, as was described in the preceding contribution. Although the ratio of the distance sample-detector versus primary neutron flight path was only 0.25 instead of 2, it was still sufficient to avoid background from scattered neutrons for almost all capture resonances in ^{58}Fe.

The data analysis is not yet completed but the preliminary evaluation of single runs shows that even for the lowest neutron energies the background was sufficiently small to allow for a proper resonance analysis. Fig. 1 shows part of such a cross section which is not yet corrected for multiple scattering and self-shielding effects. In this energy range three resonances

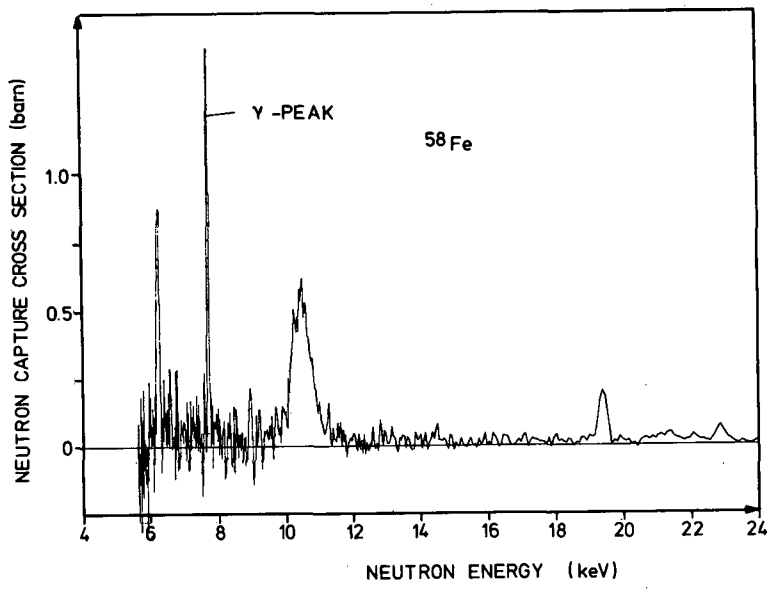

Fig. 1 Preliminary capture cross section of ^{58}Fe for a single run without corrections for multiple scattering and self-shielding effects. It demonstrates that the data allow for a reasonable resonance analysis even in the low energy range.

of ^{58}Fe can be identified. That means that the assignment of a resonance with $\ell > 0$ at 18.7 keV in the first measurement was erroneous. The position of the s-wave resonance at 10.34 keV confirms the resonance energy determined in total cross-section measurement [2] rather than the respective value of Garg et al [3].

References

[1] L.D. Hong, H. Beer, F. Käppeler, Report NEANDC(E) - 192 U, Vol. V, p. 18

[2] L.D. Hong, H. Beer, F. Käppeler, Nucl. Sci. Eng. 67 (1978) 184

[3] J.B. Garg, S.J. Jain, J.A. Harvey, Phys. Rev. C18 (1978) 1141

2.1.3 Investigation of the Validity of the Valence Model for Neutron Capture in the Mass Range 40 < A < 70

H. Beer

(Relevant to request numbers: 741033, 741034, 741035, 742033, 691104, 762179, 741059, 741063, 682013, 762139, 741065, 682014, 741068, 691106)

For a considerable number of nuclei in the mass range of the 3s giant resonance (40 < A < 70) the capture and total cross sections have been measured at the Karlsruhe pulsed 3 MV Van de Graaff-accelerator [1-4]. In the analysis of the s-wave resonances significant correlations between reduced neutron widths and total radiation widths have been detected [1] in contrast to the expectations of the model of compound nucleus formation. Correlations of that type are frequently associated with a single particle capture mechanism, the valence capture [5,6] which should exhibit strong high energy E1 transitions from $s_{1/2}$-states to low lying 2 $p_{1/2,3/2}$ levels. According to this model the partial radiation widths of these transitions can easily be calculated by means of experimentally determined resonance neutron widths and (d,p)-spectroscopic factors of the final states. The total radiation widths of the resonances are then obtained by a summation over all partial radiation widths of these high energy transitions.

In the present investigation total radiation widths were calculated via the valence model for the various nuclei which have been studied experimentally at the Karlsruhe 3 MV Van de Graaff-accelerator. The calculations were carried out using the formulae given by Cugnon [7]. In Fig. 1 the theoretical and experimental results for the s-wave resonances of the even-even nuclei are compared by white and hatched bars, respectively. For resonances located below the 5 keV energy limit of the Van de Graaff measurements, experimental values from other work were included. The experimental results of ^{54}Cr were taken from Stieglitz et al [8].

The comparison of calculation and measurement shows that in some cases valence capture seems to be responsible for essentially all the observed radiation width. In addition, the existence of a threshold effect in neutron energy is indicated. For the neutron deficient nuclei ^{54}Fe, ^{50}Cr and ^{58}Ni the agreement between theoretical and experimental values is very good up to about 100 keV resonance energy. The transition to more neutron rich nuclei which is connected with a reduction in excitation energy seems to lower

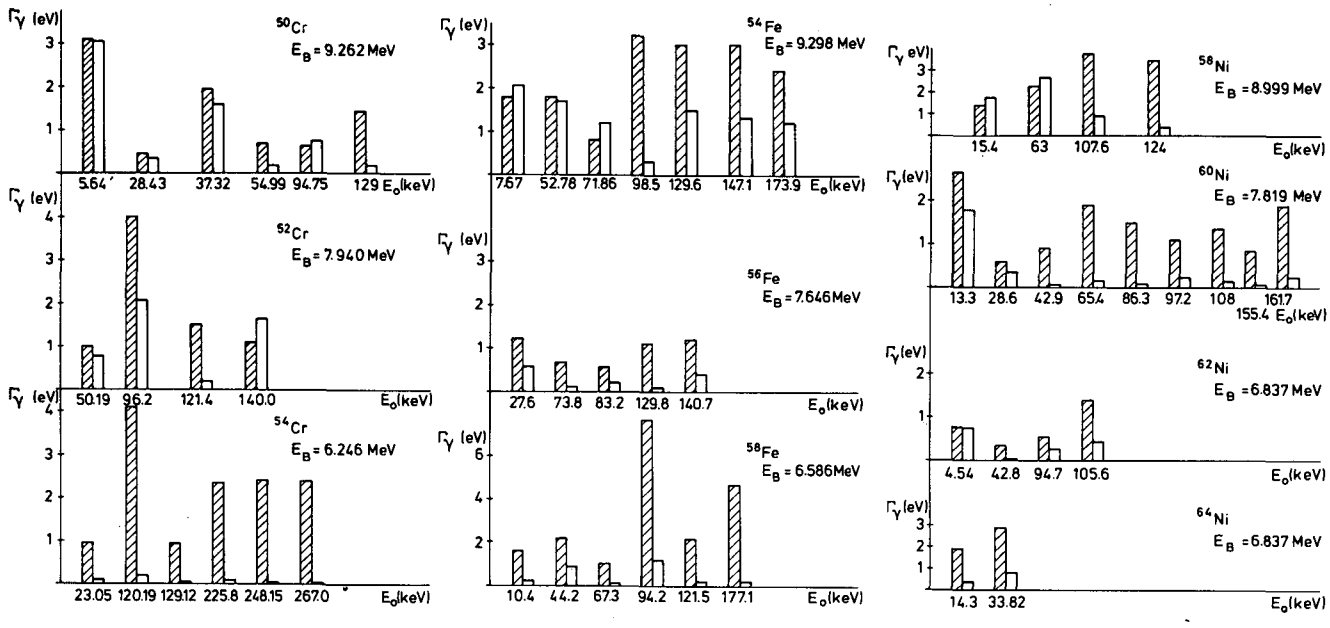

Fig. 1 Comparison of experimental and theoretical total radiation widths for the even-even nuclei of Cr, Fe and Ni (experimental values: hatched bars; theoretical values: white bars). For each resonance the neutron energy E_o and for each nucleus the binding energy E_B are specified.

this neutron energy threshold so that for the neutron richest nuclei ^{54}Cr, ^{58}Fe and ^{64}Ni the model fails totally in predicting the experimental radiation widths.

Among the studied odd target nuclei ^{53}Cr and ^{57}Fe seem to be good candidates for a valence model capture mechanism. ^{59}Co and ^{61}Ni show sizeable valence capture only for some resonances with large neutron widths whereas for the ^{47}Ti resonances the valence model fails.

Besides the comparison with calculated total radiation widths, the existence of valence capture might also be confirmed by the study of high energy gamma transitions. In a measurement carried out at our laboratory [9] this has been done for the 27 keV resonance in ^{56}Fe, the 13.3 keV resonance in ^{60}Ni and the 15.4 and 63 keV resonances in ^{58}Ni. Only in the case of ^{60}Ni the valence capture mechanism could be confirmed in this way.

The results of this investigation have been published elsewhere [10].

References

[1] H. Beer, R.R. Spencer, Nucl. Phys. A240 (1975) 29

[2] F.H. Fröhner, Report KfK-2046 (1973)

[3] R.R. Spencer, H. Beer, Nucl. Sci. Eng. 60 (1976) 390

[4] L.D. Hong, H. Beer, F. Käppeler, Specialist Meeting on Neutron Data of Structural Materials for Fast Reactors, CBNM Geel (December 1977) p. 624

[5] J.E. Lynn, Theory of Neutron Resonance Reactions, Clarendon Press, Oxford (1968)

[6] J. Cugnon, C. Mahaux, Ann. Phys. 94 (1975) 128

[7] J. Cugnon, Nucl. Phys. A 263 (1976) 61

[8] R.G. Stieglitz, R.W. Hockenbury, R.C. Block, Nucl. Phys. A 163 (1971) 592

[9] H. Beer, R.R. Spencer, F. Käppeler, Z. Phys. A 284 (1978) 173

[10] H. Beer, J. de Physique 40 (1979) 339

2.2 Fission Products

2.2.1 Capture Cross-Section Measurements on the Stable Krypton Isotopes

B. Leugers, F. Käppeler

(Relevant to request number: 742040)

The results of first measurements on natural Kr and ^{84}Kr showed that the experimental set-up must be improved to obtain overall accuracies of around 10 %. For the further measurements three major changes led to a considerable reduction in background, at least by a factor of 2:

1) The neutron shielding around the target was optimized by increasing the ^{6}Li-carbonate liner in the collimator part and by introducing a thick shield of boron resin.
2) The lead shielding around the detector was machined carefully in order to provide a thickness of 20 cm at least in any direction. In addition "white" lead was used to avoid background from the activation of antimony.

3) Instead of liquified Kr samples high pressure gas samples were designed. Steel spheres 2 cm in diameter and of 0.5 mm wall thickness are able to withstand pressures up to 500 bar. In this way the same amount of Krypton could be enclosed in less canning material as compared to liquified samples.

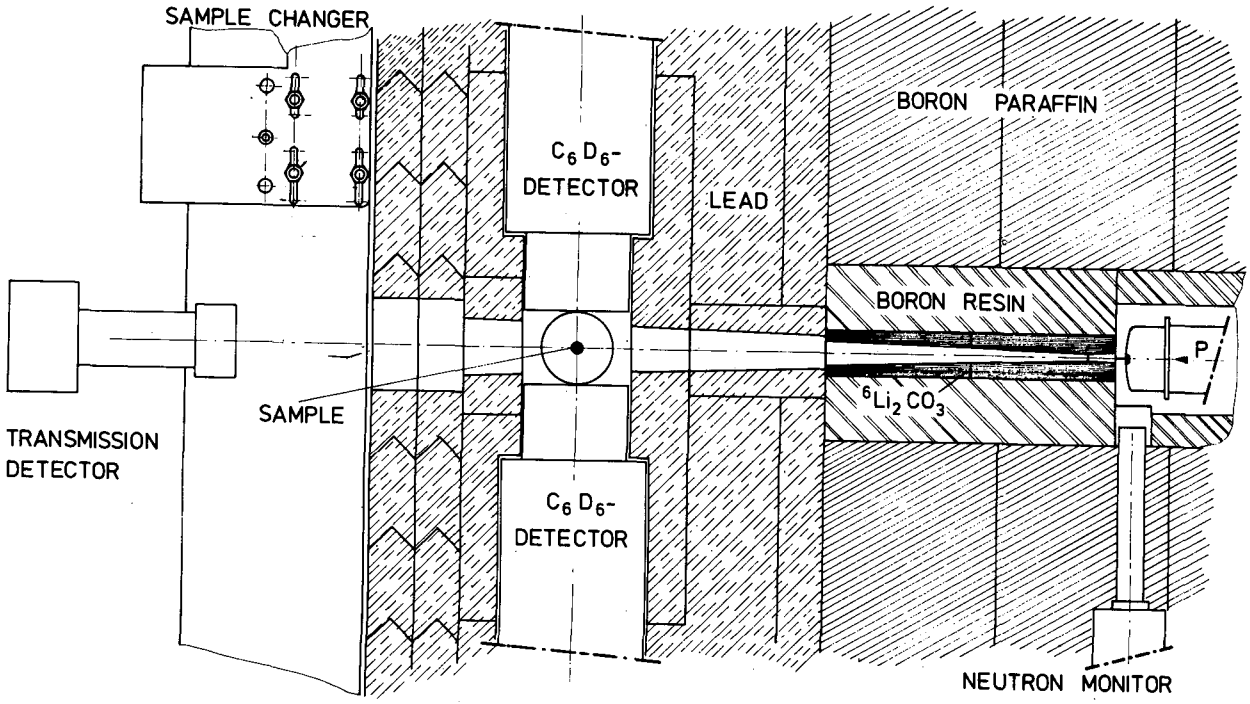

Fig. 1 Schematic sketch of the improved experimental set-up for the determination of keV neutron capture cross sections.

With this improved set-up,which is shown in Fig. 1, measurements were made on samples of natural Krypton, on isotopically pure ^{84}Kr and on three other samples enriched in ^{83}Kr, ^{82}Kr and ^{80}Kr. From these results cross sections for all the stable Kr isotopes can be deduced. As the analysis is not yet completed, only the preliminary capture cross section of natural Kr, which is not corrected for multiple scattering and self-shielding is given in Fig.2. The resolution in neutron energy is 1.5 ns/m.

The neutron energy range covered in the present work overlaps with that investigated by Maguire et al [1] and it is hoped that on the basis of

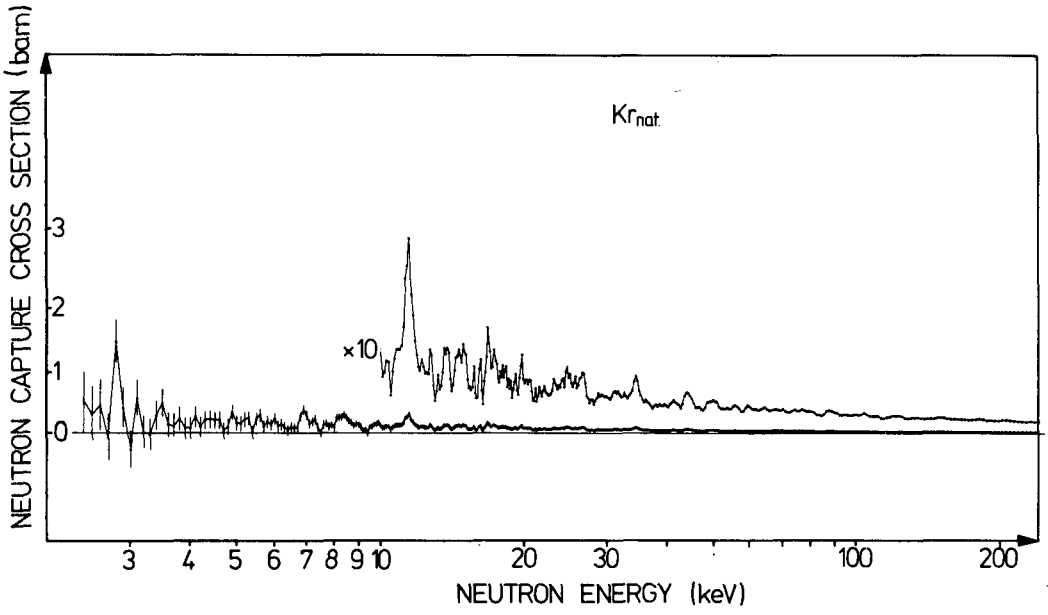

Fig. 2 Preliminary capture cross section of natural Krypton between 2 and 250 keV neutron energy. The resonances on top of the more continuous cross section are mainly due to ^{84}Kr.

our more complete set of data, the resonance assignments can be improved considerably.

Reference

[1] H.T. Maguire, H.M. Fisher, R.C. Block, Proc. Conf. on Neutron Physics and Nuclear Data for Reactors and other Applied Purposes, Harwell (September 1978) p. 472

2.2.2 Measurement of the keV Neutron Capture Cross Sections of ^{138}Ba, $^{140,142}Ce$, $^{175,176}Lu$ and ^{181}Ta with the Activation Method

H. Beer

(Relevant to request numbers: 682037, 691192)

At a Van de Graaff-accelerator the activation technique represents a powerful

tool for the measurement of neutron capture cross sections. In the present investigation neutron activation cross sections on various isotopes have been determined via the $^{7}Li(p,n)$-reaction using proton energies 10 to 15 keV above the reaction threshold. The neutron energy distribution measured by the time-of-flight technique was found to be similar to a Maxwell distribution for thermal energies around kT = 20 keV as is illustrated in Fig. 1.

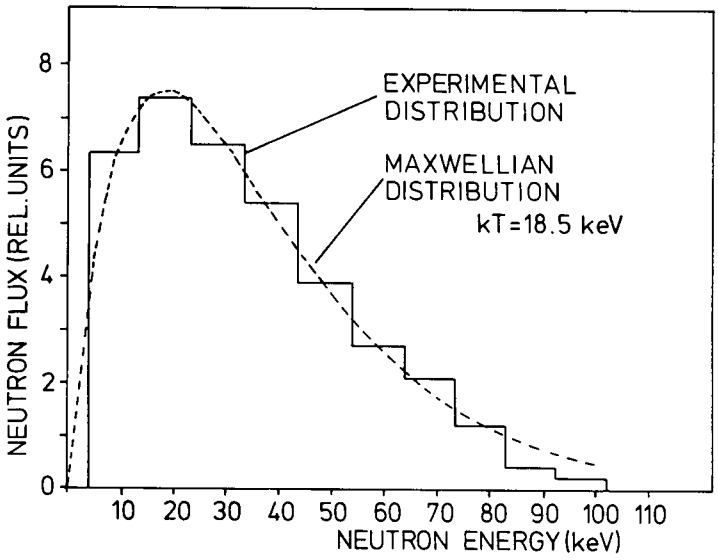

Fig. 1 Neutron flux from the $^{7}Li(p,n)$-reaction for proton energies 10 to 15 keV above threshold compared to a Maxwell distribution for a thermal energy of 18.5 keV.

During the activations the Van de Graaff-accelerator was operated in dc mode to obtain beam currents of 50 to 100 μA. The activation foil and a gold foil which served as a standard were placed in a back-to-back arrangement immediately at the neutron target. Neutron scattering corrections are very small as the neutrons from reactions just above threshold are kinematically collimated in the forward direction. Throughout the irradiation the neutron flux was recorded continuously as a function of time by a ^{6}Li glass detector. After irradiation the activated foils were analyzed by a calibrated high resolution Ge(Li) detector.

In Table I the results of the measurements are summarized in terms of the Maxwellian energy distributions which are of interest to nuclear astro-

physics. The thermal energies are given as obtained by a fit of the experimental neutron energy distribution with the Maxwell distribution function. In addition the average energies for the respective distributions were calculated by the relation

$$\bar{E} = \frac{\int E\sigma(E)\phi(E)dE}{\int \sigma(E)\phi(E)dE}$$

The unknown energy dependence of the cross sections $\sigma(E)$ was taken from theoretical work [1].

Table I. Summary of the average neutron capture cross sections obtained by the activation technique

Reaction	Thermal energy kT(keV)	Average energy (keV)	$\sigma_{n\gamma}$(mb)
$^{138}Ba(n,\gamma)^{139}Ba$	18.0	30.8	5.13 ± 0.26
$^{140}Ce(n,\gamma)^{141}Ce$	20.5	32.6	12.1 ± 0.6
$^{142}Ce(n,\gamma)^{143}Ce$	20.5	28.0	21.6 ± 1.1
$^{175}Lu(n,\gamma)^{176m}Lu$	19.6	26.4	884 ± 150
$^{176}Lu(n,\gamma)^{177}Lu$	18.0	26.8	1942 ± 97
$^{181}Ta(n,\gamma)^{182}Ta$	18.0	23.5	1245 ± 62

Reference

[1] V. Benzi, R. d'Orazi, G. Reffo, M. Vaccari, Report C.N.E.N.-RT/F1(72)6

2.3 Actinide Cross Sections

2.3.1 Neutron Capture Cross Sections of ^{241}Am in the Energy Range from 10 to 250 keV

K. Wisshak, F. Käppeler

(Relevant to request numbers: 712108, 712109, 712110, 721099, 742108, 752033, 741127, 762153, 702081)

For the capture cross-section measurement of ^{241}Am the same experimental method was applied as used recently for the isotopes ^{240}Pu and ^{242}Pu [1,2]. During the measurements three runs have been performed in the low energy range from 10 to 100 keV using flight paths between 50 and 66.2 mm, and one run in the high energy range from 50 to 250 keV. Gold has been used as a reference sample. Details of the experiments have been reported elsewhere [3,4].

The results of our measurements are shown in Fig. 1. For comparison with the data of other authors the experimental cross-section ratios have been converted to absolute values using the evaluated gold cross section from ENDF/B-IV. The statistical accuracy of the data points is 1-2 % for energies between 25 and 80 keV and increases to 5-7 % at lower and higher energies. The respective total uncertainties are 4-5 % and 8-12 %. Our data confirm the values of Gayther and Thomas [5] whereas the data of Weston and Todd [6] are systematically lower between 20 and 80 keV.

References

[1] K. Wisshak, F. Käppeler, Nucl. Sci. Eng. 66 (1978) 363

[2] K. Wisshak, F. Käppeler, Nucl. Sci. Eng. 69 (1979) 39

[3] K. Wisshak, F. Käppeler, W. Hage, Proc. of a Specialist Meeting on the Nuclear Data of Higher Plutonium and Americium Isotopes for Reactor Applications, Brookhaven (November 1978), in press

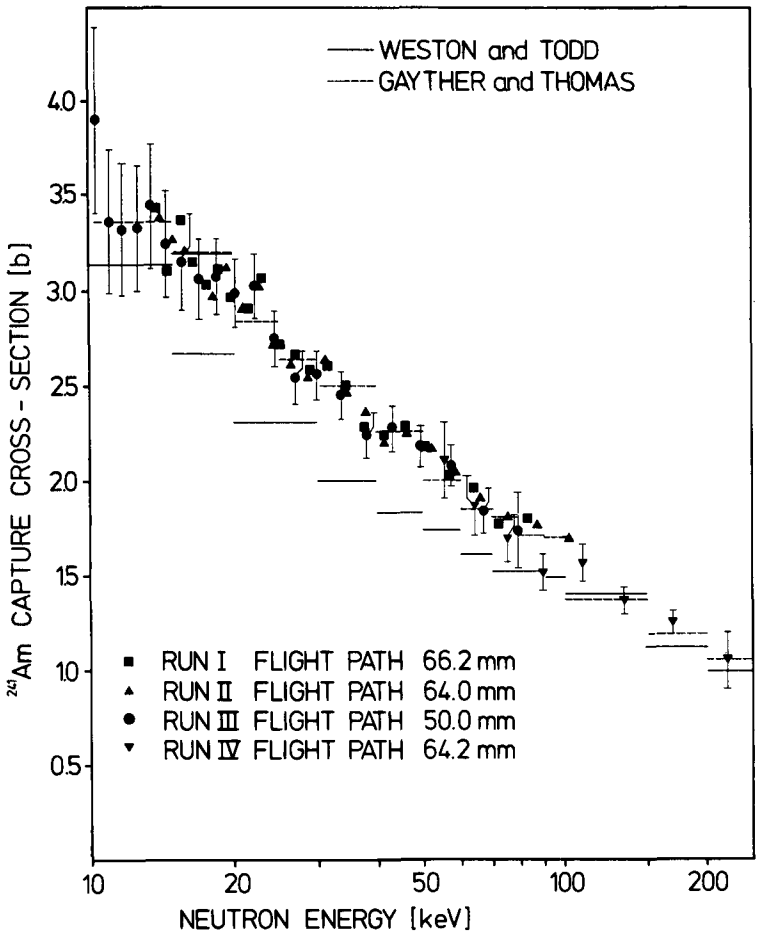

Fig. 1 The neutron capture cross section of ^{241}Am.

[4] K. Wisshak, F. Käppeler, W. Hage, Proc. Int. Conf. on Neutron Physics and Nuclear Data for Reactors and other Applied Purposes, Harwell (September 1978) p. 893

[5] D.B. Gayther, B.W. Thomas, Proc. Conf. on Neutron Physics, Kiev (1977); and private communication

[6] L.W. Weston, J.H. Todd, Nucl. Sci. Eng. 61 (1976) 356

2.3.2 The Subthreshold Fission Cross Section of ^{241}Am in the Energy Range from 10-250 keV

W. Hage*, F. Käppeler, K. Wisshak

(Relevant to request numbers: 712103, 732115, 742018, 742107, 762225, 702080)

As already reported [1] the fission cross section of ^{241}Am has been determined relative to ^{235}U in the energy range from 10 to 1000 keV via the detection of fission neutrons. Using the ^{7}Li(p,n)-reaction as a neutron source, the energy range between 120 and 1000 keV was investigated with monoenergetic neutrons from thin Li-targets, whereas a continuous neutron spectrum was applied in the lower energy range. The results obtained with the continuous spectrum are given as open circles in Fig. 1. They fit smoothly to the values obtained by monoenergetic neutrons (full circles) which have been given in ref. [1]. The total systematic and statistical accuracy of the data points is 6-10 %. These data, however, have to be quoted as preliminary because there are still some doubts about the exact sample mass.

In addition it was possible to determine the subthreshold fission cross section of ^{241}Am from the data taken during the capture cross-section mea-

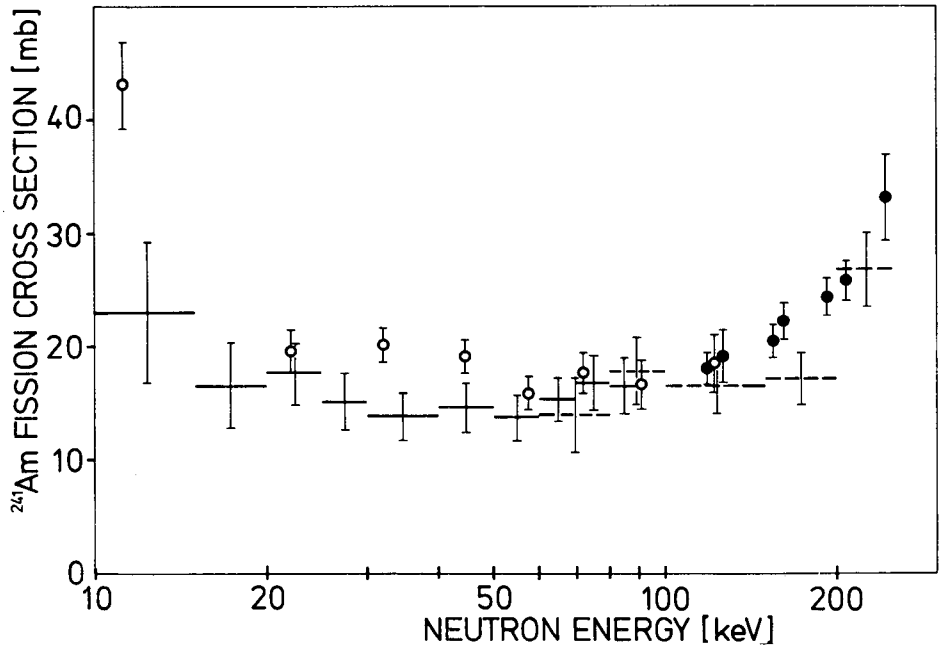

Fig. 1 The subthreshold fission cross section of ^{241}Am.

* EURATOM, Ispra, Italy

surements (see section 2.3.1). The results are shown as histograms in Fig. 1. The solid line represents the data from the three low energy runs (10-90 keV) whereas the dashed line was obtained from the data measured in the high energy run. The statistical accuracy of the data is 3-6 %, but the total uncertainty is 13-20 %. The high systematic uncertainty was caused mainly by the correction of a ∿1.6 % ^{239}Pu impurity in the sample material.

Our results indicate a minimum in the cross section of ∿15-20 mb for energies between 20 and 100 keV. This is considerably lower than the recent result of Knitter et al [2] yielding values of ∿20-30 mb in the same energy range.

References

[1] W. Hage, H. Hettinger, S. Kumpf, F. Käppeler, K. Wisshak, Report NEANDC(E) - 192 U,Vol. V, p. 26

[2] H.H. Knitter, C. Budtz-Jørgensen, Proc. Int. Conf. on Neutron Physics and Nuclear Data for Reactors and Applied Purposes, Harwell (September 1978) p. 899

2.3.3 The Distribution of Fragment Mass and Fragment Kinetic Energy from Fast Neutron Induced Fission of ^{237}Np

A.A. Naqvi, F. Käppeler, R. Müller* , F. Gönnenwein*

A 4-parameter spectrometer has been developed for the measurement of kinetic energies and velocities of correlated fragments from fast neutron induced fission. Details of this spectrometer have been reported earlier [1,2]. Measurements with this system have been performed on ^{235}U at 0.5 and 5.5 MeV neutron energy and also on ^{237}Np, where the neutron energies were chosen just above the fission threshold at 0.8 MeV and - as in the case of ^{235}U - just below the threshold for second chance fission at 5.5 MeV. The measurements have been carried out with fission targets of ∿100 μg/cm^2 thickness enriched to more than 99 % in ^{235}U and ^{237}Np, respectively. For each energy about 20 000 coincident fission fragments were observed in runs at 4 different but well defined flight paths. The overall time resolution achieved in the velocity determination of the fragments was between 600 and 800 ps. Daily energy calibration of the solid

* Physikalisches Institut, Universität Tübingen

state detectors was performed by thin ^{252}Cf sources.

In the first step of data analysis, prompt fragment mass yields and kinetic fragment energies have been derived from the observed pulse height information, only. The resulting distributions are shown in Figs. 1 and 2.

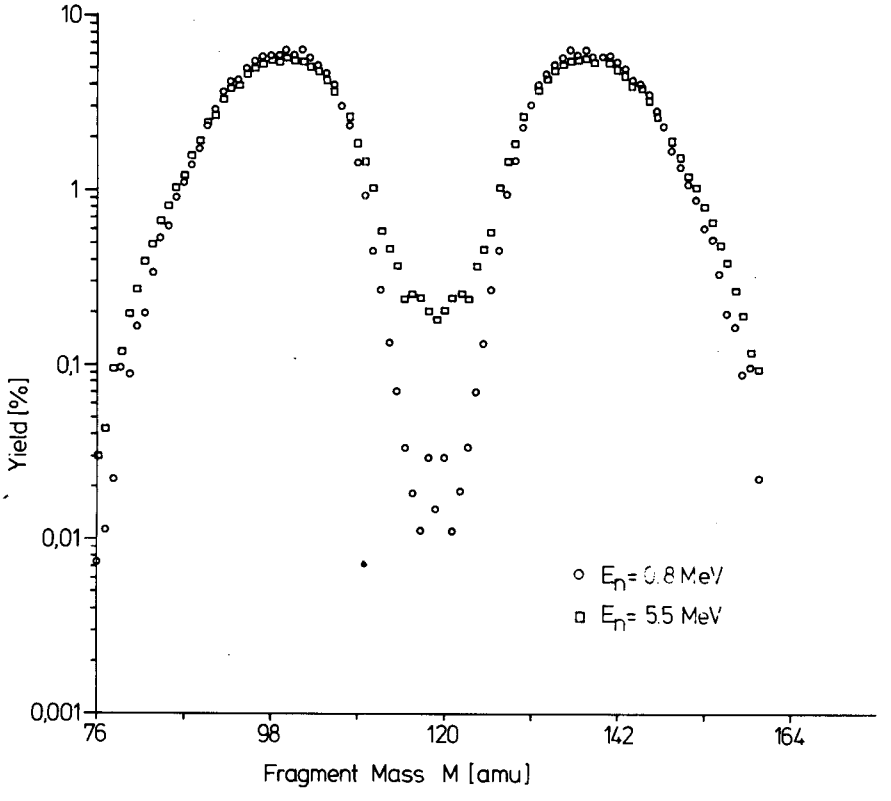

Fig. 1 Prompt fragment mass yields in the fission of (^{237}Np+n) at 0.8 and 5.5 MeV neutron energy.

The mass distribution of ^{237}Np at 0.8 MeV is characterized by a pronounced mass asymmetry with a peak/valley ratio of 250 ± 30. This value is somewhat higher than that reported for the subthreshold fission of ^{237}Np at thermal neutron energies by Asghar et al [3], who found a ratio of 125. With increasing neutron energy the symmetric fission component is somewhat enhanced and at 5.5 MeV neutron energy the peak/valley ratio decreases to 30 ± 1.5. This behaviour is compatible with the picture that shell effects decrease with the increasing excitation energy at the saddle point of the fissioning system.

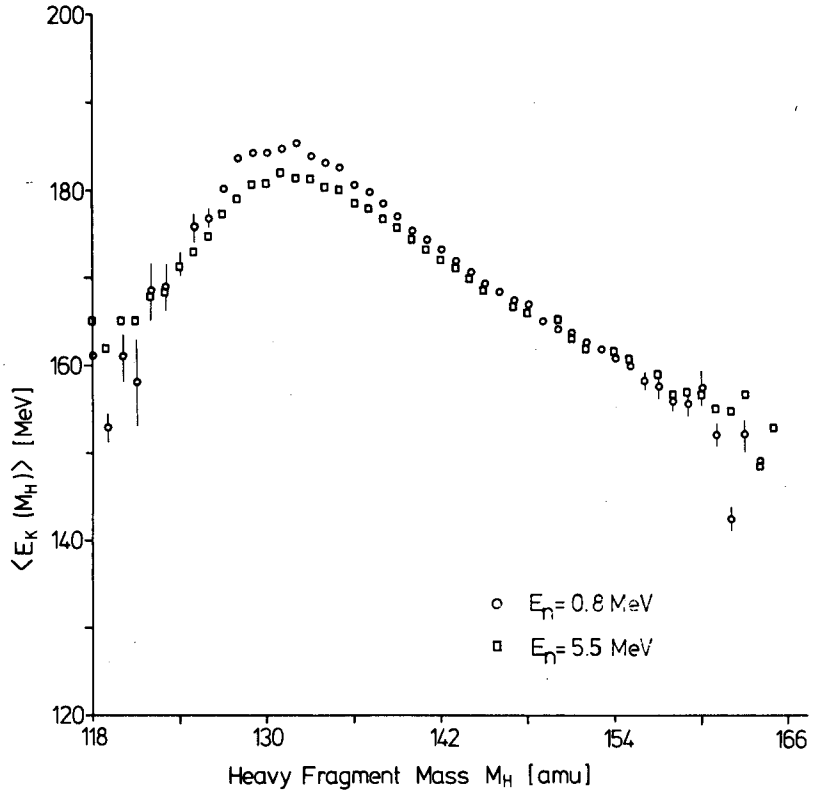

Fig. 2 Distribution of fragment kinetic energies in the fission of (^{237}Np+n) at 0.8 and 5.5 MeV neutron energy.

This trend was also present in the respective distributions of the fragment kinetic energy. One finds from Fig. 2 that the differences in the two distributions are most pronounced around the near magic fragments at mass number 132, where shell effects are rather sensitive. For higher mass numbers where shell effects are less important, additional deformations have no significant effect on the mean fragment distance at the scission point and thus on the fragment kinetic energies.

At present, data analysis is being completed by the inclusion of the fragment velocities. This yields a better mass resolution and in addition, it allows to derive the number of prompt fission neutrons as a function of fragment mass.

References

[1] R. Müller, F. Käppeler, A.A. Naqvi, F. Gönnenwein, A. Ernst, Report KfK-2379 (December 1976) p. 6

[2] R. Müller, A.A. Naqvi, F. Käppeler, Report KfK-2686 (October 1978) p. 11

[3] M. Asghar, P. D'Hondt, C. Guet, P. Perrin, C. Wagemans, Nucl. Phys. A 292 (1977) 225

2.3.4 Neutron Total Cross Sections for ^{240}Pu and ^{242}Pu in the Energy Range from 10 to 375 keV

F. Käppeler, L.D. Hong, H. Beer

(Relevant to request number: 692439)

The isotopes ^{240}Pu and ^{242}Pu are inevitable constituents of the fuel cycle of the fast breeder reactor. Fast neutron cross sections of these isotopes deserve, therefore, special attention. Since in the fast energy range above 10 keV experimental data of the respective total cross sections are only available for ^{240}Pu from 116 keV up to 1.5 MeV in increments of 25 keV [1], transmission measurements on ^{240}Pu and ^{242}Pu were carried out at the Karlsruhe pulsed 3 MV Van de Graaff-accelerator using the time-of-flight technique. The measurements covered the energy range from 10 to 375 keV with an energy resolution of 0.8 ns/m. The neutron time-of-flight spectra with and without sample were recorded with a ^{6}Li-glass detector at a flight path of about 5 m. Details of the experimental arrangement can be found elsewhere [2]. The Pu samples consisted of plutonium oxide powder (PuO_2) which was pressed into thin walled Al-cannings. The samples were enriched in ^{240}Pu and ^{242}Pu to 98.3 and 77.16 %, respectively. Therefore, besides the oxygen content impurities of other Pu isotopes had to be taken into account in the analysis. In addition the data had to be corrected for small impurities of Al from the cannings. The corrections were calculated using cross sections from KEDAK and ENDF/B-IV data files. In Figs. 1 and 2 the results of the measurements are displayed with the original energy resolution.

For comparison the KEDAK and ENDF/B-IV evaluation and the experimental values of Smith et al [1] have been included. Above 140 keV deviations between the evaluated data and the present results lie within our quoted uncertainties. Below 140 keV the evaluated data are lower than our values. The ^{240}Pu total cross section of Smith et al [1] is in good agreement with our results.

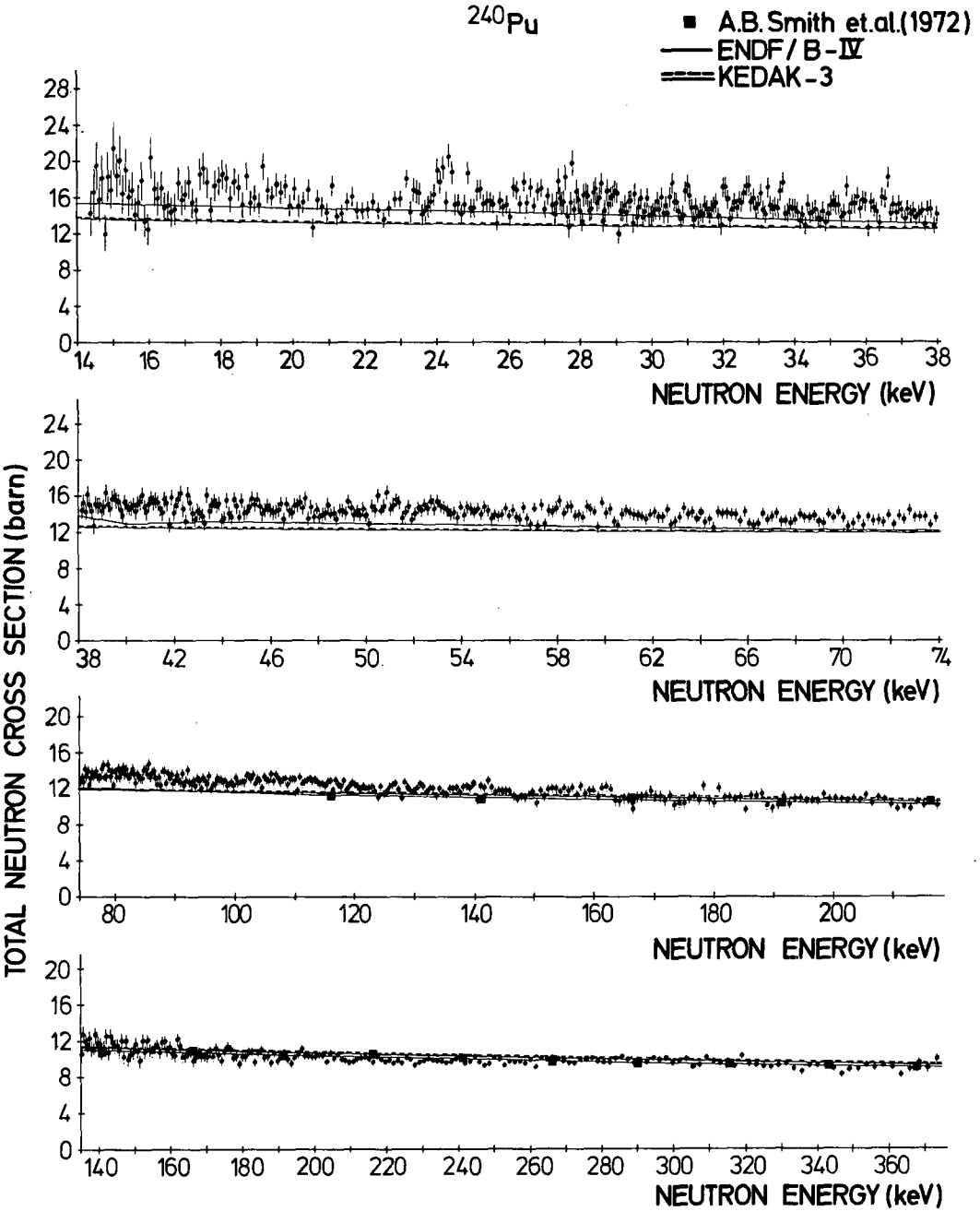

Fig. 1 The total neutron cross section of ^{240}Pu in the energy range from 14 to 375 keV.

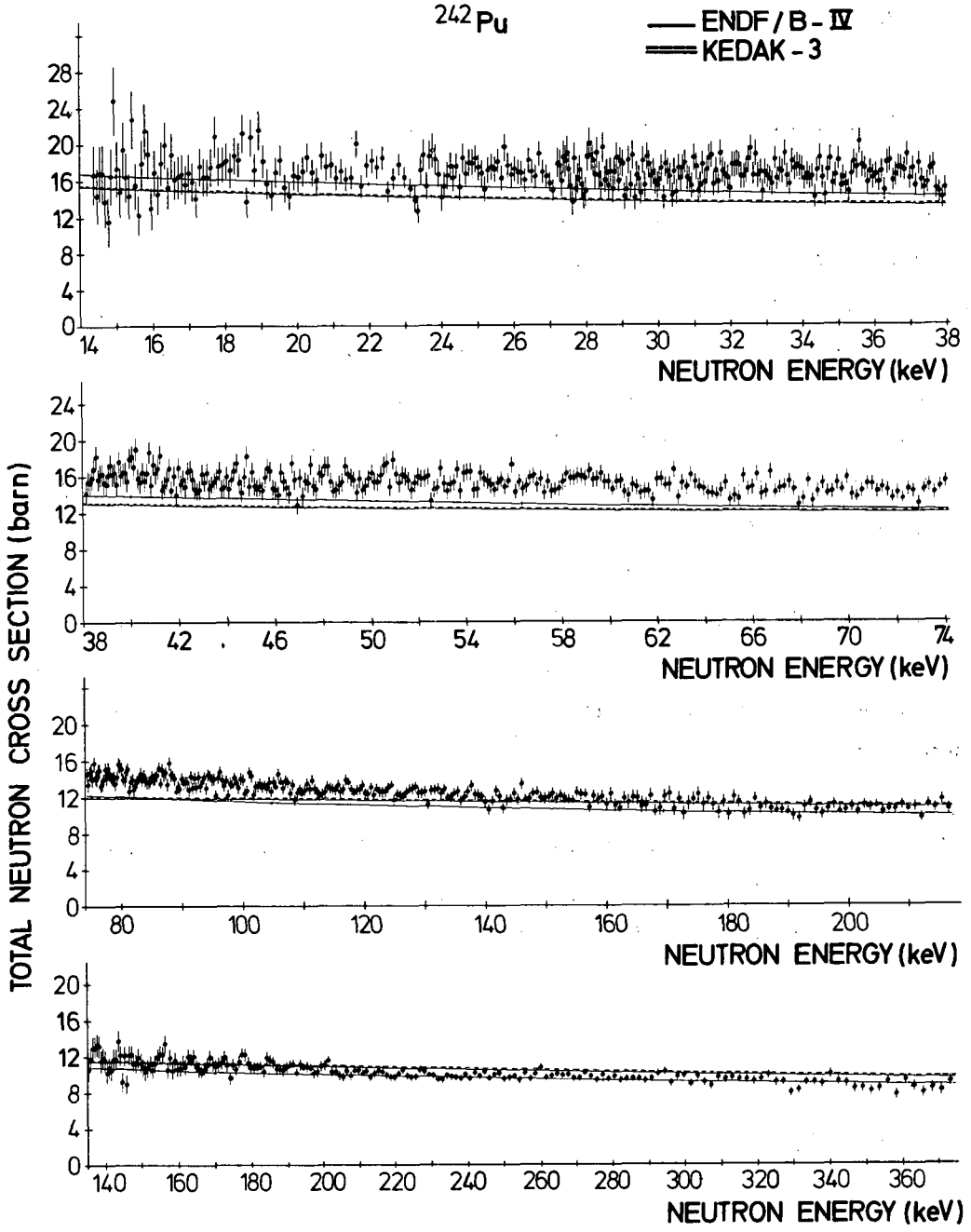

Fig. 2 The total neutron cross section of ^{242}Pu in the energy range from 14 to 375 keV.

References

[1] A.B. Smith, P. Lambropoulos, J.F. Whalen, Nucl. Sci. Eng. 47 (1972) 19

[2] H. Beer, L.D. Hong, F. Käppeler, Nucl. Sci. Eng. 67 (1978) 184

2.4 Standards

2.4.1 Resonance Analysis of the ^{10}B Total Cross Section in the Energy Range from 90 to 420 keV

H. Beer

(Relevant to request number: 691016)

The ^{10}B neutron absorption cross section is one of the important standard cross sections for neutron flux determinations. Much of the present information about this cross section has been obtained via measurements of the ^{10}B total cross section [1,2]. The broad $7/2^+$ s-wave resonance at 370 keV is primarily responsible for the well-known $E^{-1/2}$ energy dependence of the total and (n,α) cross sections from thermal energies up to 100 keV [3]. This resonance has been analyzed from polarization and differential scattering measurements [3].

In the present investigation the total cross section measured at the Karlsruhe pulsed 3 MV Van de Graaff-accelerator [4] between 90 and 420 keV has been analyzed. Special emphasis has been placed upon a broad structure with a maximum at about 230 keV.

According to the work of Lane et al [3] only one broad resonance is close to our investigated energy region, the $7/2^+$ s-wave resonance at 370 keV with a neutron width of 770 keV and a total alpha-width of 114 keV.

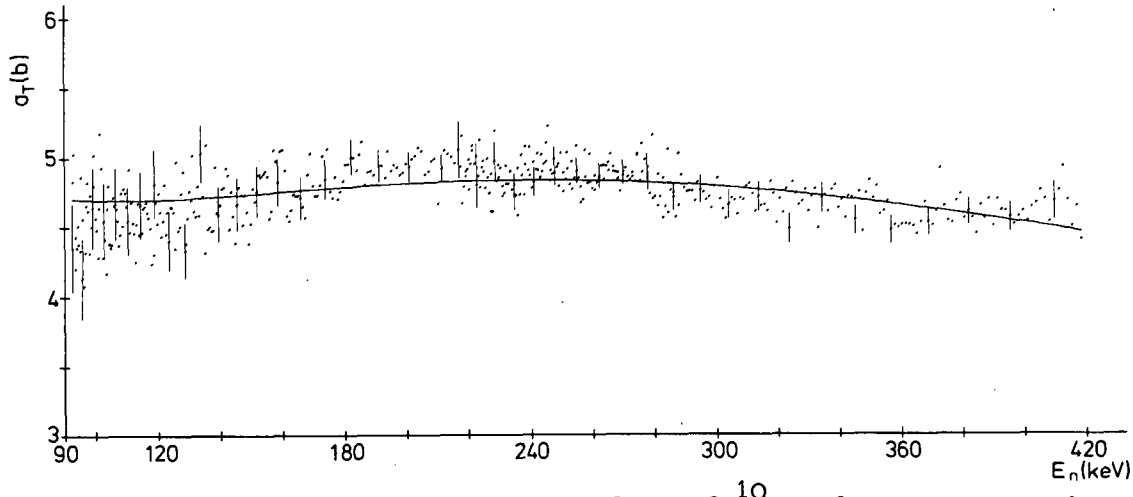

Fig. 1 The neutron total cross-section data of ^{10}B and an R-matrix shape fit represented by the full black curve. The uncertainty indicated at every tenth data point is only the statistical uncertainty.

In order to check whether the broad structure in the total cross section corresponds to this s-wave resonance,an R-matrix analysis was performed using the resonance parameters of ref. [3]. Besides neutron scattering only alpha-decay has to be considered as the contributions of other decay processes, i.e. (n,p), (n,t) and (n,γ) which are also energetically possible are negligibly small [1]. Following Lane et al [3] the variation in the alpha-penetrability was neglected and the alpha-widths were assumed to be constant. In this approximation an R-matrix multilevel analysis with the Fortran IV code FANAL [5] could be carried out treating the total alpha-decay width formally like the total radiation width. The result of our calculation shown in Fig. 1 together with the experimental data indicates that the observed structure can easily be explained with the $7/2^+$ s-wave resonance at 370 keV.

References

[1] F.P. Mooring, J.E. Monahan, C.M. Huddleston, Nucl. Phys. 82, (1966) 16

[2] M.G. Sowerby, B.H. Patrick, C.A. Uttley, K.M. Diment, Proc. Int. Conf. on Nucl. Data for Reactors, Helsinki, 1970, Vol. 1, p. 161 (IAEA, Vienna 1970)

[3] R.O. Lane, S.L. Hausladen, J.E. Monahan, A.J. Elwyn, F.P. Mooring, A. Langsdorf, jr., Phys. Rev. C4 (1971) 380

[4] R.R. Spencer, H. Beer, F.H. Fröhner, Report KfK-1518

[5] F.H. Fröhner, Report KfK-2129 (1976)

INSTITUT FÜR KERNPHYSIK
KERNFORSCHUNGSZENTRUM KARLSRUHE

1. Isochronous Cyclotron

1.1 High Precision Measurement of the Total Neutron Cross Section of the Helium Isotopes

B. Haesner, H.O. Klages, H. Dobiasch, W. Heeringa,
B. Zeitnitz, D. Erbe, F. Käppeler, B. Leugers, G. Schmalz

In the framework of investigations of the light nuclei with fast neutrons the total cross sections of the helium isotopes were measured between 1 and 40 MeV.
Transmission measurements were performed at the 190 m flight path of the Karlsruhe fast neutron spectrometer [1] . High pressure (400 bar) gaseous samples were used. The resolution of the spectrometer was below 0.008 nsec/m and therefore the d 3/2-resonance at 22.14 MeV in the ^{4}He+n-system was clearly resolved. The width of the resonance was determined to be $\Gamma = 76 \pm 12$ keV which is comparable with the former value of $\Gamma = 100 \pm 50$ keV [2] . No further narrow structure was found in the n+^{4}He-system.

The investigation of the n+^{3}He total cross section was motivated by a recent phase shift analysis [3] which gives an indication of a narrow level near 37 MeV in ^{4}He. The resolution of the existing data [4] was not sufficient to show a structure comparable to the 80 keV wide resonance in ^{5}He.

The result of our measurement is a smooth behaviour of the total cross section in the energy region of interest. So we conclude that there is no narrow level around 37 MeV in ^{4}He with a width of more than 10 keV.

The energy averaged total cross sections for both isotopes agree with the data of ref. [4] within the quoted errors.

1.2 Total Neutron Cross Sections of the Stable Hydrogen Isotopes

H. Bente, P. Schwarz, H.O. Klages, H. Dobiasch,
D. Erbe, B. Haesner, L. Husson, G. Schmalz,
J. Wilczynski, B. Zeitnitz

High resolution total neutron cross sections of hydrogen and deuterium were determined. Transmission measurements were carried out at the 190 m flight path of the Karlsruhe fast neutron facility using high pressure gaseous samples. In the experiments a resolution of the spectrometer of 0.007 nsec/m was achieved.

The data agree with recommended values in the energy range from 2 to 15 MeV and give more accuracy to the higher energy data up to 40 MeV.

No narrow structure was found for the total cross sections of both isotopes.

1.3 The Total Neutron Cross Section of ^{20}Ne and T = 3/2- States in ^{21}Ne

H. Abdel-Wahab, H.O. Klages, D. Eversheim*,
F. Hinterberger*

The investigation of low lying T = 3/2 states in nuclei with A = 4xn + 1 was continued performing a very high resolution measurement of the total neutron cross section of ^{20}Ne [5]. A high pressure gaseous sample was used at the 190 m flight path of the Karlsruhe fast neutron spectrometer. The achieved resolution of 0.006 nsec/m corresponds to 0.5 keV at a neutron energy of 2.2 MeV, at the lowest T = 3/2 level in ^{21}Ne. A great number of T = 1/2 resonances could be resolved and various parameters will be determined.

---

* Institut für Strahlen- und Kernphysik, Universität Bonn

References

[1] S. Cierjacks et al, NEANDC(E) - 192 U, Vol. V, INDC (Ger) - 20/L + Special (1978) p.1

[2] F. Ajzenberg-Selove, T. Lauritsen, Nucl. Phys. A227 (1974) 1

[3] P.W. Lisowski et al, Nucl. Phys. A259 (1976) 61

[4] C.A. Goulding et al, Nucl. Phys. A215 (1973) 253

[5] S.Cierjacks et al, NEANDC(E) - 192 U, Vol. V, INDC (Ger) - 20/L + Special (1978) p.14

INSTITUT FÜR NEUTRONENPHYSIK UND REAKTORTECHNIK
KERNFORSCHUNGSZENTRUM KARLSRUHE

1. Nuclear Data Evaluation

1.1 Clarification of ^{241}Am Thermal Cross-Section Discrepancies

B. Goel

(Relevant to request numbers: 671135, 671136, 681807, 691336, 702081)

Published data and evaluated files show large discrepancies in the thermal cross sections for ^{241}Am. In BNL 325, for example, the 2200 m/sec capture cross section is given as 832 ± 20 b while in the ENDF/B IV file a value of 582 b is stored. This discrepancy can be explained as follows. The total cross section was measured in time-of-flight experiments, which give a value precisely at 2200 m/sec. The capture cross section, on the other hand, was measured with the Cd difference method. This gives only an effective (averaged) capture cross section for a particular reactor spectrum. Due to the presence of two strong resonances at 0.31 and 0.58 eV this effective cross section is very sensitive to the Cd thickness used (Fig. 1). The published experimental data have been analysed and found to be consistent (Fig. 1) with the recommended data for 2200 m/sec listed in Table I.

Table I. Evaluated 2200 m/sec cross sections for ^{241}Am

Type of interaction	Cross section
σ_t	640 ± 20b
σ_c	625 ± 20b
σ_f	3.15 ± 0.1b
σ_n	12 ± 3b

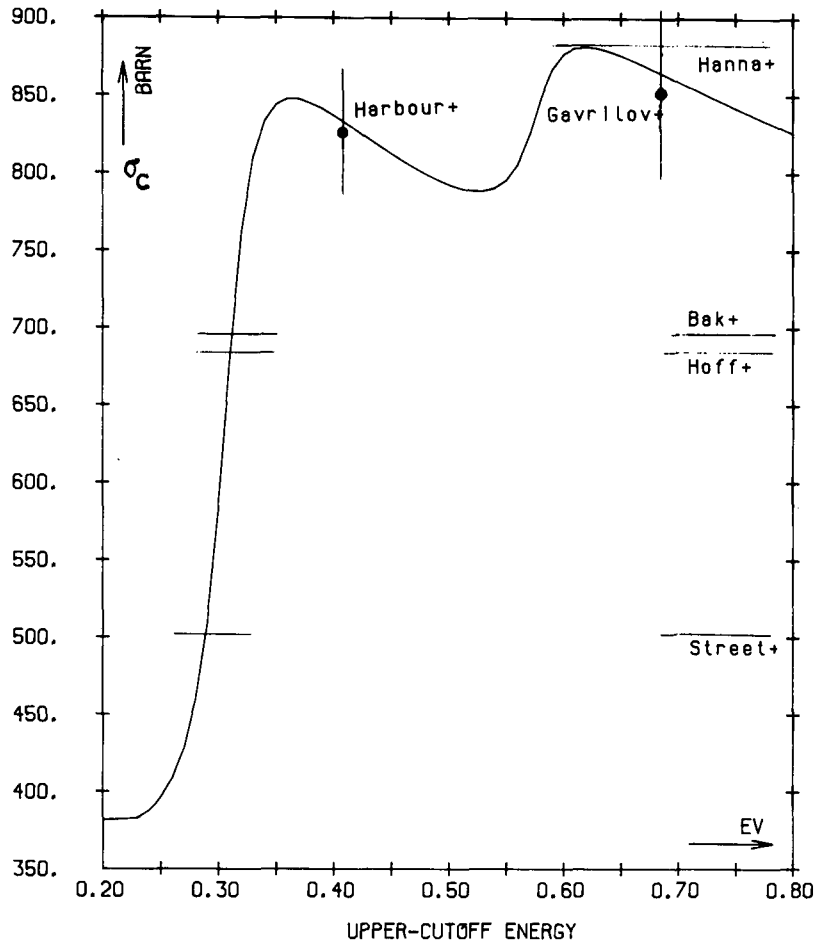

Fig. 1 Effective thermal cross section of ^{241}Am as a function of Cd cut-off energy. The indicated widely differing experimental values can be explained as corresponding to different Cd cut-off energies.

1.2 Comparative Study of Neutron Strength Functions for Actinides

F.H. Fröhner, U. Fischer, H. Jahn

(Relevant to request numbers: 671137, 691391, 692439, 692455, 741124, 753001, 753021, 762210)

Total cross sections data below about 100 keV are, apart from the quite narrow resolved-resonance region (E < 4 keV), surprisingly sparse for all actinides except ^{235}U. For theoretical prediction one needs the strength functions S_ℓ and distant-level parameters R'^{∞}_ℓ for s- and p-wave interaction (ℓ = 0 and 1) which must be obtained either from cross-section parameters determined in the resolved-resonance region or from optical model fits to average cross-section data above 100 keV.

In the first case one uses the expressions

$$S_\ell = \frac{1}{(2\ell+1)\Delta E} \sum_\lambda (g\Gamma_n^\ell)_\lambda \quad , \qquad R'_\ell = a_\ell (1-R^\infty_\ell) \quad , \qquad (1)\ (2)$$

where g is the spin factor, Γ_n^ℓ the reduced neutron width, R'_ℓ the potential scattering length, a_ℓ the R-matrix channel radius, and the sum extends over all resonances in an energy interval ΔE which are excited by the partial wave(s) with orbital angular momentum $\hbar\ell$.

Optical model fits yield essentially the complex scattering amplitudes $\bar{U}_\ell$ which, in order to reproduce average cross sections correctly, must be equal to the corresponding R-matrix collision functions averaged over resonances, i.e.

$$\bar{U}_\ell = e^{-2i\phi_\ell} \frac{1-\bar{R}_\ell L_\ell^{o*}}{1-\bar{R}_\ell L_\ell^o} \quad \text{with} \quad \bar{R}_\ell = R^\infty_\ell + i\frac{\pi S_\ell}{2k_1 a_\ell} \quad , \qquad (3)\ (4)$$

where ϕ_ℓ and L_ℓ^o are hard-sphere phase shift and logarithmic-derivative discontinuity at the channel radius a_ℓ, and $2\pi/k_1$ is the c.m.s. neutron wave length at 1 eV. Eqs. (3), (4) determine S_ℓ uniquely once a_ℓ is specified. Of course a_ℓ in Eqs. (2) and (4) and in the definition of Γ_n^ℓ for $\ell > 0$ must be the same in order to ensure consistency.

Both methods were employed to determine s-wave strength functions for a number of actinides. Resonance data were corrected for missing levels with the maximum-likelihood program STARA which simultaneously estimates strength functions and mean level spacings from observed neutron widths and resonance energies [1]. Optical-model results were obtained with the suitably modified code HAUSER-4 [2]. The spherical complex potential with surface absorption used by Wilmore and Hodgson [3] was slightly adjusted [4] so as to reproduce the average total and elastic-scattering cross sections available for ^{238}U between 50 keV and 10 MeV. The given mass and energy dependence of this potential was then utilized to extrapolate to other actinides and, for the comparison, to the resolved-resonance region below 4 keV.

Results are shown in Figs. 1 and 2 and in Table I. It is seen that in contrast to the smoothly varying optical-model strength functions those derived from resolved-resonance parameters fluctuate from nucleus to nucleus. The expected fluctuations due to the limited number of resonances per ΔE interval are covered by the stated uncertainties. Other possible sources of fluctuations not covered by the error bars include

- systematic errors in resonance measurements,
- systematic errors in resonance analysis,
- intermediate structure not averaged out in the rather narrow resolved-resonance ranges ($\Delta E < 4$ keV in all cases).

Furthermore, there is a systematic tendency of the S_o values derived from resonance data to be 10 - 30 % lower than those calculated from the optical potential. It is true that for one of the most carefully studied nuclei, ^{238}U, the most recent resonance data give reasonable agreement with the optical-model results, but for the also extensively studied nucleus ^{235}U there is quite a significant discrepancy. Coupled-channel calculations with a deformed potential do not seem to help much [5].

Cross section extrapolation from the resolved-resonance region upwards seems to be somewhat more uncertain, mainly because of intermediate structure effects, than extrapolation of good optical-model fits from above 100 keV downwards. The lack of measured total cross sections below 100 keV, properly corrected for sample thickness effects (resonance self-shielding), is embarrassing and should be remedied.

Table I. Comparison of strength functions derived from
- Resonance parameters (STARA Calculations)*)
- Average cross sections (HAUSER-4 Calculations)

Target nucleus	STARA Resonance parameters		No. of levels	ΔE (eV)	D_o (eV)	$10^4 S_o$	HAUSER-4 $10^4 S_o$
^{232}Th	Derrien	[6]	173	3010	16.9±.7	.89±.11	
^{233}Th	ENDF/B-IV		57	46	.55±.04	1.03±.17	
^{235}U	Moore+	[7]	196	100	.44±.02	.96±.10	1.34±.13
^{238}U	Keyworth+	[8]	191	4000	20.7±.3	1.18±.11	1.24±.12
^{239}Pu	KEDAK-3	[9]	257	665	2.25±.09	1.27±.11	
^{240}Pu	KEDAK-3	[9]	172	3000	13.1±.3	1.03±.11	1.20±.15
^{241}Pu	KEDAK-3	[10]	123	161	.89±.03	1.22±.15	
^{242}Pu	KEDAK-3	[11]	37	500	12.4±1.5	.84±.19	1.15±.15
^{241}Am	Derrien+	[12]	189	150	.58±.04	.93±.10	1.17±.15
^{242}Am	BNL 325	[13]	6	3.5	.21±.07	1.58±.53	
^{243}Am	BNL 325	[13]	219	90	.64±.08	.97±.10	
^{243}Cm	BNL 325	[13]	15	26	.50±.20	1.36±.30	
^{244}Cm	BNL 325	[13]	34	500	11.8±1.2	1.09±.25	1.14±.20

* STARA results for odd isotopes were calculated in the approximation that the strength functions are the same for both s-wave resonance sequences (J = I±1/2) and that the level densities are proportional to 2J+1

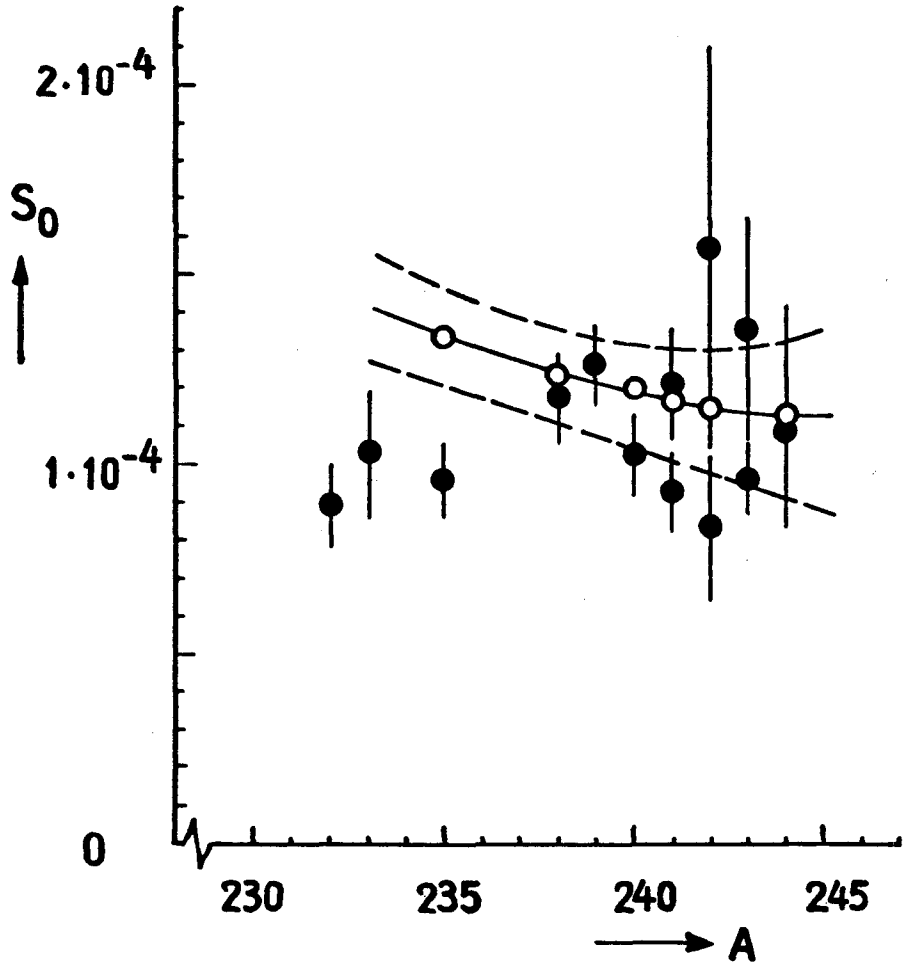

Fig. 1 Comparison of low-energy s-wave strength functions derived from resolved-resonance parameters (solid circles with error bars) and from a spherical optical potential that fits ^{238}U cross sections between roughly 50 keV and 10 MeV (open circles and curves indicating smooth behaviour and uncertainties).

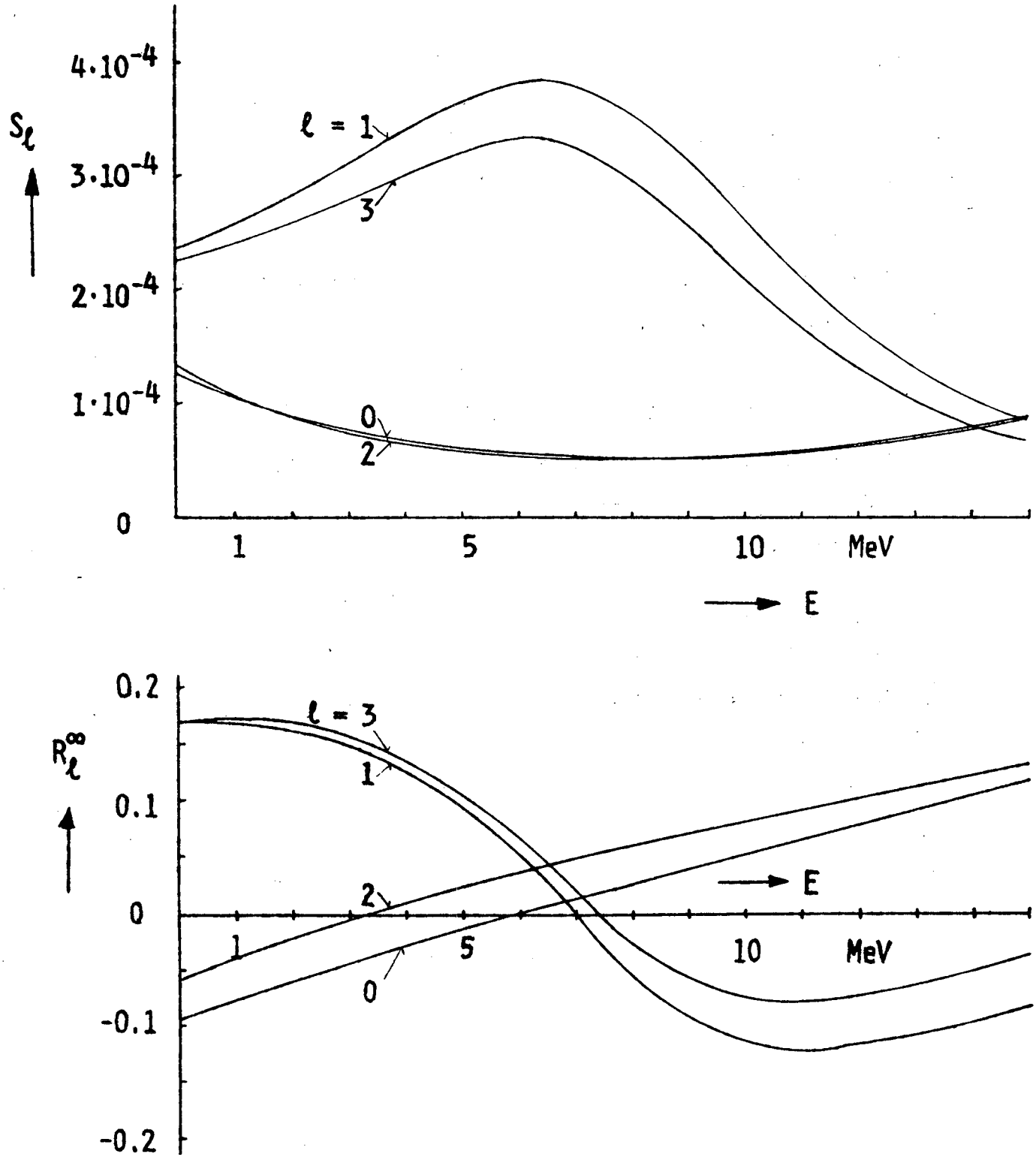

Fig. 2 Energy dependence of ^{238}U strength functions and distant-level parameters for ℓ = 0, 1, 2, 3 calculated with a spherical optical potential that fits ^{238}U cross sections between roughly 50 keV and 10 MeV.

References

[1] F.H. Fröhner, Report KfK-2669 (1978) p. 63-66

[2] F.M. Mann, Report HEDL-TME 76-80 (1976)

[3] P.E. Hodgson, D. Wilmore, Nucl. Phys. 55 (1964) 673

[4] U. Fischer, Diplomarbeit, Kernforschungszentrum Karlsruhe (1979)

[5] D.G. Madland, P.G. Young, Proc. Int. Conf. on Neutron Physics and Nuclear Data for Reactors and other Applied Purposes, Harwell (September 1978) p. 349

[6] H. Derrien, Report NEANDC(E) 163 U (1975) p. 73

[7] M.S. Moore, J.D. Moses, G.A. Keyworth, J.W.T. Dabbs, N.W. Hill, Phys. Rev. C18 (1978) 1328

[8] G.A. Keyworth, M.S. Moore, Proc. Int. Conf. on Neutron Physics and Nuclear Data for Reactors and other Applied Purposes, Harwell (September 1978) p. 241; see also G. de Saussure, D.K. Olsen, R.B. Perez, F.C. Difilippo, Report ORNL/TM-6152 (1978)

[9] B. Goel, F. Weller, Report KfK-2386/III (1977)

[10] M. Caner, S. Yiftah, Report IA-1276 (1973)

[11] M. Caner, S. Yiftah, Report IA-1275 (1973)

[12] H. Derrien, B. Lucas, Proc. Conf. Nuclear Cross Sections and Technology, NBS Special Publication 425, Washington, D.C. (March 1975) p. 637; see also L.W. Weston, J.H. Todd, Nucl. Sci. Eng. 61 (1976) 356

[13] S.F. Mughabghab, D.I. Garber, Report BNL 325, 3rd ed., vol. I (1973)

1.3 Absolute Values of Inelastic Neutron Scattering Cross Sections Calculated with Account of the Pre-equilibrium Mechanism

H. Jahn

Absolute values of secondary-energy-dependent inelastic neutron scattering cross sections can be calculated either with the master equation pre-equilibrium formalism of Cline and Blann or with Blann's more recent geometry-dependent hybrid model. The master equation formalism was used at Dubna and Dresden to reproduce experimental results for 14 MeV incident energy. The geometry-dependent hybrid model was used at Karlsruhe to cover for a number of materials the whole range from 5 to 14 MeV incident energy and to reproduce smoothed experimental spectra at 7.45 and 14 MeV. Only the geometry-dependent hybrid model accounts for scattering in the diffuse nuclear surface and thus for a certain average over the direct interaction. It is also free of any fit parameters other than those of the usual optical model. The master equation calculations, on the other hand, are based on nucleon-nucleon scattering cross sections inserted into the high-energy approximation of Kikuchi and Kawai for the intranuclear transition rate. Other approaches require either mass- or energy-dependent or more global fit parameters for a satisfactory reproduction of experimental results but a genuine prediction of the incident-energy dependence of the inelastic neutron cross section, especially below 14 MeV, is needed for transport and shielding calculations, for instance in connection with fusion reactor design studies. A review on this subject was prepared for the Winter Course on Nuclear Physics and Reactors, Part I: Course on Nuclear Theory for Applications, 17.1.-10.2.78, held at the International Centre for Theoretical Physics, Trieste, Italy.

1.4 Inelastic Neutron Scattering Calculations including the Pre-equilibrium and Direct Components using Optical Model Fit Parameters only

H. Jahn

Calculations of direct inelastic scattering cross sections by standard methods such as DWBA or coupled channels usually require knowledge of special spectral properties of the target nuclei. We find indications [1] that the secondary-energy average of the angle-integrated direct inelastic

scattering cross section depends only on general nuclear matter properties of the target nuclei such as quantities of the optical model. This is concluded from the fact that the high-energy tail of the angle-integrated secondary-energy averaged inelastic scattering cross section is roughly reproduced by calculations with Blann's geometry-dependent hybrid model as well as by averaged DWBA calculations. Since Blann's geometry-dependent hybrid model depends only on global parameters such as proton and neutron numbers and quantities of the optical model, the same global behaviour is thus also expected for the average DWBA results. The problem of a general derivation of the corresponding global average direct reaction component is discussed. It should be embedded in a formalism which is more closely related to the usual statistical reaction theory than the semiclassical geometry-dependent hybrid model. A formula for the angle-integrated average inelastic nucleon scattering cross section following from this formalism was presented in [1].

Reference

[1] H. Jahn, Proceedings of the International Conference on Neutron Physics and Nuclear Data for Reactors and other Applied Purposes, Harwell (September 1978) p. 502

1.5 Review of Applied Neutron Resonance Theory

F.H. Fröhner

A fairly comprehensive review on utilisation of resonance theory in basic and applications-oriented neutron cross-section work was prepared [1]. The practically important resonance formalisms, principal concepts and methods as well as representative computer programs for extraction of resonance parameters from measured data, evaluation of resonance data, calculation of Doppler-broadened cross sections and estimation of level-statistical quantities from resonance parameters are described in the review.

Reference

[1] F.H. Fröhner, Report KfK-2669; see also Winter Courses on Nuclear Physics and Reactors, Part I, Trieste 1978 (to be published by IAEA)

INSTITUT FÜR CHEMIE (1): NUKLEARCHEMIE
KERNFORSCHUNGSANLAGE JÜLICH

1. Neutron Data

1.1 Investigation of (n,^{3}He) Reactions

S.M. Qaim, G. Stöcklin, R. Wölfle, C.H. Wu

In continuation of earlier radiochemical studies on fast-neutron induced trinucleon emission reactions [1], (n,^{3}He) cross sections were measured at 14.6 MeV for several target nuclei and the systematics of cross sections were established [2]. The results are shown in Fig. 1.

Measurements of (n,^{3}He) cross sections were also carried out for neutrons produced via break-up of 53 MeV deuterons on a Be target (E_n = 4-50 MeV; I_{max} at 22.5 MeV; FWHM = 15.8 MeV). In addition to the radiochemical measurements, dynamic quadrupole mass spectrometric technique was also applied. The ratios of ^{3}He to ^{4}He emission cross sections, obtained using both the techniques, are shown in Fig. 2 as a function of proton number (Z) of the target element. The identity of the ^{3}He/^{4}He ratios, obtained by the activation and mass spectrometric methods, suggests that the contribution of the processes like (n,2pn) and (n,n'2p), which lead to the same activation product as the (n,^{3}He) reaction, is small. This observation leads to the conclusion that over the energy region considered the emission of a bound ^{3}He-particle is favoured over that of three single nucleons (2pn).

1.2 Cross-Section Measurements on Hydrogen and Helium Producing Reactions

S.M. Qaim, G. Stöcklin, R. Wölfle
(Relevant to request numbers: 692135, 692136, 692137, 692291, 693030, 741299)

Following the recommendation of the 1977 Specialist Meeting in Geel, we measured cross sections by the activation technique using specific

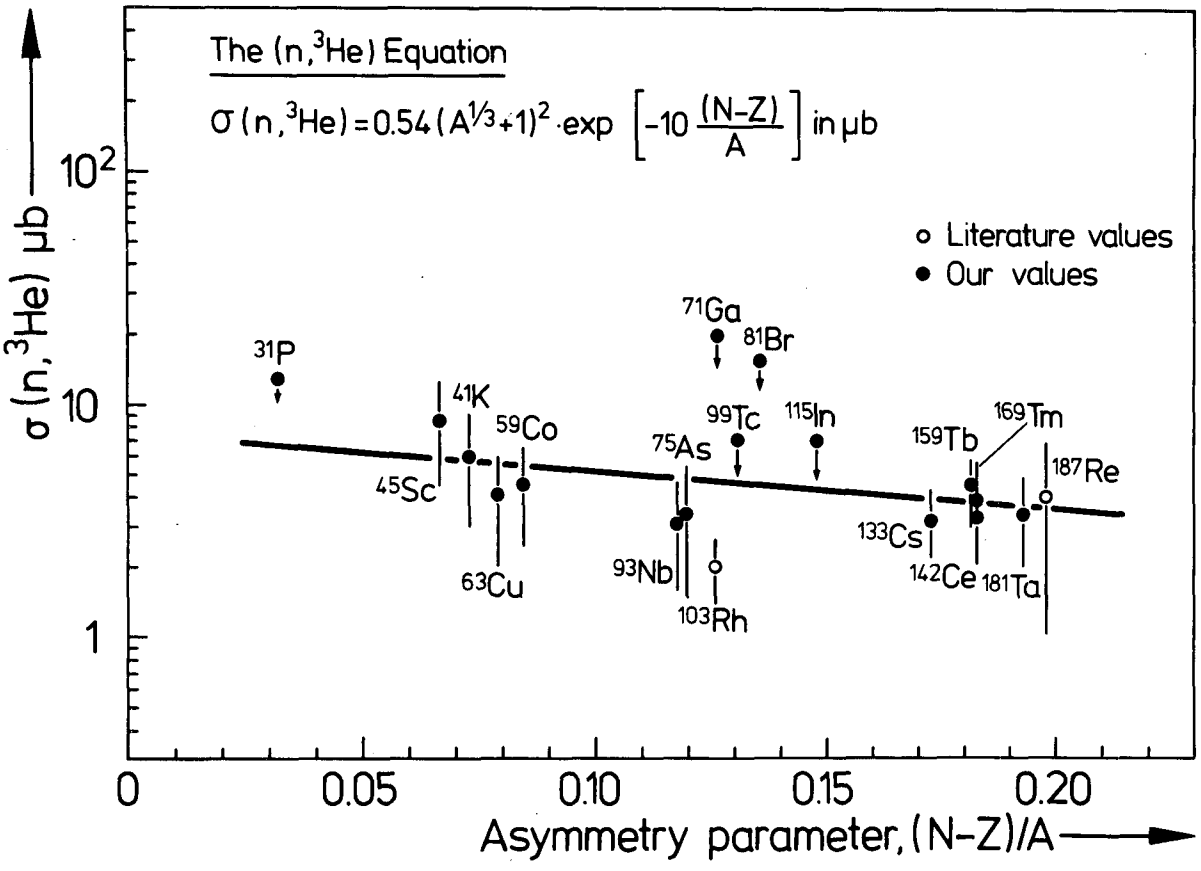

Fig. 1 (n,^{3}He) reaction cross sections at 14.6 ± 0.4 MeV for medium and heavy mass elements as a function of the asymmetry parameter (N-Z)/A of the target nucleus.

radiochemical separations and high-precision counting methods for the relatively less known hydrogen and helium producing reactions $^{50}Cr(n,n'p)^{49}V$, $^{58}Ni(n,n'p)^{57}Co$, $^{58}Ni(n,\alpha)^{55}Fe$ and $^{62}Ni(n,\alpha)^{59}Fe$ induced by fission neutron spectrum.

Several (n,p) and (n,α) reaction cross sections were measured for 14.7 MeV neutrons, especially in the region of rare earths, where the technique of high pressure liquid chromatography (HPLC) was extensively applied for the separation of the reaction products from the bulk of the target material.

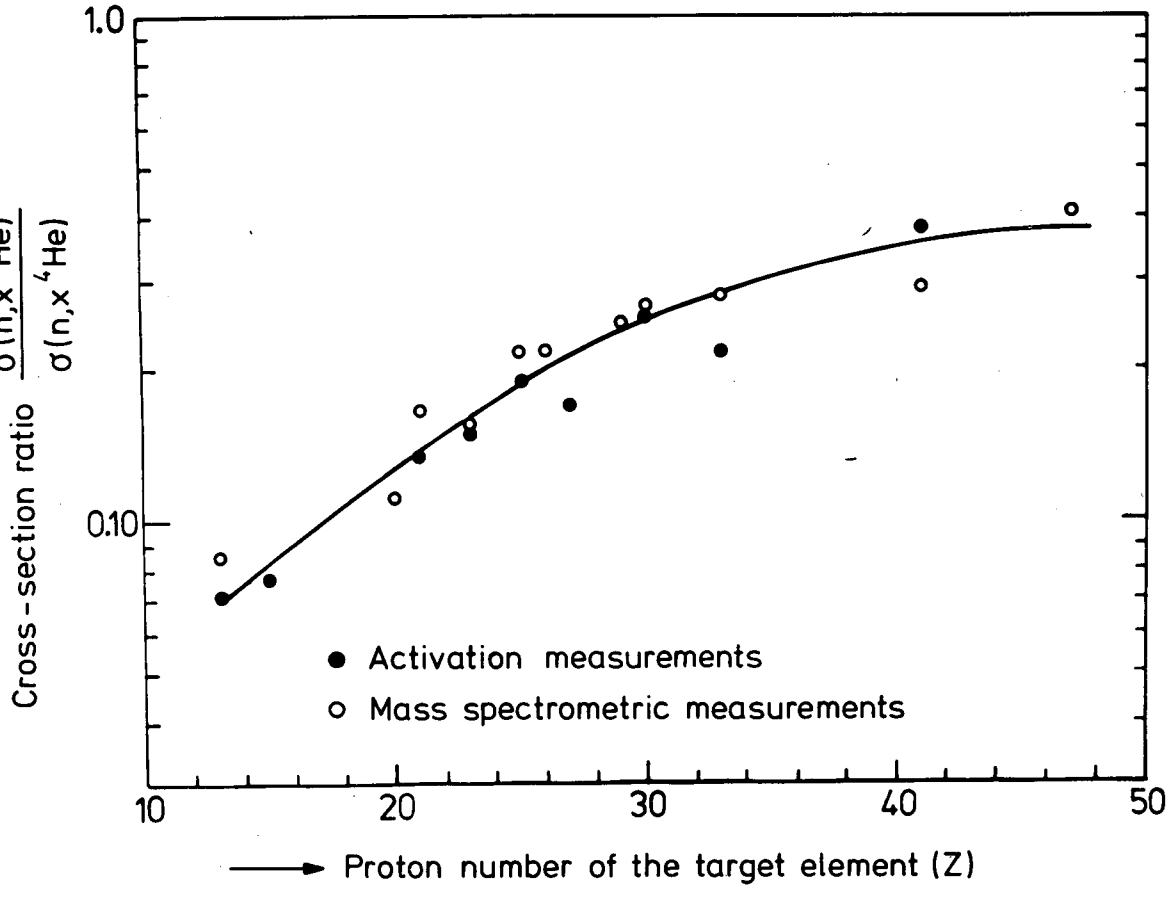

Fig. 2 ^{3}He to ^{4}He emission cross-section ratios as a function of Z of the target element.

A new system for producing neutrons from a 30 MeV d/Be target was constructed and integral cross-section measurements on FRT-related structural materials were initiated.

1.3 Evaluation, Systematics and Review of Fast Neutron Induced Reaction Cross-Section Data

S.M. Qaim

Extensive Hauser-Feshbach calculations using a global set of optical model parameters showed that the cross sections of 14.6 MeV neutron

induced (n,p) and (n,α) reactions on target nuclei with A = 27 to 50 are well described by the statistical model. In the case of rare trinucleon emission reactions, i.e. (n,t) and (n,^{3}He), the agreement is not so good. Whereas the (n,t) reaction on target nuclei in the (2s,1d)-shell is described by the statistical model, in heavier nuclei considerable contribution from direct processes appears to be present. The contribution of non-statistical processes appears to be appreciable in the case of (n,^{3}He) reactions as well.

The gross trend in the (n,^{3}He) cross sections at 14.6 MeV was analysed [2]. It was found that the (n,^{3}He) cross section can be described by the following formulation:

$$\sigma(n,^3He) = 0.54(A^{1/3} + 1)^2 \exp[-10(N-Z)/A]\mu b.$$

A survey of the recent advances in the study of neutron threshold reactions was carried out and presented at the Harwell Conference [3]. Similarly the nuclear data needs for radiation damage studies relevant to fusion reactor technology were critically reviewed and presented at the IAEA-Advisory Group Meeting held in Vienna [4].

2. Charged Particle Data for Radioisotope Production

2.1 Cross-Section Data for the Production of Organic Radioisotopes

Z.B. Alfassi, S.M. Qaim, G. Stöcklin, R. Weinreich

Measurements of cross sections of nuclear reactions potentially useful for the production of short-lived organic radioisotopes were continued. In view of the increasing importance of positron coincidence tomography in nuclear medical in-vivo diagnostics, emphasis was placed on the development of methods for the production of short-lived β^+ emitters. Thus, cross section information for the production of 2.5 min ^{30}P was completed [5]. For the production of ^{74m}Br ($T_{1/2}$ = 42 min) and ^{75}Br ($T_{1/2}$ = 1.6 h) excitation functions of ^{3}He-induced reactions on ^{75}As

were measured over the energy range of 20 to 100 MeV. Radiation dose considerations show that ^{75}Br is potentially a very useful radioisotope and the reaction $^{75}As(^{3}He,3n)^{75}Br$ is very suitable for its production at medical compact cyclotrons.

2.2 Excitation Functions for the Production of Inorganic Radioisotopes

S.M. Qaim, R. Weinreich

Cross-section measurements for the production of ^{201}Tl and ^{203}Pb, reported in the last Progress Report, were completed and the optimum conditions for the routine production worked out [6].

2.3 Cross Sections for the Production of Rare Gases

J. Knieper, R. Weinreich

Excitation functions for the production of $^{77,79}Kr$ via $^{79,81}Br(p,xn)^{77,79}Kr$ were determined over the proton energy range up to 45 MeV. It is possible to produce enough quantities of ^{79}Kr for medical and industrial applications.

2.4 Survey of Charged Particle Data for Radioisotope Production

S.M. Qaim, G. Stöcklin, R. Weinreich

A survey of the status of available cross-section data for radioisotope production was carried out and presented at the Oxford Symposium [7]. Similarly a critical review on the data needs was presented at the Harwell Conference [8].

References

[1] S.M. Qaim, R. Wölfle, Triton emission in the interactions of fast neutrons with nuclei, Nucl.Phys. A295 (1978) 150

[2] S.M. Qaim, A systematic investigation of (n,^{3}He) reactions at 14.6 MeV and an analysis of the gross trend in the cross-section data, Radiochimica Acta 25 (1978) 13

[3] S.M. Qaim, Recent advances in the study of some neutron threshold reactions, Proc.Int.Conf. on Neutron Physics and Nuclear Data for Reactors and other Applied Purposes, Harwell (September 1978) p. 1088

[4] S.M. Qaim, Nuclear data needs for radiation damage studies relevant to fusion reactor technology, Proc. IAEA-Advisory Group Meeting on Nuclear Data for Fusion Reactor Technology, Vienna (December 1978), in press

[5] S.M. Sahakundu, S.M. Qaim, G. Stöcklin, Cyclotron production of short-lived ^{30}P, Int.J.appl.Radiat.Isotopes 30 (1979) 3

[6] S.M. Qaim, R. Weinreich, H. Ollig, Production of ^{201}Tl and ^{203}Pb via proton induced nuclear reactions on natural thallium, Int. J.appl.Radiat.Isotopes 30 (1979) 85

[7] S.M. Qaim, R. Weinreich, Nuclear data for the production of medically useful radioisotopes, Review paper presented at the 2nd Int.Symp. on Radiopharmaceutical Chemistry, Oxford (July 1978)

[8] G. Stöcklin, S.M. Qaim, Recent trends in nuclear reaction data needs for nuclear medicine, Proc.Int.Conf. on Neutron Physics and Nuclear Data for Reactors and other Applied Purposes, Harwell (September 1978) p. 667

INSTITUT FÜR KERNPHYSIK: EXPERIMENTELLE KERNPHYSIK II
KERNFORSCHUNGSANLAGE JÜLICH

1. Slow Neutron Induced Nuclear Reactions

1.1 Cross Section of the Reaction $^{16}O(n,\gamma)^{17}O$

N. Wüst, H. Seyfarth, L. Aldea

Due to the use of a H_2O target ($\sim$1 cm in length, $\sim$ 1 cm in diameter) the investigation of two-quantum radiative thermal neutron capture in ^{1}H [1] has allowed to determine at the same time the cross section of the reaction $^{16}O(n,\gamma)^{17}O$. At an external Bi-filtered slow neutron beam [2] of the research reactor DIDO γ-γ coincidence data have been recorded using two NaI(Tl) detectors and a two-dimensional data acquisition system [2]. Absolute coincidence efficiencies have been determined with calibrated radioactive sources at the target position. With normalization to the single-photon capture cross section of ^{1}H ((334.2 $\pm$ 0.5) mb [3]) the partial cross section of the 1088 - 2184 - 871 keV γ cascade has been determined as (153 $\pm$ 6) μb. With the known branching ratio of (82 $\pm$ 3) % [4] for this cascade the total capture cross section of the reaction $^{16}O(n,\gamma)^{17}O$ results as (187 $\pm$ 10) μb which has to be compared with earlier values of (178 $\pm$ 25) μb [5] and (202 $\pm$ 27) μb [4].

1.2 Partial Cross Sections of the Reactions $^{123}Te(n,\alpha)^{120}Sn$, $^{143}Nd(n,\alpha)^{140}Ce$, $^{123}Te(n,\gamma\alpha)^{120}Sn$, and $^{143}Nd(n,\gamma\alpha)^{140}Ce$

L. Aldea, H. Seyfarth, N. Wüst

Metallic targets (310 $\mu g/cm^2$ enriched to 70 % in ^{123}Te and 85 $\mu g/cm^2$ enriched to 88 % in ^{143}Nd) have been exposed to an external Bi-filtered slow neutron beam [2] of the research reactor DIDO. The α-particle spectra have been recorded with silicon surface-barrier detectors (100 or 200 mm^2 surface and 100 μm thickness) positioned near to the target. Details of the investigations are found in ref. [6]. Preliminary results have been presented elsewhere [7,8]. The resulting partial cross sections [6] for the single-step reactions $^{123}Te(n,\alpha)^{120}Sn$ and $^{143}Nd(n,\alpha)^{140}Ce$ with α transitions from the capture states in $^{144}Nd(I^{\pi} = 3^{-}$, attributed to bound state at -6 eV [9]) and in $^{124}Te(I^{\pi} = 0^{+}$, attributed to postulated bound state [6] to the ground state and excited states in ^{120}Sn and ^{140}Ce are collected in Table I. From the observed α spectra the $(n,\gamma\alpha)$ cross sections for α-particle energies between those of the α_0 and α_1

Table I. Partial cross sections of the reactions $^{123}Te(n,\alpha)^{120}Sn$ and $^{143}Nd(n,\alpha)^{140}Ce$ from the present work

		E_{ex} [a] (keV)	I^{π}_{final} [a]	E_{α} (keV)	σ (μb)
$^{123}Te(n,\alpha)^{120}Sn$	α_0	0	0^+	7334.5 [b]	53 ± 5
	α_1	1171.5	2^+	6201.3 [b]	12 ± 5
$^{143}Nd(n,\alpha)^{140}Ce$	α_0	0	0^+	9449.1±0.1 [b]	21280 ± 180 [c]
	α_1	1596.5	2^+	7897.4±1.7	91.4± 3.0
	α_2	1903.3	0^+	7598.7±0.5 [b]	185.2± 4.0
	α_3	2083.5	(4^+)	7424 ±2	36.8± 2.0
	α_4	2348.2	2^+	7162 ±3	41.5± 4.0
	α_5	2350.1	$4^+,5^+$		
	α_6	2412.3	3^+	7103 ±3	31.2± 3.0
	α_7	2464.3	3^-	7051 ±3	22.8± 3.0
	α_8	2516.1	$3^+,4^+$	7003 ±4	21.2± 3.0
	α_9	2547.5	$1^+,2^+$	6963 ±6	12.8± 4.0

a) Excitation energies and spin/parity values of ^{120}Sn and ^{140}Ce from refs. [10] and [11], respectively.

b) α energy calculated from Q values, used for energy calibration.

c) for normalization taken from ref. [12]

transitions (Table I) in the (n,α) reactions have been deduced [6] for the two-step reactions $^{143}Nd(n,\gamma\alpha)^{140}Ce$ and $^{123}Te(n,\gamma\alpha)^{120}Sn$ as (768 ± 14) μb and (9 ± 5) μb, respectively.

References

[1] N. Wüst, H. Seyfarth, L. Aldea, Phys. Rev. C, in press

[2] W. Delang, P. Göttel, H. Seyfarth, Nucl. Instr. Meth. 99 (1972) 13

[3] A.F. Cox, S.A.R. Wynchank, C.H. Collie, Nucl. Phys. 74 (1965) 497

[4] A.B. McDonald, E.D. Earle, M.A. Lone, F.C. Khanna, H.C. Lee, Nucl. Phys. A281 (1977) 325

[5] E.T. Jurney, H.R. Motz, Proc. of the International Conference on Nuclear Physics with Reactor Neutrons, edited by F.E. Throw (Report ANL-6797, Argonne, Illinois, 1963) p. 236

[6] L. Aldea, Ph. D. Thesis, Universität zu Köln (1979)

[7] L. Aldea, B. Kardon, O.W.B. Schult, H. Seyfarth, N. Wüst, Z. Physik A283 (1977) 391

[8] L. Aldea, H. Seyfarth, Proc. 3rd Int. Symp. on Neutron Gamma-Ray Spectroscopy and Related Topics, Brookhaven (September 1978), in press

[9] S. Mughabghab, D.I. Garber, BNL-325, 3rd Edition Vol. 1 (1973)

[10] Nuclear Data Sheets 17 (1976) 39

[11] Nuclear Data Sheets 12 (1974) 343

[12] N.S. Oakey, R.D. Macfarlane, Phys. Lett. 26B (1968) 662

ZENTRALABTEILUNG FÜR CHEMISCHE ANALYSEN
KERNFORSCHUNGSANLAGE JÜLICH

Gamma-Ray Data Compilations for Applied Gamma-Ray Spectrometry

G. Erdtmann, W. Soyka

With respect to the requirements of applied gamma ray spectrometry, data on gamma rays from radioactive decay have been collected, evaluated and compiled. This compilation should enable an easy identification of radionuclides from gamma ray spectra. Usually the following data are necessary to ascribe a certain line found in a gamma spectrum to a certain radionuclide:

- energy and intensity of a gamma ray transition
- energies and intensities of other gamma lines emitted by this radionuclide
- the half-life of this radionuclide
- daughter nuclides and their gamma transitions, if present
- long-lived parent nuclides, if present
- modes of production or natural abundance of the nuclides

These data have to be clearly arranged in printed tables or they should be stored on a magnetic tape or some other computer accessible data store if computer aided evaluation of gamma ray spectra has to be carried out. The gamma ray data compilation "GAMDAT'78" contains this information for all the radionuclides. It is stored on magnetic tape and copies of this tape can be made available to possible users [1] . From this data set printed tables have been prepared [2] . The computer accessible data set as well as the book will be shortly introduced here.

1. GAMDAT'78

1.1 Description of the Information Stored

This data compilation is based on an older one, which had been edited in 1973 [3] . Since that time, all data have been revised and corrected, completed and updated where necessary. Thus, about 80% of the data contained in GAMDAT'78 are new. They are stored on computer compatible magnetic tape.

The data file consists of 2055 data sets, one for each radionuclide. The data sets are composed of two records containing general information on each nuclide and a number of records containing the gamma-ray data. This number corresponds to the number of gamma lines of the radionuclide concerned. Each record has a length of 100 bytes; they are arranged in blocks of 4000 bytes, so that the tape my be handled also with small computers. The information contained in the data set for each nuclide may be seen from a section of the printout of GAMDAT'78.(see Fig.1)

In field 1 the nuclide is given.

Isomeric nuclides are marked by M or N, where N means the m2-state. If the mesomeric sequence of two isomers is unknown, letters A and B are used to distinguish them.

In field 2 the half-life is given.

In field 3 the daughter nuclides are listed.

They are included since their gamma ray lines often are used to support the identification of radionuclides. If more than three daughters exist, the most important ones are selected since in this field space is available only for three nuclide symbols. With very long or branched decay chains having no especially important members we have written "COMPLX" in this space. If mesomeric states occur in the decay scheme they are usually listed, provided their half-lives are longer than 1/10 s. The fission products from nuclides with spontaneous fission such as ^{252}Cf

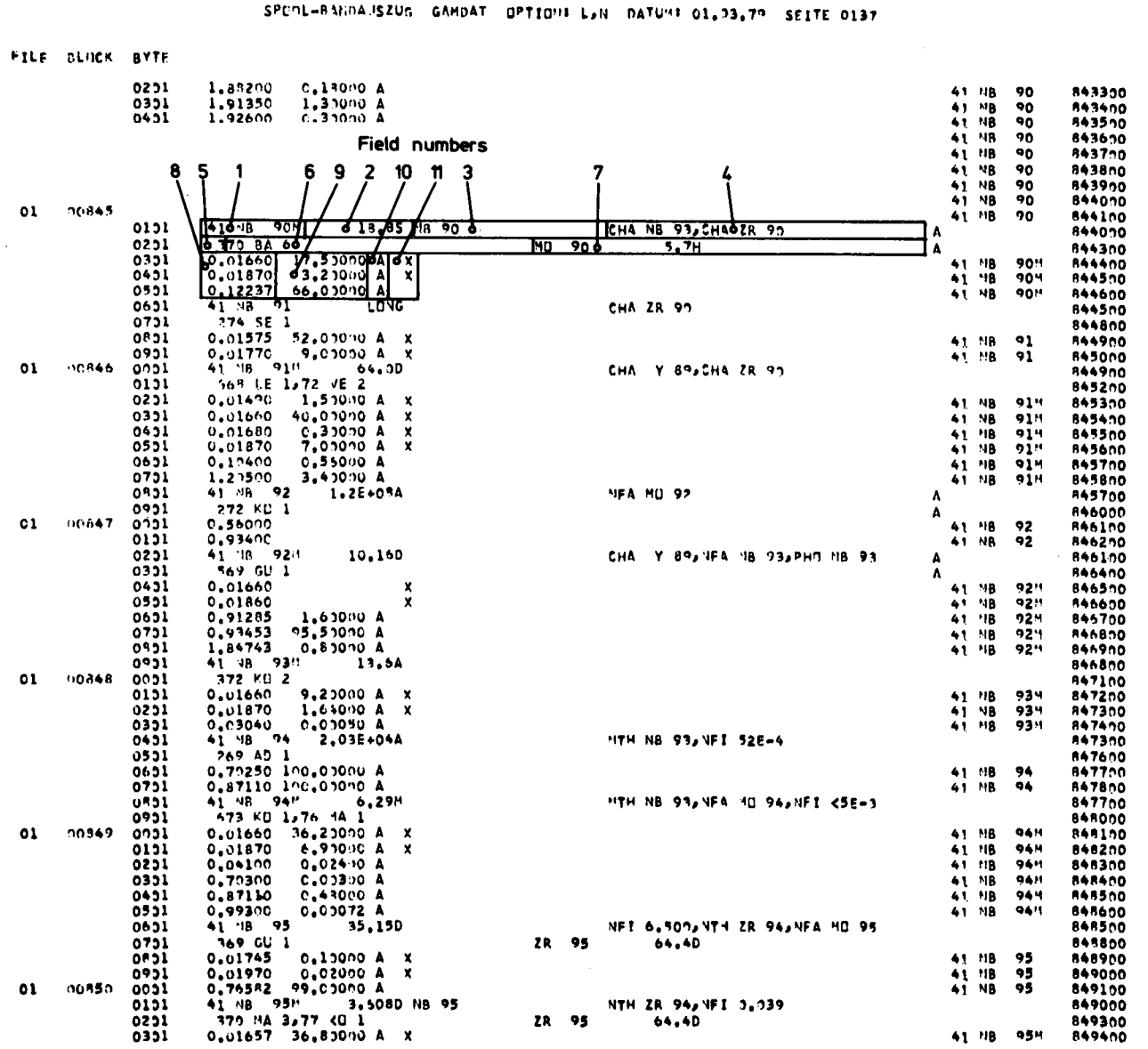

Fig. 1 A section of the printout of "GAMDAT '78".

may also be understood as daughter nuclides. Accordingly, this type of decay is indicated by the symbol "SFI" and its abundance per 100 decays is given.

In field 4 the possible origin of the radionuclide may be seen.

Naturally occurring nuclides are marked by the symbol NAT and the value of its isotopic abundance. Nuclides available by irradiation with thermal neutrons are marked by NTH and the symbol of the stable nuclide from which it is produced. Accordingly NFA stands for production by fast neutrons, CHA for irradiation with all types of charged particles from protons to heavy ions, and PHO means high energy photons, usually bremsstrahlung from electron accelerators. NFI indicates fission products. It is followed by the value for its cumulative yield for thermal neutron fission of ^{235}U, which could be taken or calculated from refs. [4-7] . From consideration of space only three generating reactions could be listed.

In field 5 the total number of gamma- and X-ray lines observed in the spectrum is given.

In field 6 up to four references used for the compilation of the nuclide data set are listed.
A list with the bibliographic data is not contained in "GAMDAT'78" but may be found in ref. [2] .

In this field instead of references occasionally certain additional remarks have been made.

"No GAMMA LINES" means that the nuclide decays by pure alpha- or beta-emission or by pure electron capture. It may also mean that the gamma-rays have not yet been investigated.

"GAMMA LINES?" means that gamma-lines are expected but have not yet been detected.

"INCL.LINES OF..." means that the gamma-lines of a short-lived daughter or another inseparable nuclide are included in the list of gamma-lines.

"LINES SEE..." means that the gamma-lines of this nuclide cannot be clearly separated from that of a parent, daughter or isomeric nuclide. They are included therefore in the list of the nuclide cited.
"FURTHER LINES SEE..." means that only the lines listed can be clearly separated from those of a parent, daughter or mesomeric nuclide. Additional lines, which cannot be clearly ascribed to one of the inseparable nuclides or whose contribution to a line occurring in both decay schemes cannot be determined, are included in the list of the other nuclide.
"LINES OF ..." means that all lines belong to the decay of the daughter nuclide indicated.
"NOT EXT" plus reference means that this nuclide does not exist. Although described in earlier papers, the authors of the references cited refuted these findings.
"EXIST.DOUBTFUL" means that the existence of this nuclide is not unequivocally proven.

In field 7 data on long-lived parent nuclides are presented.

Their knowledge will also be important for the analysis of gamma-ray spectra. In an old mixture of radionuclides the presence of short-lived nuclides is usually not to be expected, though they may still be present if they have long-lived precursors. For this reason one must check for long-lived parent substances when in the gamma-ray spectra of materials with long cooling periods short-lived radionuclides are detected. To facilitate rapid recognition of such cases, precursors with half-lives longer than that of the actual nuclides are presented with their symbol and half-life.

All the subsequent fields contain data on gamma- and X-ray lines. The latter ones are produced by internal conversion or electron capture processes during radioactive decay and can usually be seen in gamma-ray spectra, particularly if "low energy photon detectors", Ge(Li)-, Si(Li)- or pure Ge-detectors with an extremely good resolution in the region below 100 keV, are used. For the identification and measurement of radionuclides X-ray lines

can be used just as well as gamma-ray lines. Therefore they are included in the table. However, with a few exceptions, only the K X-rays above 20 keV are given.

The list of gamma-ray lines for each nuclide is as complete as possible. Doublets, as far as they can be resolved, e.g. by coincidence measurements, are listed as separate lines. Otherwise they are indicated by D in field 11. Also included are internal transitions presently known only from conversion electron measurement. Furthermore, the list of lines contains the "escape peaks", which are produced from gamma rays with energies higher than 1022 keV by pair production processes in the gamma detector followed by the escape of one or both the annihilation quanta.

In field 8 are given the gamma ray or X-ray energies and in field 9 the gamma ray or X-ray intensities.

As far as possible absolute intensities have been calculated, i.e. the number of gamma or X-ray photons emitted per hundred decay events of the radionuclide concerned. This absolute intensity values are necessary if the absolute activities of the radionuclides found in the gamma spectrum have to be calculated. If by no means a normalisation factor could be calculated, relative intensities are given in field 9. Here, the intensity of the most intense line, is set to 100 and all others are related to this line. All intensities are photon abundances, not transition probabilities. Details on the calculation of the intensities are given in refs. [2] and [3].
If no intensity data are found, field 9 is empty. If an escape peak is concerned it contains the text "PAIR PEAK".

In field 1o A means absolute and R means relative intensity.

In field 11 "D" means doublet, "C" complex, "X" X-ray and "W" weak line. "?" means that the existence of the gamma line is not ensured and "<" means that the intensity value is an upper limit.

1.2 Format of the Data File and Hints to its Handling

The data set is a non-labelled file and stored on a 9-track, 1600 BPI magnetic tape. It is coded in EBCDIC and built up from more than 50000 records. Each logical record has a length of 100 bytes and a block size of 4000 bytes.

The data set has been compiled on an IBM computer 370/168 of the Central Institute of Mathematics of the KFA Jülich. However, the data control parameters are so defined that it is possible to process this file also on small computers.

The whole data set consists of the data sets of 2055 nuclides which are arranged in order of increasing atomic number and, within each atomic number, in order of increasing mass number. Each nuclide data set consists of three different types of records with a length of 100 bytes each. Type 1 and 2 records contain general information on the radionuclide whereas type 3 records contain the gamma and X-ray data, as described in the section above.

This tape may be obtained from the KFA Jülich [1] . Modified copies with the following track numbers and densities may be delivered on special request:

1. 7-track, 200 BPI (DEN=0)
2. 7-track, 556 BPI (DEN=1)
3. 7-track, 800 BPI (DEN=2)
4. 9-track, 800 BPI (DEN=2)
5. 9-track, 6250 BPI (DEN=4)

Users may also be provided with original tape print-outs (ca. 420 pages) on paper or on microfilm.

The tape can be handled on very different computers using appropriate programs, e.g. in PL/1 or in FORTRAN. Useful programs are described and detailed information on the tape is given in a booklet [8] which is delivered with each copy of the tape.

Since for many applications the total amount of data is too large, excerpts may be easily prepared according to different aspects

by simple retrieval procedures , e.g., if fission products have to be investigated, sorting out all nuclides containing "NFI" in field 4 will yield a data set of only the fission products. Accordingly "NAT" will select all natural isotopes and so on. Further reduction may be done by discrimination against short or long half-lives, or against gamma lines with low intensities. Also mass or atomic numbers can be used for selection of specific data sets.

1.3 Applications of the Magnetic Tape

Most of the users need the tape for the evaluation of gamma ray spectra. The data set or, more often, special reduced excerpts and the data from the gamma spectrum measured are stored in a computer. The lines found are compared with those of the gamma ray table with respect to energy and intensity. If conformity is found, the relevant radionuclides are stored for a "first choice"-list. Looking for further criteria, such as other lines and their relative intensities, half-lives and generating reactions leads to the identification of the radionuclides present in the sample. Additionally, in most of the cases the absolute decay rates are calculated, which can be done if the gamma ray spectrometer is calibrated for peak counting efficiency, and decay corrections are carried out.

Another group of users needs the tape to calculate gamma ray dose rates of radionuclides or mixtures of them. These dose rates depend on the gamma ray energy and intensity and both of these values may be found in this file. Dose rates are needed, e.g. for medical applications of radionuclides or for industrial applications. Their knowledge is also necessary for the construction of shieldings for radioactive materials and installations.

2. The Printed Gamma Ray Table

For many purposes the use of the data file by a computer is inconvenient, complicated or, where no computer is accessible, impossible. Therefore a printed version of these tables has been prepared [2] .

```
 0.99200   0.09412 A
 1.00450   0.09774 A
 1.06050   0.27150 A
 1.12700   2.17200 A
 1.24250   0.24620 A
 1.25900   1.26700 A
 1.30300   0.32580 A
 1.33230   1.26700 A
 1.37750   0.07240 A
 1.41200   0.01810 A
 1.44770   0.39820 A
 1.46480   0.90500 A
 1.51140   1.99100 A
 1.58080   0.54300 A
 1.62720   3.62000 A
 1.64120   0.20270 A
 1.83340   3.36700 A
 1.94800   0.06878 A
 2.10110   0.61540 A
 2.12820   0.57920 A
 2.13200   0.13390 A
 2.22100   0.18820 A
 2.27900   0.03620 A
 2.29700   0.11580 A
 2.38860   0.05430 A
 2.57230   2.75100 A
 2.61210   0.30770 A
 2.71400   0.03620 A
 2.73000   0.06878 A
 2.74000   0.02896 A
 2.75350   0.47060 A
 2.88960   0.20630 A
 2.92580   0.18820 A
 2.96010   1.81000 A
 2.98100   0.04706 A
 3.01620   0.21720 A
 3.09270   3.14900 A
 3.14120   0.02172 A
 3.28090   0.03620 A
 3.46690   0.04344 A
 3.51270   0.06516 A
 3.53100   0.03258 A
 3.53400   0.01810 A
 3.55720   0.05430 A
 3.57580   0.20270 A
 3.83700   0.06516 A
 3.90700   0.00905 A
 3.93100   0.00362 A
 3.94800   0.00543 A
 3.96550   0.01086 A

 41 NB  89M
HALF LIFE:          1.1H
GEN: CHA    BR
DAU:
PAR:
REF: 75 KO 2

 0.01660   9.50000 A  X
 0.01860   1.70000 A  X
 0.50740  85.00000 A
 0.51100 163.80000 A
 0.58800 100.00000 A
 0.65030   0.80000 A

 0.76960   6.50000 A
 1.27750   1.60000 A

 41 NB  90
HALF LIFE:          14.6H
GEN: CHA ZR 90
     PHO MO 92
DAU: ZR 90M
PAR:
REF: 75 KO 3,71 ZA 1,
     70 TU 2,68 PE 1

 0.01580  55.00000 A  X
 0.01780  10.00000 A  X
 0.13260   4.40000 A
 0.14120  67.00000 A
 0.33700   0.50000 A  ?
 0.37100   1.70000 A
 0.51100  10.00000 A
 0.51800   0.50000 A
 0.55450   0.30000 A
 0.75800   0.15000 A
 0.78400   0.14000 A
 0.82770   0.90000 A
 0.89060   1.73000 A
 0.89900   0.20000 A  ?
 1.05400   0.20000 A
 1.12910  92.00000 A
 1.16400 PAIR PEAK
 1.23500   0.04000 A
 1.27050   1.45000 A
 1.29700 PAIR PEAK
 1.47050   0.53000 A
 1.52200   1.60000 A  ?
 1.57500   0.47000 A
 1.61200   2.40000 A
 1.65600   0.23000 A
 1.67500 PAIR PEAK
 1.69850   0.17000 A
 1.71600   0.52000 A
 1.74000   0.15000 A
 1.76100   0.40000 A
 1.78750   0.44000 A
 1.80800 PAIR PEAK
 1.84300   0.75000 A
 1.87600   0.27000 A
 1.88200   0.18000 A
 1.91350   1.30000 A
 1.92600   0.30000 A
 1.97000   0.09000 A
 1.98400   0.63000 A
 2.08500   0.44000 A
 2.18600  18.00000 A
 2.22300   0.64000 A
 2.31900  82.00000 A

 41 NB  90M
HALF LIFE:          18.8S
GEN: CHA ZR 90
     CHA NB 93
DAU: NB 90
PAR: MO  90         5.7H
REF: 70 BA 6

 0.01660  17.50000 A  X
 0.01870   3.20000 A  X
 0.12237  66.00000 A

 41 NB  91
HALF LIFE:          LONG
GEN: CHA ZR 90
DAU:
PAR:
REF: 74 SE 1

 0.01575  52.00000 A  X
 0.01770   9.00000 A  X

 41 NB  91M
HALF LIFE:          64.0D
GEN: CHA ZR 90
     CHA Y  89
DAU:
PAR:
REF: 68 LE 1,72 VE 2

 0.01490   1.50000 A  X
 0.01660  40.00000 A  X
 0.01680   0.30000 A  X
 0.01870   7.00000 A  X
 0.10400   0.56000 A
 1.20500   3.40000 A

 41 NB  92
HALF LIFE:       1.2E+08A
GEN: NFA MO 92
DAU:
PAR:
REF: 72 KO 1

 0.56000
 0.93400

 41 NB  92M
HALF LIFE:          10.16D
GEN: NFA NB 93
     CHA Y  89
     PHO NB 93
DAU:
PAR:
REF: 69 GU 1

 0.01660                X
 0.01860                X
 0.91285   1.60000 A
 0.93453  95.50000 A
 1.84743   0.80000 A

 41 NB  93M
HALF LIFE:          13.6A
GEN:
DAU:
PAR:
REF: 72 KO 2

 0.01660   9.20000 A  X
 0.01870   1.64000 A  X
 0.03040   0.00050 A

 41 NB  94
HALF LIFE:       2.03E+04A
GEN: NTH NB 93
     NFI 52E-4
DAU:
PAR:
REF: 69 AD 1

 0.70250 100.00000 A
 0.87110 100.00000 A

 41 NB  94M
HALF LIFE:          6.29M
GEN: NTH NB 93
     NFA MO 94
     NFI <5E-3
DAU:
PAR:
REF: 73 KO 1,76 MA 1

 0.01660  36.20000 A  X
 0.01870   6.90000 A  X
 0.04100   0.02400 A
 0.70300   0.00300 A
 0.87110   0.48000 A
 0.99300   0.00072 A

 41 NB  95
HALF LIFE:          35.15D
GEN: NTH ZR 94
     NFA MO 95
     NFI 6.500
DAU:
PAR: ZR  95         64.4D
REF: 69 GU 1

 0.01745   0.10000 A  X
 0.01970   0.02000 A  X
 0.76582  99.00000 A
```

Fig. 2 A typical page (reduced size) of the printed gamma ray table arranged in order of atomic and mass numbers.

The book consists of two parts. In the first all radionuclides are listed in order of atomic and mass numbers together with their gamma rays. A typical page of this list is shown in Fig.2. The second part is a list of all gamma lines, except the weak ones, arranged in order of increasing gamma ray energy. This arrangement, the first example of which is to be found in the book of Crouthamel [9] has proved to be very useful for the identification of radionuclides in mixtures of unknown composition. A typical page of the second table is shown in Fig. 3.

NUCLIDE	ENERGY	INTENSITY	OTHER LINES	PRODUCTION
J 120M 53.M	0.7632	3.5 A	0.5110 131.0 A 0.5604 100.0 A 0.6011 87.0 A 0.6147 67.0 A 0.9760 35.0 A	CHA LA CHA J
IN 119 2.4M	0.7635	99.5 A	0.7635 99.5 A	NFA SN119 NFI <0.01
AG 110M 249.9D	0.7639	22.3 A	0.6577 94.7 A 0.7639 22.3 A 0.8846 72.8 A 0.9374 34.3 A 1.3842 24.3 A	NTH AG109 NFA IN113 NFA CD110
ES 250 8.3H	0.7640	5.0 R	0.1334 15.6 R X 0.3032 29.4 R 0.3494 27.1 R 0.3838 18.5 R 0.8288 100.0 R	CHA BK249
IR 182 15.M	0.7643	5.6 A	0.0614 29.0 A X 0.0630 54.0 A X 0.0713 18.5 A X 0.1273 34.8 A 0.2730 43.6 A	
HO 156 55.6M	0.7644	6.6 R	0.1378 95.5 R 0.2665 100.0 R 0.3664 20.0 R 0.6843 10.0 R 0.8846 13.2 R	CHA DY156 CHA TA
TB 152 17.5H	0.7648	3.9 A	0.0423 22.0 A X 0.0430 42.0 A X 0.0487 13.0 A X 0.3442 86.0 A 0.5110 17.4 A	CHA EU151
HO 160 25.0M !PAR!	0.7652	5.8 A	0.0460 61.0 A X 0.5110 196.0 A 0.7281 61.0 A 0.9619 37.0 A 0.9658 37.0 A	CHA TB159 CHA TA181
PA 238 2.3M	0.7652	4.0 A	0.0984 83.0 A X 0.4485 76.0 A 0.6352 88.0 A 0.6802 73.0 A 1.0150 100.0 A	NFA U 238
HO 160M 5.1H !PAR!	0.7652	0.9 A	1.1985 2.3 A 1.2715 2.9 A 1.2854 1.8 A 2.6300 1.3 A 2.6732 1.6 A	CHA TB159 CHA TA181
TB 160 72.1D	0.7653	2.0 A	0.0868 13.4 A 0.2985 27.4 A 0.8763 30.0 A 0.9661 25.5 A 1.1779 15.5 A	NTH TB159 NFA DY160
AU 186 10.7M	0.7654	17.0 R	0.1915 100.0 R 0.2988 41.0 R 0.4155 13.7 R 0.7654 17.0 R 0.7987 8.6 R	CHA PB
GD 147 1.588D	0.7655	49.5 A	0.2299 57.0 A 0.3705 13.2 A 0.3965 26.2 A 0.7655 49.5 A 0.9280 16.2 A	CHA SM147 CHA SM144
NB 95 35.15D !PAR!	0.7658	99.0 A	0.7658 99.0 A	NTH ZR 94 NFA MO 95 NFI 6.500
TC 95 20.H	0.7658	94.3 A	0.0174 55.0 A X 0.0197 10.3 A X 0.7658 94.3 A 1.0741 3.7 A	CHA MO 95 CHA MO 94
PB 211 36.1M	0.7662	0.5 A	0.4048 3.0 A 0.4271 1.4 A 0.7033 0.3 A 0.7662 0.5 A 0.8318 2.8 A	NAT U 235
BI 211 2.16M !PAR!	0.7664	0.6 A	0.0728 1.2 A X 0.3511 12.2 A 0.4048 4.1 A 0.4269 1.9 A 0.8318 3.3 A	NAT U 235
PA 234M 1.17M !PAR!	0.7666	0.2 A	0.0136 0.4 A X 0.0946 0.1 A X 0.0984 0.1 A X 0.7666 0.2 A 1.0010 0.5 A	NAT U 238
J 134 52.6M	0.7666	3.8 A	0.5954 11.2 A 0.6217 10.9 A 0.8470 96.0 A 0.8840 66.0 A 1.0725 14.3 A	NFA XE134 NFI 7.250
RH 102 2.89A	0.7668	33.4 A	0.0192 50.0 A X 0.4750 93.0 A 0.6311 55.8 A 0.6971 44.6 A 0.7668 33.4 A	NFA RH103 NFA PD102 CHA RU102
PB 201 9.4H	0.7672	3.2 A	0.0708 25.0 A X 0.0728 46.0 A X 0.0825 16.0 A X 0.3311 82.0 A 0.3612 10.7 A	CHA TL203
TE 134 41.8M	0.7672	30.4 A	0.0794 21.2 A 0.2104 22.1 A 0.2779 21.5 A 0.5659 19.1 A 0.7672 30.4 A	NFI 5.210

Fig. 3 A typical page (reduced size) of the gamma ray table arranged in order of increasing gamma ray energy.

References

[1] Inquiries should be directed to
Dr. W. Heidrich, Kernforschungsanlage Jülich GmbH
Technologie-Transfer Büro, Postfach 1913, D-5170 Jülich

[2] G. Erdtmann, W. Soyka,
The gamma ray of the radionuclides: Tables for applied gamma ray spectrometry, Verlag Chemie, Weinheim, New York (1979)

[3] G.Erdtmann, W. Soyka,
Die γ-Linien der Radionuklide, JÜL-1003-AC (1973)

[4] E.A.C. Crouch,
Assessment of known independent yields and the calculation of those unknown in the fission of ^{232}Th, ^{235}U, ^{238}U, ^{239}Pu, ^{240}Pu, AERE-R 7680 (1974)

[5] E.A.C. Crouch,
Independent and chain yields for ^{235}U thermal neutron fission, priv. comm. (1976)

[6] E.A.C. Crouch,
Fission product chain yields from experiments in reactors and accelerators producing fast neutrons of energies up to 14 MeV, AERE-R 7394 (1973)

[7] E.A.C. Crouch,
Fission product chain yields from experiments in thermal reactors, Proc. of the Conf. on Nuclear Data in Science and Technology, Paris (March 1973) Vol. I, IAEA, Vienna (1973)

[8] G. Erdtmann, W. Soyka,
The radionuclide gamma ray file 'GAMDAT'78, JÜL-Spez-34 (1979)

[9] C.E. Crouthamel,
Applied gamma ray spectrometry, Pergamon Press, Oxford (1960)

I. INSTITUT FÜR EXPERIMENTALPHYSIK
UNIVERSITÄT HAMBURG

1. Study of the (α,xn)-Reactions on ^{59}Co and ^{60}Ni

A. Alevra*, H.H. Bissem, R. Langkau, P. Plischke, W. Scobel

Analyses of double differential cross sections for (α,xn)- and (α,xp)-reactions performed with 28-32 MeV projectiles and target nuclei in the mass range A ≈ 60 indicate [1] that for even-even targets the preequilibrium (PE) contributions are best described with an initial $n_o = 4$ exciton configuration composed of 2 neutrons, 2 protons and 0 hole. For odd A target nuclei, e.g. ^{59}Co, best agreement is obtained with the initial configuration $n_o = 5$ (2n,3p,0h). This behaviour may be related to a decomposition of the α-particle into 4 nucleons in contact with the target and the interaction of the projectile with the impaired nucleon.

In order to further study this correlation at higher energies, we have measured the (α,xn)-reaction on ^{59}Co (^{60}Ni) with 28 MeV (31.7 MeV) projectiles. Neutron spectroscopy was performed with time-of-flight (TOF) spectrometers consisting of heavily shielded 4" Ø x 2" NE 213 detectors. Neutrons with energies down to 1 MeV were detected with TOF-paths of 6-8 m and an overall time resolution of 2-3 ns. Measurements were performed for 8-10 angles ranging from 30°-150°, including individual background runs with a shadow bar inserted into the TOF-path.

Some of the energy spectra and angular distributions are shown in Fig. 1. For energies $\varepsilon_n \leq 6$ MeV the equilibrium component dominates whereas for $\varepsilon_n > 10$ MeV most of the neutron yield in the forward hemisphere can be attributed to PE emission. The resulting angle integrated spectra are in quantitative agreement with the predictions of the hybrid model for the PE component, applying a mean free path multiplier $1 \leq k \leq 2$ [2], followed by equilibrium as described [3] by an Ewing-Weißkopf-Model (Fig. 2). According to these calculations, PE emission depletes the initial reaction

---

*Permanent address: Institutul de Fizica si Inginerie Nucleara, Bukarest, Romania

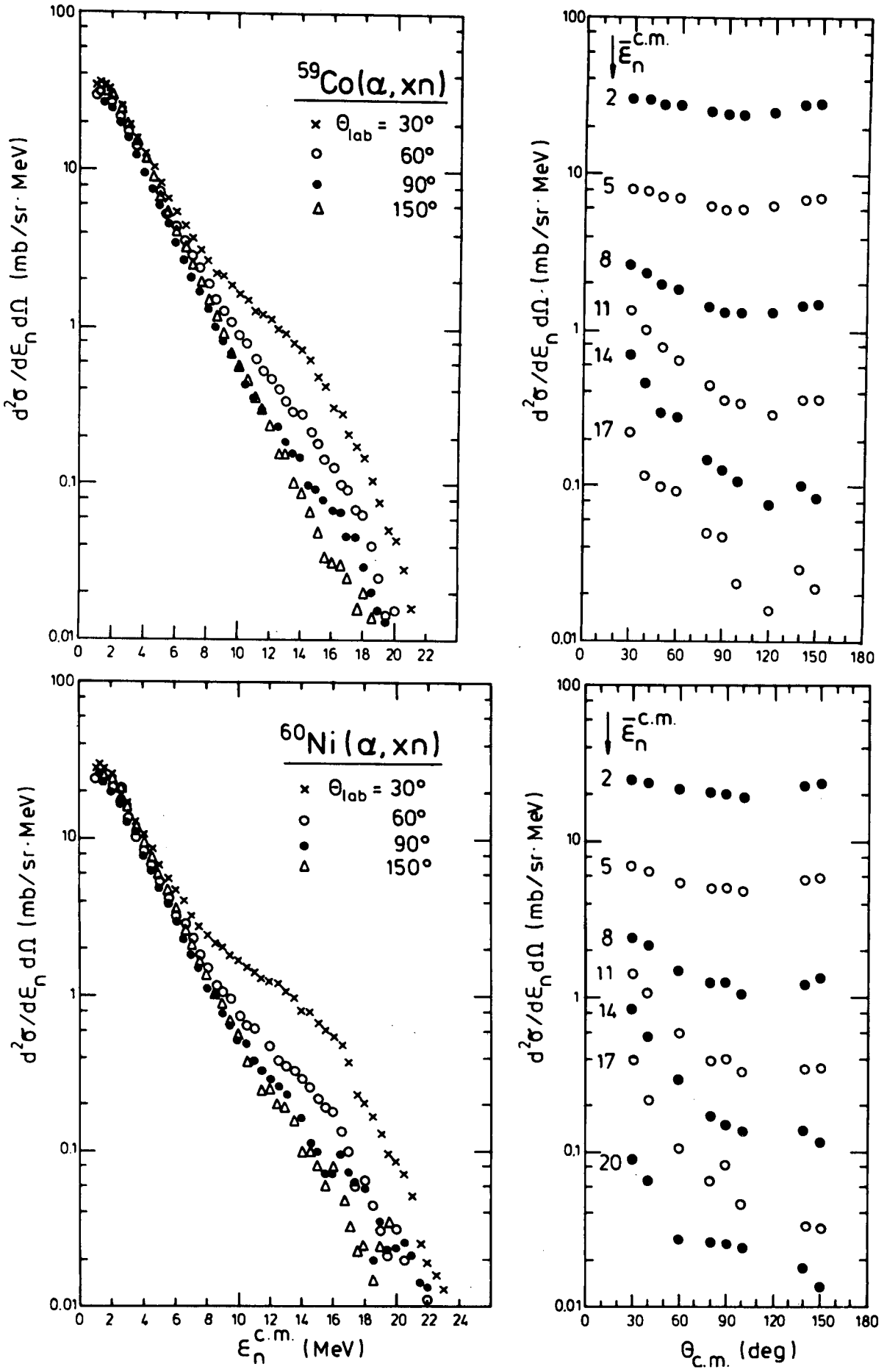

Fig. 1 Energy spectra and angular distributions for 1 MeV bins centered around $\bar{\varepsilon}_n^{cm}$ (MeV) for neutron yield from reactions of 28 MeV (31.7 MeV) α-particles with ^{59}Co (^{60}Ni).

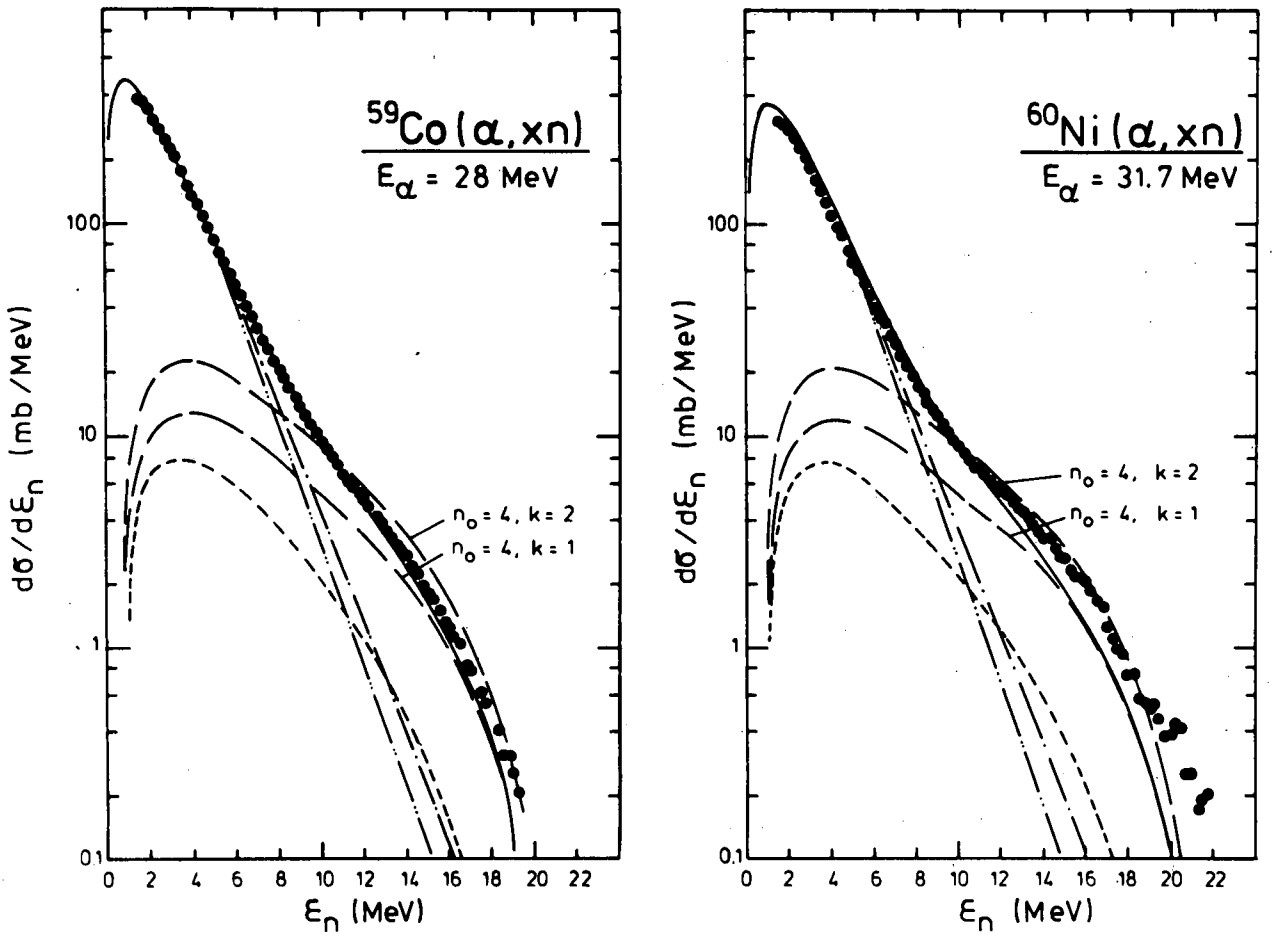

Fig. 2 Resulting experimental angle integrated spectra (points). Calculations:

a) Hybrid model for internal transition rates λ_+^{NN}/k with k = 1 and initial configuration $n_o = 4$ ($n_p = 2$, $n_n = 2$, $n_h = 0$) (long dashed).

b) Same as a) but k = 2 (long dashed).

c) Same as a) with k = 1 and $n_o = 5$ (3; 2; 0) (short dashed).

d) Ewing-Weisskopf-model with level density parameter $a = A/9$ MeV^{-1} (dot-dashed).

e) Same as d) with $a = A/7.5$ MeV^{-1} (double dot-dashed).

f) Sum of a) and d) (solid line).

cross section by 20 ± 4% and contributes about 7.5 ± 1.5% (for ^{59}Co) and 9 ± 2% (for ^{60}Ni) of the total neutron yield. For both reactions an initial configuration of $n_o = 4$ excitons provides a better agreement than the choice $n_o = 5$.

2. Continuous Spectra of Light Particles from p + ^{58,60,61,62,64}Ni and p + ^{63,65}Cu at $E_p = 27$ MeV

J. Friese, H.H. Bissem, H.J. Langanke, W. Scobel, R. Wien

Particle emission in proton induced reactions with all stable Ni and Cu isotopes prior to and during the equilibration has been studied for the neutron, proton and α exit channels. Double differential cross sections have been measured for charged particle (neutron) emission for 13-20 (8-10) angles between 10° and 160° (30° and 150°) with solid state detector telescopes (TOF techniques). The total neutron yields obtained by integration over angle are shown in Fig. 3 together with the results of a calculation combining preequilibrium (PE) and equilibrium (EQ) decay modes. Details are given elsewhere [4].

The resulting decomposition into EQ and PE contributions is listed in Table I; it shows for nucleons the expected correlation with neutron excess (N-Z) and binding energies S_n, S_p. The total nucleon PE yield amounts to ≈35% of the reaction cross section σ_R. The PE yield of α particles is in the order of 1% of σ_R and shows no distinct mass dependence.

Assuming the spectral shape of PE and EQ contributions to be independent of angle, their angular distributions may be obtained (Fig. 4). It is satisfying to note that the EQ contribution reveals the expected symmetry around 90°, indicating a correct decomposition in the forward hemisphere, where PE and EQ yields are comparable.

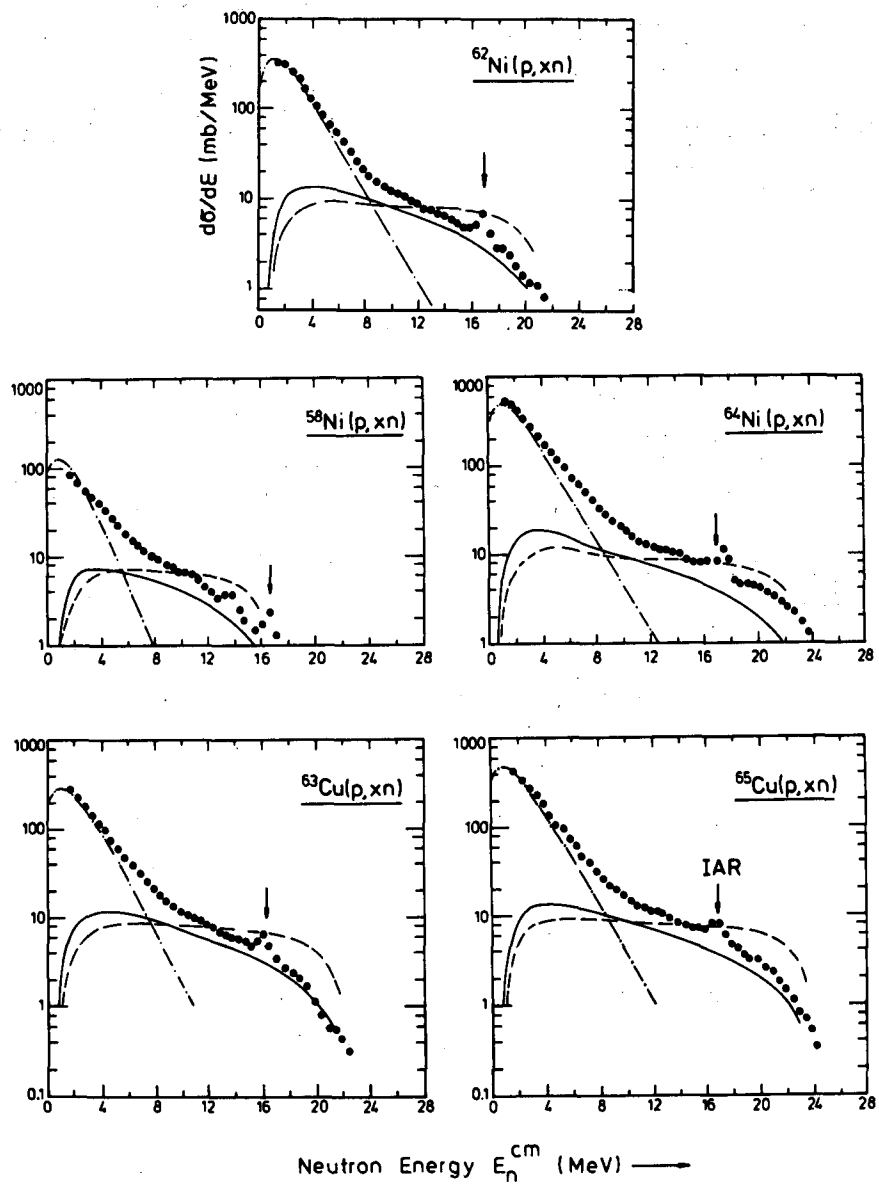

Fig. 3 Angle integrated neutron energy spectra. Calculations: EQ contribution (dash-dotted); PE contributions: hybrid model with λ_+^{NN} and k=2 (solid), GDH model with λ_+^{NN} (dashed).

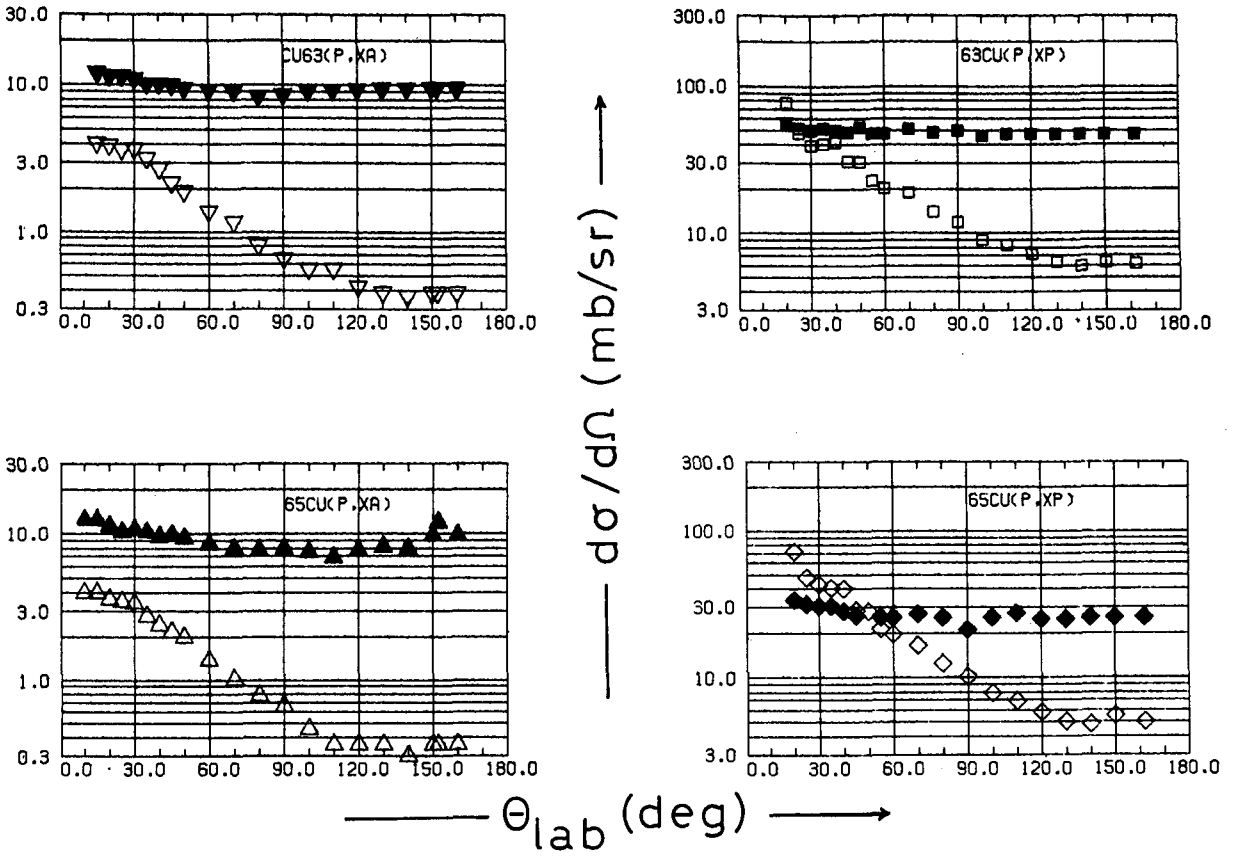

Fig. 4 Angular distribution of α-particles and protons for $p + {}^{63,65}Cu$. Solid (open) symbols: EQ (PE) component

Table I. PE and EQ yields of nucleons and α-particles obtained from decomposition of angle integrated spectra. Error estimates: $\Delta\sigma_N \approx 10\%$, $\Delta\sigma_\alpha \approx 15\%$

Target	$N-Z_{CN}$	S_n-S_p (MeV)	σ_n (mb) PE	EQ	σ_p (mb) PE	EQ	σ_α (mb) PE	EQ
^{58}Ni	1	9.35	101	408	277	854	11	77
^{60}Ni	3	6.91	-	-	242	626	11.5	100
^{61}Ni	4	3.03	-	-	276	505	10.5	106
^{62}Ni	5	4.73	170	1240	255	351	13	84
^{64}Ni	7	2.45	263	1770	198	254	12	60
^{63}Cu	4	4.15	147	907	228	578	15.5	121
^{65}Cu	6	2.13	200	1481	202	330	14.4	97

3. Measurement of Neutrons Emitted in Fission of $^{235,236,238}U$ by Protons

P. Plischke, H. Krause, R. Langkau, W. Scobel

We have started a programme devoted to the neutron-fission competition of highly excited neptunium isotopes as observed in $^{235,236,238}U(p,nf)$ reactions. In order to separate pre- and post-fission neutron contributions, neutron emission has been measured at 0° and 90° with respect to the fission fragment direction (Fig. 5). Fission fragments have been detected with NE 102A scintillator foils F_1, F_2 of 700 $\mu g/cm^2$ thickness, subtending solid angles of 106 msr and 227 msr perpendicular to the projectile direction. Neutrons in coincidence with F1, F2 were measured with two time-of-flight detectors N1, N2 (NE213, 4" Ø x 2", flight path 2m).

Neutrons emitted after fission from the fully accelerated fragments are correlated with the fission fragment direction in the lab system, whereas the pre-fission neutrons do not show such a correlation (they are, however, correlated with the projectile direction if they are emitted prior to equilibration, and this decay mode contributes substantially at high excitation energies, cf. [6-8]). A decomposition may be obtained from the comparison of the spectra measured under 0° and 90°, respectively.

The proton Coulomb barrier restricts these measurements to $E_p > 10$ MeV, allowing for multiple chance fission. Determination of Γ_n/Γ_f therefore requires measurements with different projectile energies and a sequence of target isotopes. So far we have completed $p + ^{238}U$ at $E_p = 12.7$ MeV, 18.5 MeV, 25.6 MeV and $p + ^{235}U$, ^{236}U at 12.7 MeV.

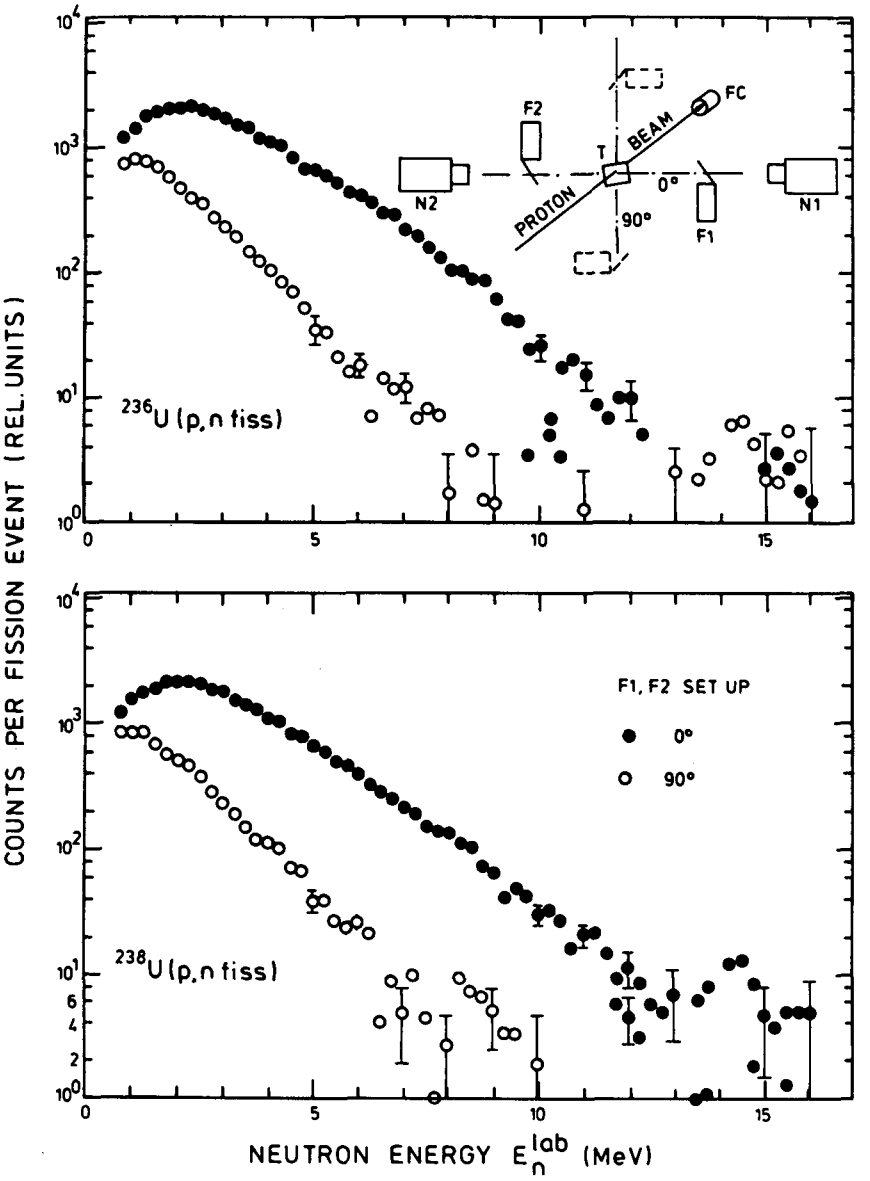

Fig. 5 Lab neutron energy spectra for E_p = 12.7 MeV at 0° and 90° with respect to the fission axis. Data are normalized to the same number of F1-F2-coincidences.

References

[1] A. Alevra, M. Duma, I.R. Lucas-Koch, M.T. Magda, M.E. Nestor, Nucl.Phys. A265(1976)376

[2] M. Blann, Nucl.Phys. A213(1973)570

[3] V. Schröder, W. Scobel, L. Wilde, M. Bormann, Z.Physik A287(1978)353

[4] W. Scobel, Proc. Workshop on Reaction Models for Continuous Spectra of Light Particles (Bad Honnef, 1978) p. 65

[5] C.J. Bishop, I. Halpern, R.W. Shaw, R. Vandenbosch, Nucl.Phys. A198(1972)161

[6] J.R. Boyce, T.D. Hayward, R. Bass, H.W. Newson, E.G. Bilpuch, F.W. Purser, H.W. Schmitt, Phys.Rev. C10(1974)231

[7] J. Gilat, A.F. Delagrange, J.H. Alexander, Phys.Rev. C16(1977)694

[8] H. Karius, A. Ackermann, W. Scobel, J.Phys.G: Nucl.Phys., in press

INSTITUT FÜR KERNCHEMIE

UNIVERSITÄT ZU KÖLN

1. Integral Excitation Functions for p-Induced Reactions

R. Michel, G. Brinkmann, W. Herr

In 1978 we extended our former work [1-3] on the measurement and hybrid model [4] analysis of excitation functions for p-induced reactions on Ti, V, Fe, Co and Ni, both with respect to the Z of the target element as well as to the energy range of the incident particles.

1.1 p-Induced Reactions on Ti, V, Fe, Co and Ni for p-Energies between 2 and 17 MeV

While applying the stacked foil technique for the determination of excitation functions, the total thickness of the stacks is limited by the increasing energy error due to stopping power uncertainties as well as due to the energy straggling. For these reasons, a total stopping of the protons was not adequate in our former investigations [1-3] including irradiations of the stacks at the Jülich isochronous cyclotron JULIC. The lowest available external proton energy at that accelarator is 22.5 MeV. In order to complete the low energy part of some of our excitation functions, we have measured the cross sections for p-induced reactions on Ti, V, Fe, Co and Ni irradiating stacks of those elements at the compact cyclotron CV 28 of the KFA Jülich. The experimental procedure is the same as that described earlier [1]. The results are presented in Table I.

Table I. Experimental cross sections for p-induced reactions on Ti, V, Fe, Co and Ni for proton energies between 2 and 17 MeV

TARGET ELEMENT: TITAN						
E_p [MeV]	16.42 ± 0.19	14.77 ± 0.26	12.97 ± 0.35	10.93 ± 0.38	8.02 ± 0.48	3.90 ± 0.58
$\sigma(E_p)$ [mb]						
^{48}V	2.13 ± 0.26	3.24 ± 0.39	3.95 ± 0.47	3.79 ± 0.45	3.58 ± 0.31	
^{47}Sc	1.26 ± 0.18	0.76 ± 0.10	0.49 ± 0.05	0.22 ± 0.04		
$^{46m+g}Sc$	2.75 ± 0.36	1.84 ± 0.24	1.22 ± 0.16	0.667 ± 0.087	0.141 ± 0.021	
^{44m}Sc	1.12 ± 0.17	0.78 ± 0.10	0.44 ± 0.06	0.16 ± 0.02		
TARGET ELEMENT: VANADIUM						
E_p [MeV]	15.91 ± 0.21	14.21 ± 0.27	12.36 ± 0.35	10.23 ± 0.39	7.13 ± 0.49	2.95 ± 0.61
$\sigma(E_p)$ [mb]						
^{51}Cr	293. ± 35.	505. ± 61.	692. ± 83.	676. ± 81.	514. ± 62.	1.26 ± 0.21
TARGET ELEMENT: IRON						
E_p [MeV]	16.06 ± 0.25	14.38 ± 0.30	12.55 ± 0.39	10.44 ± 0.43	7.41 ± 0.55	3.44 ± 0.68
$\sigma(E_p)$ [mb]						
$^{58m+g}Co$	0.77 ± 0.12	1.32 ± 0.18	2.02 ± 0.24	2.04 ± 0.24	1.35 ± 0.2	
^{57}Co	5.47 ± 0.60	5.81 ± 0.64	7.72 ± 0.85	10.6 ± 1.1	7.43 ± 0.82	0.102 ± 0.016
^{56}Co	228. ± 23.	342. ± 34.	371. ± 37.	319. ± 32.	97.3 ± 10.	
^{54}Mn	0.75 ± 0.18					
^{51}Cr	2.13 ± 0.26	1.42 ± 0.17	0.86 ± 0.15			
TARGET ELEMENT: COBALT						
E_p [MeV]	15.34 ± 0.69	13.59 ± 0.77	11.65 ± 0.93	9.39 ± 1.07	5.98 ± 1.43	
$\sigma(E_p)$ [mb]						
$^{58m+g}Co$	217. ± 26.	45.2 ± 5.4	0.189 ± 0.028			
^{57}Co	0.459 ± 0.055					
TARGET ELEMENT: NICKEL						
E_p [MeV]	16.26 ± 0.24	14.59 ± 0.30	12.78 ± 0.39	10.71 ± 0.43	8.89 ± 0.58	7.75 ± 0.54
$\sigma(E_p)$ [mb]						
^{61}Cu	4.48 ± 0.76	2.37 ± 0.32	3.89 ± 0.65	5.04 ± 0.60		3.27 ± 0.38
^{57}Ni	18.6 ± 2.4	2.49 ± 0.40	0.317 ± 0.046			
$^{58m+g}Co$	1.08 ± 0.12	1.18 ± 0.13	1.06 ± 0.12	0.860 ± 0.095	0.533 ± 0.099	0.375 ± 0.041
^{57}Co	192. ± 19.	74.4 ± 8.2	14.4 ± 1.6	7.67 ± 0.84	1.18 ± 0.16	0.51 ± 0.06
^{55}Co	23.2 ± 2.3	20.7 ± 1.9	14.9 ± 1.6	8.32 ± 0.92		0.058 ± 0.008

The present cross sections fit very well into the excitation functions measured by us for the higher proton energies [1-3], as can be seen by a comparison of the data for ^{44m}Sc, $^{46m+g}Sc$ and ^{47}Sc produced from titanium as target material [1]. A comparison with excitation functions given in the literature is, for example, possible in the case of nickel. Here our cross sections are in very good agreement with the work of the authors cited in [2].

1.2 Redetermination of the Excitation Function for the Reaction $^{27}Al(p, 3p3n)^{22}Na$

The p-induced reactions on Al were reviewed extensively by Tobailem et al in 1971 [5]. However, there exists a discrepancy for the reaction $^{27}Al(p,3p3n)^{22}Na$ between the adopted values of Tobailem et al [5] and those of Myano [6] which were published in 1973. So we have redetermined the excitation function for the production of ^{22}Na from Al. The resulting cross sections are:

(44.80 ± 0.09 MeV)	45.1 ± 5.0 mb	(43.06 ± 0.13 MeV)	48.3 ± 5.8 mb
(41.28 ± 0.17 MeV)	45.3 ± 4.9 mb	(39.44 ± 0.21 MeV)	41.0 ± 4.5 mb
(37.82 ± 0.24 MeV)	34.2 ± 4.1 mb	(36.14 ± 0.27 MeV)	25.5 ± 2.8 mb
(34.40 ± 0.29 MeV)	16.21± 1.8 mb	(32.59 ± 0.32 MeV)	7.5 ± 0.9 mb
(30.69 ± 0.33 MeV)	2.20± 0.26mb	(28.70 ± 0.37 MeV)	0.417± 0.36mb
(26.58 ± 0.40 MeV)	0.380± 0.004mb		

As shown in Fig.1, our data are in excellent agreement with the adopted values of Tobailem et al [5] and in contrast to those given by Myano [6].

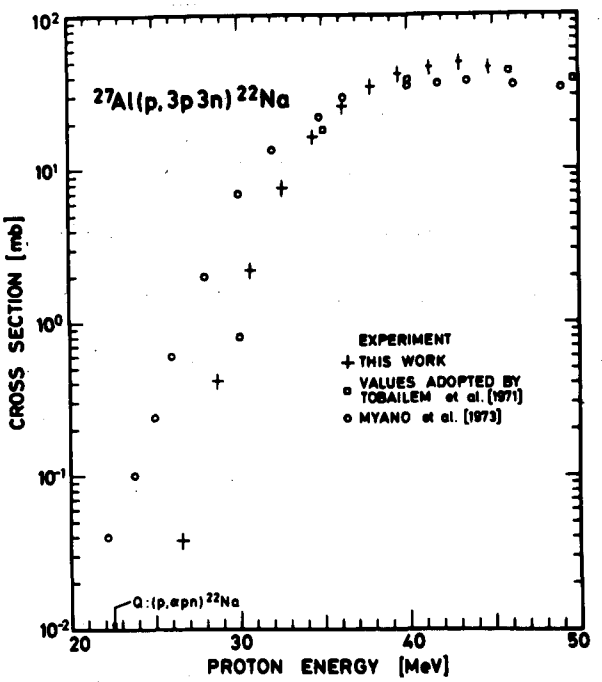

Fig.1 Comparison of our cross-section data for the reaction ^{27}Al(p,3p3n)^{22}Na with the literature values. For references to earlier work see text.

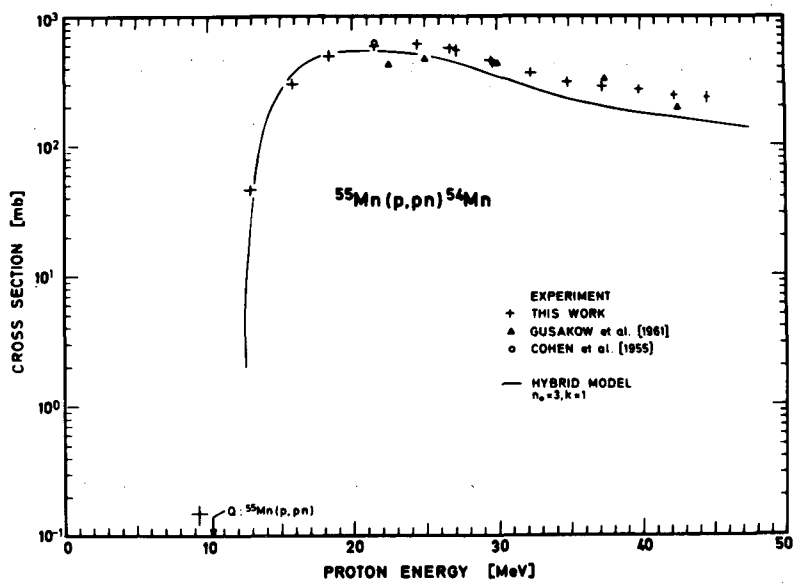

Fig.2 Experimental measurement and hybrid model analysis of the cross section for the reaction ^{55}Mn(p,pn)^{54}Mn.

1.3 Excitation Functions for the Production of ^{54}Mn, $^{52m+g}Mn$ and ^{51}Cr from Manganese with Proton Energies up to 45 MeV

Using 25 µm metal foils of Mn/Ni alloy containing 88% of Mn and 12% of Ni, we measured the excitation functions for the production of ^{54}Mn, $^{52m+g}Mn$ and ^{51}Cr from manganese. The cross-section data are presented in Table II. Up to now, experimental values are to be found in the literature only for the reaction $^{55}Mn(p,pn)^{54}Mn$ by Gusakov et al [7] and Cohen et al [8], which fit quite well into ours (see Fig.2). The data were compared with model calculations applying the code OVERLAID ALICE [9]. The general good agreement between theory and experiment obtained for p-induced reactions is shown typically in Fig.2. However, some discrepancies still exist, mainly with regard to the emission of complex particles, as it is shown in Fig.3 for the reaction $^{55}Mn(p,p3n)^{52m+g}Mn$, where the cross sections below 32 MeV can only be explained by the emission of ^{3}H. A detailed discussion of the problem related to complex particle emission is given elsewhere [3].

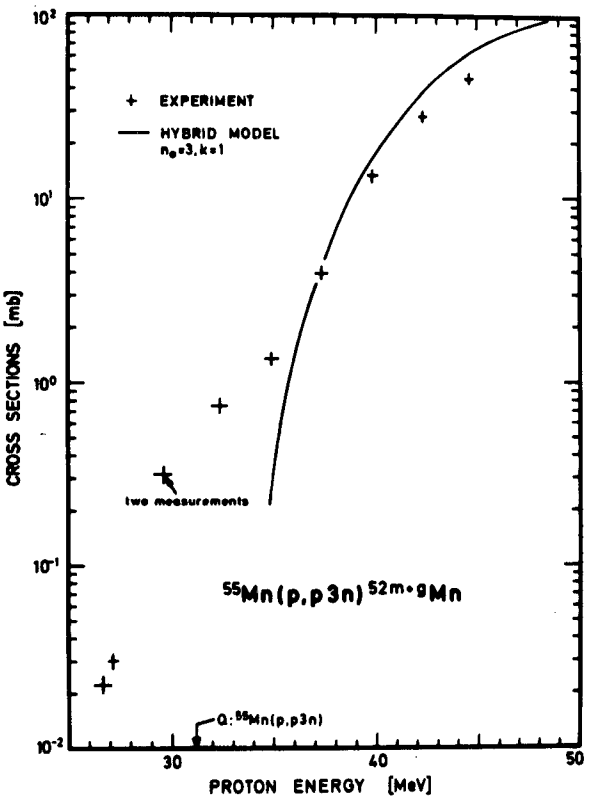

Fig.3 Experimental measurement and hybrid model analysis of the cross section for the reaction $^{55}Mn(p,p3n)^{52m+g}Mn$.

Table II. Experimental cross section for the production of ^{51}Cr, ^{54}Mn and $^{52m+g}Mn$ in p-induced reaction on Mn in the proton energy range of 9 to 45 MeV

$E_p \pm \Delta E_p$ [mb]	CROSS SECTION [mb]			$E_p \pm \Delta E_p$ [mb]	CROSS SECTION [mb]		
	^{51}Cr	^{54}Mn	$^{52m+g}Mn$		^{51}Cr	^{54}Mn	$^{52m+g}Mn$
44.63 ± 0.13	18.7 ± 2.4	236. ± 25.	44.97 ± 3.14	27.17 ± 0.23	98.5 ± 8.4	544. ± 49.	0.0306 ± 0.0030
42.30 ± 0.22	19.8 ± 2.2	242. ± 18.	28.09 ± 1.96	26.73 ± 0.45	98.6 ± 9.2	570. ± 51.	0.0226 ± 0.0024
39.86 ± 0.27	25.2 ± 1.8	269. ± 22.	13.37 ± 1.00	24.48 ± 0.30	88.5 ± 6.7	611. ± 55.	
37.32 ± 0.32	36.0 ± 3.6	284. ± 23.	3.95 ± 0.30	21.53 ± 0.34	64.4 ± 5.5	590. ± 47.	
34.91 ± 0.36	52.7 ± 4.1	309. ± 25.	1.36 ± 0.10	18.43 ± 0.38	23.2 ± 2.1	495. ± 45.	
32.36 ± 0.40	77.7 ± 7.8	363. ± 25.	0.759 ± 0.060	15.86 ± 0.43	1.52 ± 0.29	300. ± 24.	
29.66 ± 0.42	98.6 ± 8.4	453. ± 36.	0.315 ± 0.030	12.89 ± 0.48		46.0 ± 3.7	
29.66 ± 0.17	97.1 ± 7.8	437. ± 42.	0.314 ± 0.030	9.28 ± 0.53		0.149 ± 0.025	

At the moment, we are extending our work on integral reaction cross-section data to α-induced reactions for the same target elements.

References

[1] R.Michel,G.Brinkmann,H.Weigel,W.Herr,J.Inorg.Nucl.Chem.40(1978) 1845

[2] R.Michel,H.Weigel,W.Herr,Z.Phys.A 286 (1978) 393

[3] R.Michel,G.Brinkmann,H.Weigel,W.Herr, Nucl.Phys.A, in press

[4] M.Blann, Phys.Rev.Lett.27 (1971) 337

[5] J.Tobailem, C.-H.de Lassus St-Genies,C.Leveque, CEA-N-1466(1)(1971)

[6] K.Myano, J.Phys.Soc.Japan 34 (1973) 853

[7] M.M.Gusakov, G.Albouy, N.Poffe, C.Riehl,J.Phys.Radium 22(1961)636

[8] B.L.Cohen, E.Newman, Phys.Rev.99 (1955) 718

[9] M.Blann, COO-3494-32 (1976) and UR-NSRL-181 (1978)

INSTITUT FÜR KERNCHEMIE
JOHANNES GUTENBERG-UNIVERSITÄT MAINZ

1. Some Decay Properties and Yields in Fission Product Chains 131, 133 and 135

H. Braun, T. Izak-Biran*, Z. Alfassi**, W. Lauppe†, H.O. Denschlag

Some decay properties and/or yields of the members of the decay chains with the mass numbers A = 131, 133 and 135 were examined using fast chemical separations of antimony and tellurium from fission product mixtures in $^{235}U(n_{th},f)$. In addition, a direct measurement of the conversion coefficient (α) of the 334 keV isomeric transition deexciting ^{133m}Te was carried out using the on-line mass-separator JOSEF of the Jülich Nuclear Research Centre.

A somewhat surprising result of these studies is the finding that the 334 keV γ-ray is produced in two separate transitions:

(i) it arises in the isomeric transition of ^{133m}Te to ^{133g}Te (6.6 % absolute photon yield, $\alpha_T = 1.43$) and

(ii) it is emitted following the ß-decay of ^{133m}Te to ^{133}I (3.1 ± 0.4 % absolute yield). This finding was confirmed by γ-γ coincidence experiments [1].

Further analysis of our data resulted in the branching fractions indicated in Table I and in some absolute γ-ray intensities given in Table II. In addition, new values of the cumulative yields of ^{133m}Te and ^{131m}Te in $^{235}U(n_{th},f)$ were obtained (Table III). The new values differ substantially from some older values also given in the tables.

---

*SOREQ Nuclear Research Centre, Yavne, Israel
**Ben Gurion University, Beer Sheva, Israel
†Institut für Kernphysik, Kernforschungsanlage Jülich

Table I. Branching fraction in chain 133

Decay from	to	Fraction of total decay: This work	Literature [ref.]
Sb	^{m}Te	0.29±0.03	0.42±0.06 [2], 0.15±0.01 [3]
Sb	^{g}Te	0.71±0.03	0.58±0.06 [2], 0.85±0.04 [3]
^{m}Te	^{g}Te	0.16±0.02	0.13±0.03 [4], 0.29±0.01 [3]
^{m}Te	^{g}Te	0.84±0.02	0.87±0.03 [4], 0.71±0.01 [3]

Table II. Absolute photon intensities of the main γ-rays in the decay of ^{133}Sb, ^{133m}Te and ^{135}Te

Isotope	E_γ (keV)	Absolute photon intensity, I_γ (%): This work	Literature [ref.]
^{133}Sb	1096	32±2	42 [1]
^{133}Sb	817	15±3	
^{133m}Te	912	62±5	32±3 [5], 88±4 [3], 63±7 [6]
^{135}Te	603	25±3	
^{135}Te	267	5.8±0.7	

Table III. Cumulative yields of ^{133m}Te and ^{131m}Te in ^{235}U(n_{th},f)

Isotope	Cumulative yield (%): This work	Literature [ref.]
^{133m}Te	3.79±0.15	4.68±0.11 [7]
^{131m}Te	0.50±0.05	0.43 [8]

References

[1] R. A. Meyer, private communication

[2] B. Parsa, G. E. Gordon, A. Wenzel, J. Inorg. Nucl. Chem. 31 (1969) 585

[3] I. Fujiwara, N. Imanishi, T. Nishi, J. Inorg. Nucl. Chem. 36 (1974) 1921

[4] T. Alväger, G. Oelsner, Arkiv Fysik 12 (1957) 319

[5] V. Berg, K. Fransson, C. E. Bemis, Arkiv Fysik 37 (1968) 213

[6] L. M. Lederer, V. S. Shirley (eds.) Table of Isotopes (7th Edition) Wiley, New York (1978)

[7] A. C. Pappas, MIT Technical Report No. 63 (1953) p.92

[8] S. Katcoff in C.D. Coryell and N. Sugarman (eds.), Radiochemical Studies: The Fission Products, McGraw-Hill (1951) p.980

2. Spectroscopy of Beta Delayed Neutrons in Coincidence with Gamma-Rays Depopulating Excited States in the Final Nucleus

H. Ohm, A. Schröder, W. Rudolph*, K. Sümmerer, U. Tharun, K.D. Wünsch+, G. Jung+, K.-L. Kratz

As has originally been indicated by γ-ray measurements [1,2], beta-delayed neutron emission from precursors with large energy windows ($Q_\beta - B_n$) can not only lead to the ground state but also to excited states of the final nucleus. In these cases the construction of β^--strength functions (S_β-) requires unfolding of the neutron singles spectra. The optimum spectroscopic method therefore is the measurement of delayed neutrons in coincidence with γ-rays depopulating those excited final states.
This technique has been developed at Mainz utilizing three high-resolution ^{3}He ionization chambers operated in parallel for neutron detection and a Ge(Li) spectrometer of 23% relative efficiency for γ-ray detection. Due to the rather long and variable charge collection times[3] in the ^{3}He ionization chambers a resolving time of about 5 μs was required [4]. The overall efficiency of the Ge(Li) - ^{3}He detector arrangement was as low as 10^{-7}. Consequently, this implies severe restrictions on the data aquisition rates, results in rather long measuring times and requires isotopically clean sources. With this set-up high resolution nγ-coincidence spectra were measured for $^{94-97}$Rb(βnγ) decays at the alkali isotope separator OSTIS in Grenoble [5].

* Present Address: Nukem, D-6540 Hanau, Germany

+ II. Physikal.Inst., Univ.Giessen, D-6300 Giessen, Germany and Inst. Laue-Langevin, F-38042 Grenoble, France

Fig. 1 shows the singles neutron spectrum of ^{95}Rb (upper part), together with the partial spectrum in coincidence with the 837 keV γ-rays corresponding to the $2^+ \rightarrow 0^+$ transition in ^{94}Sr (middle part) and the spectrum of neutron decay to the ground state of the final nucleus (lower part). Combining nγ-coincidence and γ-singles data [2], one can deduce that about 59% of the total neutron emission leads to the ground state of ^{94}Sr, about 37% to the 2^+-state and only a total of 4% feeds the four higher excited levels between 1926 and 2604 keV in ^{94}Sr. In this case the singles spectrum thus represents a superposition of only two intense partial spectra, their individual neutron peaks still being well resolved. The strongest neutron lines appearing in the singles spectrum [2] are seen in only one or the other of the partial spectra, not in both. This is most clearly demonstrated for the 13.6 keV peak which surprisingly corresponds to a transition to the 0^+ ground state in ^{94}Sr though from the hindrance of the required f-wave neutrons at this low energy one would expect it to be seen in the partial spectrum to the 2^+-state where p-wave neutrons are dominating. Recent results of Crawford et al [6] who measured the low energy part of the ^{95}Rb delayed neutron spectrum with an energy resolution of 0.2 keV using the TOF-method confirm that the 13.6 keV peak consists of a single component. Another interesting feature of the partial spectrum to the ^{94}Sr ground state is the drop in neutron intensity at 837 keV, exactly corresponding to the energy difference of the ground- and the 2^+-state in the final nucleus. This supports an earlier qualitative explanation that the apparent lack of high-energy neutron intensity in the singles spectra is due to preferential neutron decay to excited final states [1,2], their configurations being strongly connected to the main configurations of neutron emitting states populated in β^--decay [7].

Quite a different situation is found for ^{94}Rb ($\beta^- n\gamma$)-decay, where many low-lying levels in the final nucleus ^{93}Sr can be reached after neutron emission [2]. Fig. 2 shows several nγ-coincidence spectra (a-d) representing the neutron decay to the 4 lowest excited states in ^{93}Sr. The relative neutron branching ratios p_n^i to these levels are in general agreement with the previous results from γ-ray measurements [2]. The partial spectrum of neutron decay to the ground state (e) was obtained by subtracting all coincidence spectra from the singles neutron spectrum of ^{94}Rb (f). Compared to the nearly continuous shape of this singles spectrum, the partial spectra exhibit clear peak structure, confirming our earlier expalnation that the extent of fine structure in a singles neutron spectrum depends on the density of levels in the final nucleus accessible to neutron decay [2].

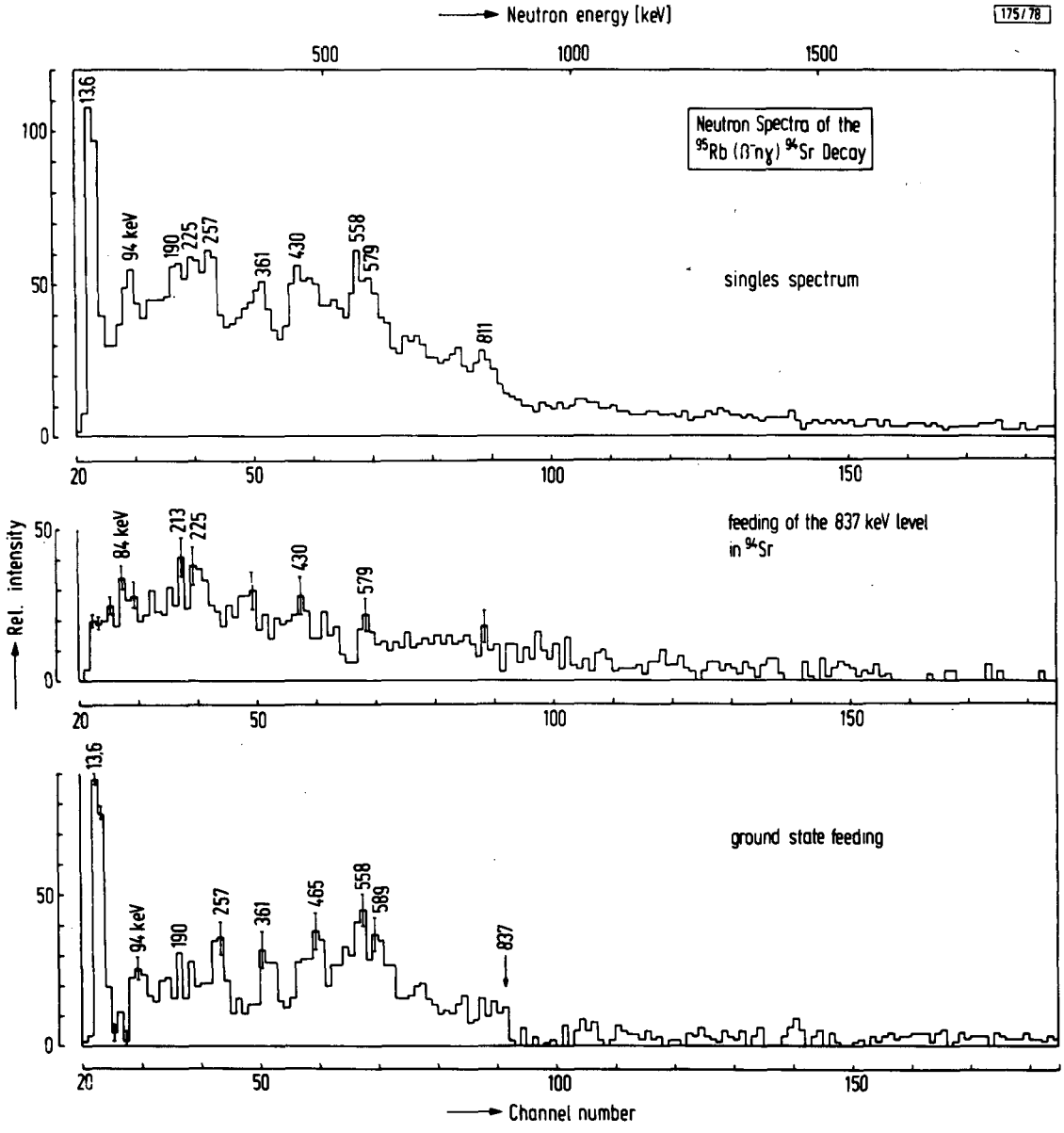

Fig. 1 Singles neutron spectrum of ^{95}Rb decay (upper part), and partial spectrum in coincidence with the 837 keV γ-rays correpsonding to the $2^+ \rightarrow 0^+$ transition in ^{94}Sr (middle part). The partial spectrum of neutron decay to the ground state (lower part) was obtained by subtracting the coincidence spectrum from the singles spectrum.

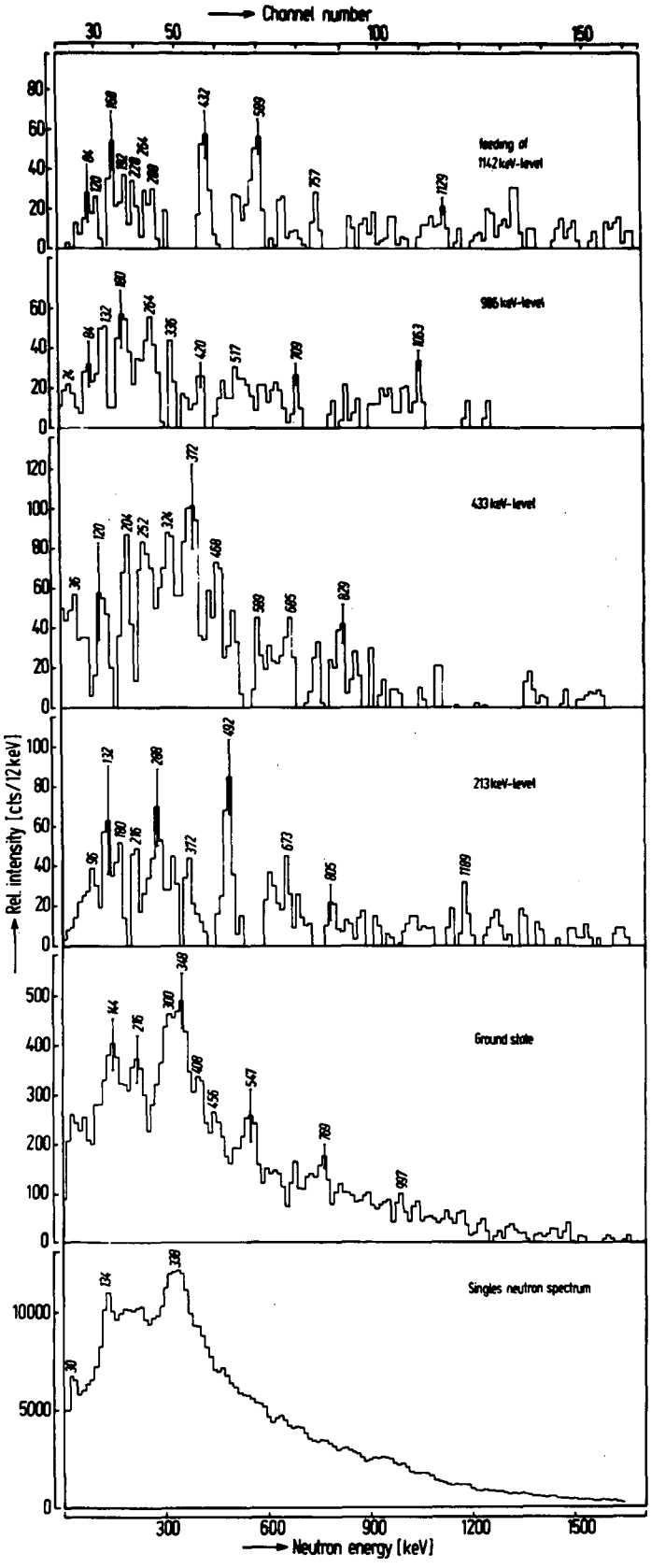

Fig. 2 ^{94}Rb partial neutron spectra in coincidence with γ-rays depopulating excited states in ^{93}Sr (a-d), neutron spectrum to the ground state in ^{93}Sr (e), and singles neutron spectrum (f).

In the case of ^{94}Rb the singles spectrum represents a superposition of 8 partial spectra containing about 95% of the total neutron intensity $p_n^{tot} \simeq 10\%$, and some further 20 partial spectra with very low p_n^i. Thus, with an average neutron detector resolution of about 18 keV in this experiment the individual peaks of the partial spectra can no longer be resolved in the singles neutron spectrum.

The partial neutron spectra directly yield information on the β^--decay preceding neutron emission and allow the construction of unique β^--strength functions in the energy range B_n to near Q_β of the emitter nuclides. Furthermore, these data make possible detailed comparison with nuclear model estimates of neutron transmission coefficients, neutron spectrum envelopes and β-strength distributions.

First analysis of our data demonstrate - besides nuclear structures in the β^--strength functions [8] - that the experimental neutron branching ratios do not follow in the manner predicted by optical model transmission coefficients [9]. This implies that intermediate structure [7] in neutron emitter and final states must be considered explicitly.

References

[1] H. Franz et al, Phys. Rev. Lett. 33 (1974) 859

[2] K.-L. Kratz et al, Proc AED-Conf. 77-017-001, Hirschegg (1977), p.208

[3] H. Franz et al, Nucl. Instr. Nethods 144 (1977) 253

[4] W. Rudolph, Doctoral Dissertation, Univ. Mainz (1976)

[5] K.D. Wünsch, Nucl. Instr. Methods 155 (1978) 347

[6] G.I. Crawford et al, ILL-Report 03-03-61 (1977)

[7] A.A. Shihab-Eldin et al, Phys. Lett. 69B (1977) 143

[8] K.-L. Kratz et al, Report NEANDC(E)-192 U Vol. V (1978) p.72

[9] E.H. Auerbach, F.G.J. Perey, Brookhaven Report BNL-765 (1962)

REAKTORSTATION GARCHING, FACHBEREICH PHYSIK
TECHNISCHE UNIVERSITÄT MÜNCHEN

1. Coherent Neutron Scattering Lengths

1.1 Neutron Refractometer

L. Koester, W. Waschkowski, H. Reiner

Highly precise neutron reflection measurements on liquid mirrors of the molten metals Pb, Bi and Sn have shown small deviations of the measured reflection curve from the calculated curve near the critical fall height. These deviations lead to a systematic error in the order of the statistical uncertainty of about ± 0.02 % for the coherent scattering lengths of the mirror substance.
For tin a scattering length b(Sn) = 6.2170 + 0.0015 fm per bound atom was obtained from the reflection experiment. Reflection measurements on evaporated layers are planned.

1.2 Christiansen Filter Technique

L. Koester, K. Knopf

In the course of a work for the determination of the spin state scattering lengths of light nuclei the coherent scattering lengths for the bound atoms of the following nuclides and elements were measured:

^{12}C : b = 6.6535 ± 0.0014 fm
^{13}C : b = 6.19 ± 0.09 fm
^{14}N : b = 9.37 ± 0.03 fm
^{15}N : b = 6.44 ± 0.03 fm
^{16}O : b = 5.805 ± 0.005 fm
^{17}O : b = 5.62 ± 0.45 fm
^{18}O : b = 5.84 ± 0.07 fm
^{19}F : b = 5.654 ± 0.012 fm
Mg : b = 5.376 ± 0.020 fm

The presented data are in good agreement with the values compiled in BNL 325, Vol. 1, third edition (1973), but, in general, they are more accurate. Measurements on isotopically enriched mixtures of Rb resulted in preliminary values for

Rb : b = 7.12 ± 0.03 fm,

^{85}Rb : b = 7.23 ± 0.06 fm and
^{87}Rb : b = 6.98 ± 0.03 fm.

2. Neutron Cross Sections

L. Koester, W. Waschkowski, P. Hurst

Exact values for scattering cross sections at "zero-energy" and coherent scattering lengths are needed for the determination of the fundamental spin state scattering lengths, which describe completely the scattering of slow neutrons by nuclei.

Zero-energy scattering cross sections are derived from total cross sections measured in the eV-region of the neutron energy. Transmission measurements were carried out on powdered samples of compounds of ordinary elements or separated isotopes with neutrons of 1.2 eV and 5.2 eV energy detected by means of rotating resonance detectors. From the measured total cross section the value of the scattering cross section at zero energy was obtained by taking into account the absorption, solid state effects and resonance contributions.

The following scattering cross sections have been determined:

^{19}F : σ_o = 3.64 ± 0.02 b
^{23}Na : σ_o = 3.03 ± 0.02 b
Mg : σ_o = 3.4140 ± 0.0024 b and
^{27}Al : σ_o = 1.4134 ± 0.0010 b.

The evaluation of these values and other data with the corresponding scattering lengths led to the following spin state scattering lengths (per bound nucleus)

^{13}C : b_+ = 4.8 ± 0.5 fm; b_- = 10.2 ± 1.6 fm
^{14}N : b_+ =10.7 ± 0.2 fm; b_- = 6.5 ± 0.3 fm
^{15}N : $b_+ = b_-$ = 6.45 (13) fm
^{19}F : b_+ = 5.56 ± 0.03 fm; b_- = 5.98 ± 0.10 fm
^{23}Na : b_+ = 6.457 ± 0.021 fm; b_- = -1.04 ± 0.02 fm
^{27}Al : b_+ = 3.22 ± 0.02 fm; b_- = 3.82 ± 0.02 fm.

Because of discrepancies in the published values for the fundamental neutron-proton scattering cross section at zero-energy we made a new experiment to measure σ_{np} at 1.2 eV and 5.2 eV neutron energy. Transmission measurements on H_2O, C_6H_6, C_2Cl_4 and CCl_4 yielded the following data:

O : σ_o = 3.76 ± 0.04 b

C : σ_o = 4.76 ± 0.02 b

Cl : σ_o = 15.9 ± 0.1 b and

H : σ_{np} = 20.401 ± 0.015 b.

The latter value is in fair agreement with the value 20.436 ± 0.023 b reported by Houk [1].

On the other hand, the new value is in sharp contradiction to the σ_{np} = 20.491 ± 0.014 b published by Dilg [2].

References

[1] T.L. Houk, Phys.Rev. C3 (1971) 1886

[2] W. Dilg, Phys.Rev. C11 (1975) 103

PHYSIKALISCH-TECHNISCHE BUNDESANSTALT (PTB)
BRAUNSCHWEIG

1. Radionuclide Data

1.1 Gamma-Ray Emission Probabilities

K. Debertin, W. Peßara, U. Schötzig, K.F. Walz

The radionuclides ^{67}Ga, ^{99m}Tc and ^{201}Tl have found wide applications in nuclear medicine. In medial practice, ^{99m}Tc ($T_{1/2}$ = 6.006 h) is usually extracted from a $^{99}Mo/^{99m}Tc$ generator while ^{67}Ga ($T_{1/2}$ = 3.2594 d) and ^{201}Tl ($T_{1/2}$ = 3.0375 d) are commercially supplied in directly applicable solutions. Gamma- and X-ray emission probabilities of these nuclides were determined by means of Ge(Li)-spectrometry. The emission probabilities per decay were calculated from relative emission rates either by forming the ground-state balance (^{99}Mo) or by deducing the number of K X-rays emitted per decay from the K-capture probability, the fluorescence yield and conversion coefficients.

Results for ^{67}Ga and ^{201}Tl have been forwarded for publication [1], those for $^{99}Mo/^{99m}Tc$ are given in Table I. The quoted uncertainties correspond to one standard deviation.

1.2 Half-lives

K.F. Walz, K. Debertin, U. Schötzig

Half-lives of ^{67}Ga, ^{111}In, ^{131}I, ^{154}Eu and ^{201}Tl were determined by following the radioactive decay with a high pressure ionization chamber. In addition, Ge(Li) measurements were carried out for ^{67}Ga and ^{201}Tl. Results are given in Table II. The quoted uncertainties correspond to one standard deviation and include systematic uncertainties.

Table I. Gamma-ray emission probabilities p per decay of ^{99}Mo in radioactive equilibrium with ^{99m}Tc

Energy in keV	p in %
140.5	90.5 ± 0.5
181.1	6.03 ± 0.07
366.4	1.22 ± 0.02
739.5	12.31 ± 0.09
777.9	4.33 ± 0.04
823.0	0.140 ± 0.005
960.7	0.099 ± 0.003

Table II. Half-lives of some radioisotopes

Nuclide	Half-life
^{67}Ga	(3.2594 ± 0.0012) d
^{111}In	(2.8045 ± 0.0008) d
^{131}I	(8.021 ± 0.001) d
^{154}Eu	(8.57 ± 0.07) a
^{201}Tl	(3.0380 ± 0.0007) d

2. Fission Yields

2.1 Fission Product Yields in ^{238}U Fission by ^{252}Cf-neutrons

K. Debertin

Because of the growing importance of fast reactors it is desirable to have more accurate ^{238}U fission yields in well defined neutron fields.

Three ^{238}U samples were irradiated in the PTB low scattering irradiation facility [2] which consists of a cylindrical ^{252}Cf source mounted to a mast 15 m above the ground in the open air. Two methods were applied for determining relative cumulative fission yields. Common to both is the simultaneous measurement of the activities of several fission products in irradiated uranium samples by recording the gamma-ray spectrum with a Ge(Li) detector. In the first method, gamma-ray emission probabilities are used to determine the fission product activities. The second evaluation method, also called R-value method, relates ^{238}U fast yields to ^{235}U thermal yields. This method demands additional measurements of ^{235}U samples irradiated in a thermal neutron field. As we did not determine the total number of fissions in the samples we obtained only relative yields.

In Table III we quote results obtained by both methods. Yields are given for 20 fission products with respect to a mass number 140 chain yield of 6.05 %. The uncertainties of our results are of the order of ± 2 % for high yield fission products. Further details were reported in a contribution to the "International Conference on Neutron Physics and Nuclear Data for Reactors and Other Applied Purposes", Harwell, 25th-29th September 1978 [3].

3. Neutron Cross Sections and Californium-252 Data

3.1 Covariance Matrix of Average Cross Sections Measured in the Neutron Field of Cf-252

W. Mannhart

Besides energy-dependent cross sections, valuable information on nuclear cross-section data is also contained in integral experiments (for example,

Table III. ^{238}U fast fission yields

Mass number	Fission yields in % *	
	Method 1	Method 2
88	2.38 (17)	2.38 (13)
91	4.16 (17)	3.98 (13)
92	4.68 (50)	4.37 (16)
95	5.30 (9)	5.16 (13)
97	5.81 (13)	5.71 (18)
99	6.64 (10)	6.49 (17)
103	6.25 (9)	6.30 (43)
105	3.87 (10)	4.06 (19)
127	0.175 (12)	0.164 (21)
129	0.67 (10)	0.49 (13)
131	3.41 (6)	3.18 (8)
132	5.32 (10)	5.14 (11)
133	6.98 (16)	6.74 (24)
135	7.34 (17)	7.35 (22)
138	6.84 (45)	6.55 (49)
140	6.05	6.05
142	4.26 (24)	4.60 (17)
143	4.73 (23)	4.64 (10)
147	2.43 (16)	2.68 (15)
151	0.80 (4)	0.90 (5)

*Uncertainties are given in parentheses in units of the last digit

in the measurement of average cross sections). The IAEA plans to distribute an "International Reactor Dosimetry File" (IRDF) [4] which includes the complete information available on neutron cross sections. The IRDF is thought as an extension of the ENDF/B Dosimetry File and will additionally contain information about neutron benchmark fields and average cross sections measured in these fields with the inclusion of the covariance matrices of both.
To generate a set of best average cross-section values for the IRDF, it is necessary to combine various experiments on the basis of their complete uncertainty information, i.e. including their covariance. As a first step the PTB-measurements of average cross sections in the Cf-252 neutron field [5,6] were reanalyzed to generate their covariance matrix. The result is given in Table IV as a correlation matrix. The strong correlations between the data are mainly due to the neutron source strength measurement and due to scattering corrections in the neutron source and in the detector foils. Similar work based on the data of other experiments is in progress.

3.2 Sensitivity Coefficients of Cf-252 Spectrum Averaged Cross Sections

W. Mannhart

To estimate the uncertainty of calculated average cross sections in comparing those data with experiments, it is necessary to combine the uncertainty resulting from the energy-dependent cross-section data and from the neutron spectrum with coefficients describing the influence of both quantities on the final value.

These coefficients, called sensitivity coefficients (or relative sensitivities), were calculated for a lot of reactions measured in the Cf-252 neutron field. Fig. 1 shows, as an example, sensitivity profiles of the reaction $^{27}Al(n,\alpha)$ based on the ENDF/B-IV neutron cross-section data. In the upper part of the figure, the relative uncertainty of the calculated average cross sections, $\langle\sigma\rangle$ due to a given relative uncertainty of the energy-dependent cross-section, $\sigma(E)$, is plotted per lethargy width. The figure shows, for example, that an uncertainty (or a change) of 10 % in $\sigma(E)$ between 8 MeV and 9 MeV results in an uncertainty (or a change) of 2.4 % in $\langle\sigma\rangle$. The lower part of the figure gives in a similar way the influence due to an error dE (in MeV) in the neutron energy scale of $\sigma(E)$. Here the given sign indicates an increase or a decrease in $\langle\sigma\rangle$.

Table IV. Correlation matrix of Cf-252 spectrum average cross sections

Reaction		<σ> (mb)																
$^{27}Al(n,\alpha)$	A*	1.006	±	2.14%	1.00													
$^{46}Ti(n,p)$	A	13.8	±	2.37%	0.74	1.00												
$^{47}Ti(n,p)$	A	18.9	±	2.29%	0.77	0.74	1.00											
$^{48}Ti(n,p)$	A	0.42	±	2.54%	0.69	0.77	0.69	1.00										
$^{54}Fe(n,p)$	A	84.6	±	2.36%	0.74	0.67	0.70	0.63	1.00									
$^{56}Fe(n,p)$	A	1.45	±	2.39%	0.74	0.67	0.69	0.62	0.71	1.00								
$^{58}Ni(n,p)$	A	118	±	2.35%	0.75	0.68	0.70	0.63	0.68	0.67	1.00							
$^{64}Zn(n,p)$	A	39.4	±	2.51%	0.70	0.64	0.66	0.59	0.64	0.63	0.64	1.00						
$^{113}In(n,n')$	B*	160	±	2.42%	0.73	0.66	0.68	0.61	0.66	0.65	0.66	0.62	1.00					
$^{115}In(n,\gamma)$	B	124.1	±	2.89%	0.61	0.55	0.57	0.51	0.55	0.55	0.55	0.52	0.77	1.00				
$^{115}In(n,n')$	A	198	±	2.53%	0.70	0.63	0.65	0.74	0.63	0.62	0.63	0.60	0.66	0.55	1.00			
$^{115}In(n,n')$	B	195	±	2.46%	0.71	0.65	0.67	0.60	0.65	0.64	0.65	0.61	0.90	0.75	0.67	1.00		
$^{197}Au(n,\gamma)$	B	76.2	±	2.38%	0.74	0.67	0.69	0.63	0.67	0.66	0.68	0.63	0.89	0.75	0.69	0.88	1.00	
$^{197}Au(n,2n)$	B	5.50	±	2.59%	0.68	0.62	0.64	0.57	0.62	0.61	0.62	0.58	0.82	0.69	0.63	0.80	0.87	1.00

A* : ref. [5]

B* : ref. [6]

$^{27}Al(n,\alpha)^{24}Na$ ENDF/B-IV

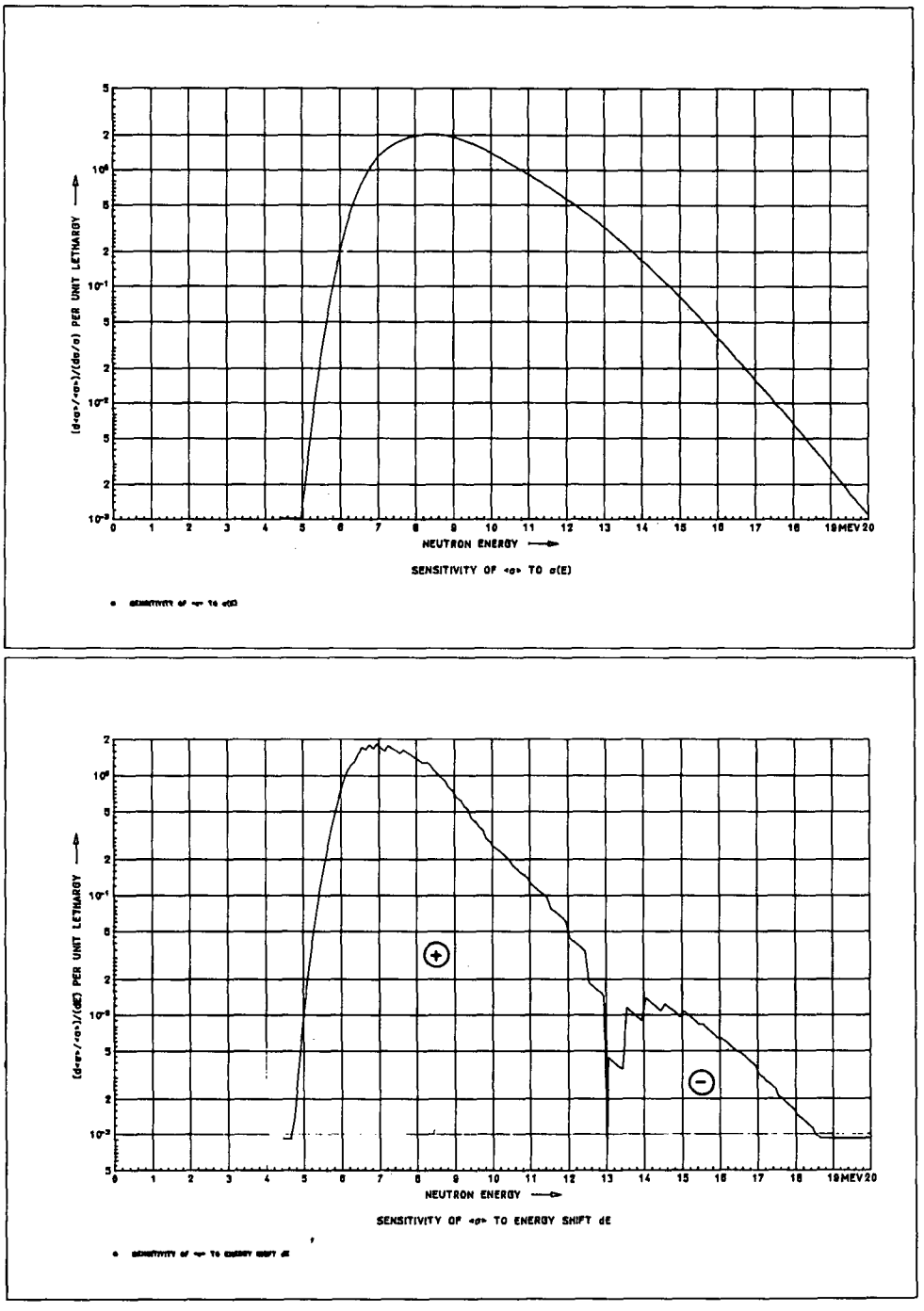

Fig. 1 Sensitivity profiles for the reaction $^{27}Al(n,\alpha)^{24}Na$.

3.3 Half-life of Californium-252

W.G. Alberts, W. Mannhart, M. Matzke

From neutron source strength measurements extended over a period of 5.3 years, the half-life of the spontaneous fission isotope Cf-252 was determined. The source strength measurements were performed with a waterbath method, i.e. the determination of the spatial distribution of neutrons thermalized in water with gold activation detectors. Whilst the source strength measurement has an uncertainty of ± 1.6 % (1σ-level), the determination of the half-life can be done more precisely as most of the uncertainty is due to corrections which are independent of the actual source strength value. The contribution due to neutrons from the isotopes ^{250}Cf and ^{254}Cf with half-lives of 61.9 days and 13.2 years, respectively, was corrected for. This time-dependent correction was of the order of 0.12 % up to 0.31 %. A preliminary result is:

$$T_{1/2}(^{252}Cf) = (2.6489 \pm 0.0024) \text{ years}$$

The quoted uncertainty corresponds to the 1σ-level and is mainly based on the fitting procedure. The most recent value from the literature is (2.638 ± 0.007) years [7].

4. Variable Energy Cyclotron
A New High-Precision Fast Neutron Time-of-Flight Facility

H.J. Brede, G. Dietze, R. Jahr, H. Klein, D. Schlegel-Bickmann, H. Schölermann, B. Siebert

The progress achieved in setting up the time-of-flight facility described in the last year's report was as follows:

The stability of the pulsed cyclotron was greatly improved by replacing the original power supplies for the magnetic trim coils and the harmonic coils by more stable ones. A redesign of the deflector modulator reduced the intensity of satellite pulses by an order of magnitude. In addition the pulsed beam current available at the target increased by a factor of two.

The Monte-Carlo calculations for the optimization of the collimator were completed and a detailed description of the calculations and the results which include the calculated neutron background due to various sources, was published [8]. According to these guide lines the collimator was constructed, set up and adjusted with an accuracy of better than 0.3 mm. The total mass amounts to about 110 t.

The design of the liquid scintillation counters (NE 213, 25 cm in diameter and 5 cm in thickness) with an optimized light guide has been completed. The results will be published shortly [9].

First experiments revealed the requirement of continuously monitoring the primary neutrons which are emitted from the gas-target by means of a shielded TOF - detector. Consequently, an optimized collimator shield for a small NE 213 spectrometer is mounted on a separate swivel-arm. The neutron production can be monitored in forward direction (20^{o}) for all scattering angles moving the cyclotron and the monitor simultaneously.

The experimental neutron scattering data are to be corrected in general since the finite geometry of source, scattering sample and detector cause attenuation, multiple scattering and finite resolution in angle and energy. Multiple scattering will be corrected iteratively by means of standard Monte-Carlo simulation, while the flux attenuation, the source characteristics and finite angular resolution are taken into account by a new technique. In a separate Monte-Carlo run we compute the moments of the cosine of the scattering angles. These moments, the normalized number of detector events and the Legendre expansion coefficients define an overdetermined system of linear equations, which may be solved by means of matrix inversion codes. A computer program based on this new correction technique is being developed.

References

[1] K. Debertin, W. Peßara, U. Schötzig, K.F. Walz, Decay data of ^{67}Ga and ^{201}Tl, Int. J. appl. Radiat. Isotopes, to be published

[2] W.G. Alberts, J. Bortfeldt, E. Günther, K. Knauf, M. Matzke, G. Rassl, V. Siegel, K.F. Walz, Proc. Conf. on Nuclear Cross Sections and Technology, Vol. I, NBS Special Publication 425 (1975) p. 273

[3] K. Debertin, Fission product yields in ^{238}U fission by ^{252}Cf-neutrons, Proc. Int. Conf. on Neutron Physics and Nuclear Data for Reactors and Other Applied Purposes, Harwell (September 1978) p. 229

[4] A. Lorenz, Report INDC(NDS)-100/M (January 1979)

[5] W.G. Alberts, E. Günther, M. Matzke, G. Rassl, Proc. First ASTM-EURATOM Symp. Reactor Dosimetry, EUR 5667 e/f, Part I (1975) p.131

[6] W. Mannhart, W.G. Alberts, Nucl. Sci. Eng. 69 (1979) 333

[7] V. Spiegel, Nucl. Sci. Eng. 53 (1974) 326

[8] D. Schlegel-Bickmann, Report ND-14 (January 1979), Physikalisch-Technische Bundesanstalt, Braunschweig

[9] H. Klein, H. Schölermann, Contribution to the 1978 Nuclear Science Symposium, October 18-20, 1978, Washington D.C., to be published in IEEE-Transact. on Nucl. Sci.

INSTITUT FÜR KERNENERGETIK UND ENERGIESYSTEME
UNIVERSITÄT STUTTGART

1. Study of Nuclear Data Requirements for the Application of Fast Neutrons in Radiation Therapy

G. Pfister, G. Hehn, H.P. Friedlein, M. Mattes

1.1 Calculations for Neutron Generators used in Cancer Treatment

Transport calculations have been performed to optimize the neutron collimator and source shielding [1, 2]. The main effort is devoted to accurate determination of the depth dose of neutrons and secondary gamma rays in the patient. Neutron spectra were calculated to predict local changes of the tissue response and the mean RBE [3, 4]. Energy flux spectra of the secondary charged recoils in tissue were calculated [5] to apply cell kinetic models for the simulation of cell reactions induced by radiation.

1.2 The IKE Cross Section Sensitivity and Uncertainty Analysis Code System

For the target quantities as kerma of neutrons and secondary gamma rays and RBE-dose of interest in the patient, the requirements of neutron data have been determined [6].

For studying the relationships beween uncertainties in nuclear reaction cross sections and the accuracy of calculated integral responses several computer programs were combined to a code system shown in Fig. 1. This system includes multigroup cross section processing, uncertainty file processing, transport calculations, sensitivity profile generation, uncertainty analysis, and plotting routines.

Starting from the Evaluated Nuclear Data File ENDF/B-IV a coupled neutron and gamma multigroup cross section library EURLIB-4 with 100 neutron groups and 20 gamma groups was generated by the use of the codes MINX, LAPHAN, and SMUG. For the use in the sensitivity and uncertainty analysis EURLIB-4 was extended to include partial scattering matrices.

Uncertainty analysis requires multigroup covariance matrices. These are produced from ENDF/B-IV format uncertainty files by the PUFF code. The matrices are placed in the Multigroup Covariance Matrix Library in the COVERX format.

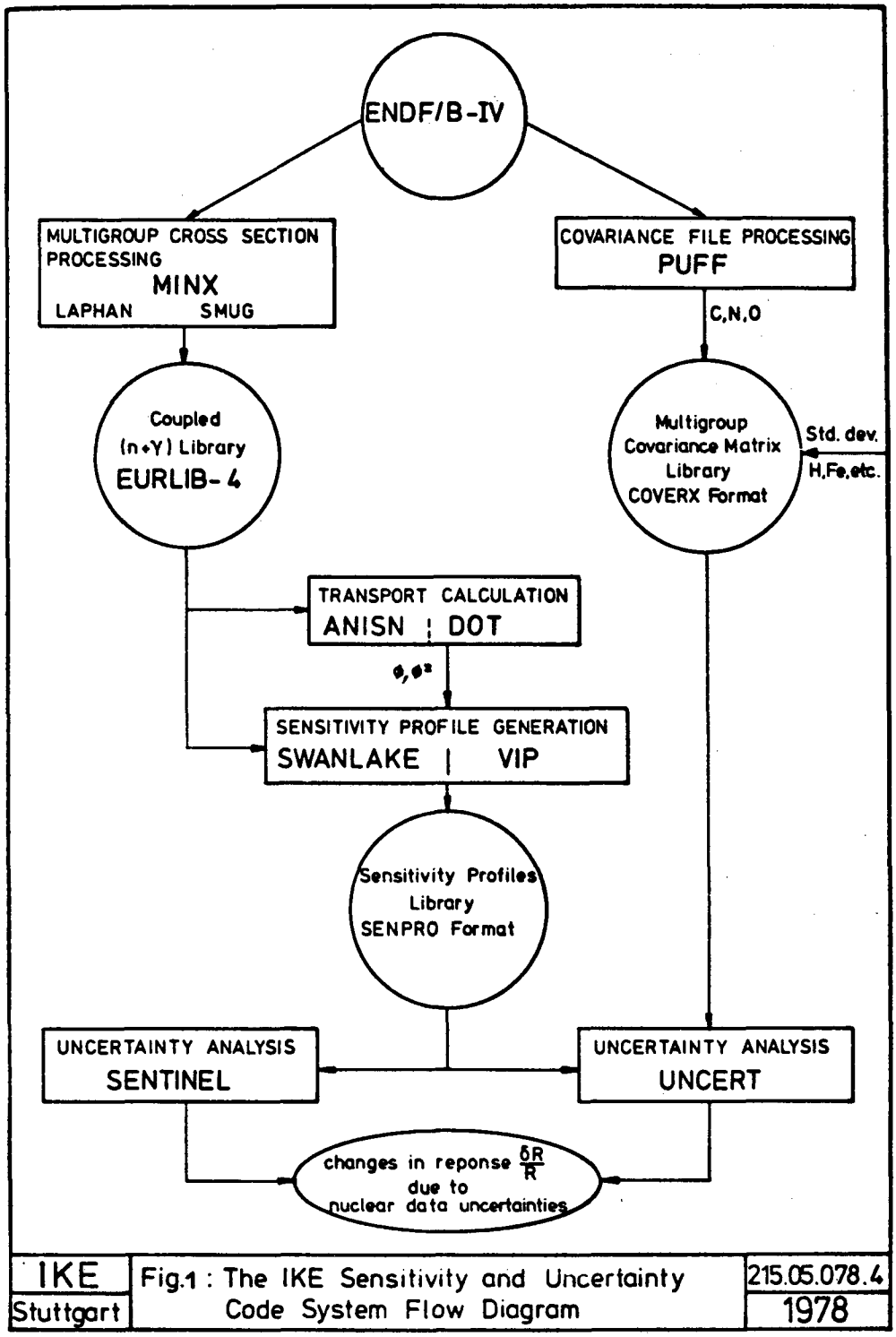

Fig. 1 The IKE sensitivity and uncertainty code system flow diagram.

In ENDF/B-IV uncertainty files are available only for carbon, nitrogen, and oxygen. For further materials we use the estimates of the uncertainties in the evaluated cross sections to generate uncorrelated and fully (+ 1) correlated relative covariance matrices. In addition to C, N, and O we need H and Fe covariance matrices to represent tissue and collimator materials.

SWANLAKE calculates the sensitivity of a target quantity such as dose or reaction rate obtained from a one-dimensional discrete ordinates solution of the Boltzmann transport equation to the cross sections used in the calculation. In the linear perturbation theory applied by SWANLAKE forward adjoint transport calculations in one-dimensional (ANISN) or two-dimensional (DOT) geometry are required together with microscopic cross-section sets. The sensitivity coefficients calculated by SWANLAKE are placed in the SENPRO format.

Using the sensitivity profiles the SENTINEL module computes the percentage change in the integral response of a given therapy unit due to specified percentage changes in designated reaction cross sections over a number of energy regions.

When COVERX and SENPRO libraries are available, uncertainty analysis may be initiated. The UNCERT module folds the sensitivity profiles (SENPRO) and the relative covariance matrices (COVERX) to estimate changes in the response which result from uncertainties in nuclear data.

1.3 Nuclear Data Requirements in Radiation Treatment Planning

For the improvement of treatment planning in neutron therapy the depth dose of neutron and secondary gamma rays must be determined with high precision. Energy spectra of neutrons and their recoil particles produced in tissue must be calculated if biological effects have to be compared between different neutron therapy facilities.

We have shown quantitatively that the nuclear data available are sufficient for cyclotron facilities with a mean neutron energy of about 7 MeV. But most neutron therapy units are (D,T)-generators with 15 MeV neutrons and for these generators the nuclear data evaluated in ENDF/B-IV are not sufficient. The uncertainty in the neutron cross sections,especially of the inelastic scattering cross section of carbon and oxygen,contributes to the error of kerma and RBE-dose in the tumor with 8 %, which is a factor of three too high compared with the target accuracy specified. For carbon and oxygen the uncertainties of the inelastic cross sections should be reduced,especially

above 12 MeV.

In earlier studies [3, 5] we have shown that for 15 MeV generators the portions of alpha particles to the kerma in the tumor region reaches 6 - 10 % resulting in a higher contribution to the RBE-dose. Therefore we need an improved accuracy of neutron cross sections with α-production in carbon and oxygen.

References

[1] G. Pfister, Untersuchungen zur optimalen Kollimation schneller Neutronen für die Neutronentherapie, IKE-Bericht 6 - 73D (1973)

[2] H.P. Friedlein, Neutronenspektrum und Tiefendosisverlauf im Wasserphantom für das Neutronentherapiegerät CIRCE mit Fehleranalyse, IKE-Bericht 6D - 14 (1979)

[3] J.K. Böhm, H.M. Eissa, G. Hehn, G. Pfister, G. Stiller, Transport calculations, analytical representations of absorbed dose and determination of isoeffect curves for therapy with fast neutrons, EUR 5848 DE/EN/FR, (1977)

[4] G. Pfister, J.K. Böhm, G. Hehn, G. Prillinger, Computer treatment planning for neutron therapy including radiobiological effects, 6th Int. Conf. on the use of Computers in Radiation Therapy, Göttingen (September 1977)

[5] G. Pfister, P. Stiller, G. Hehn, Recoil spectra in neutron irradiated tissues and TE-materials, 6th Symp. on Microdosimetry, Brussels (May 1978)

[6] G. Pfister, G. Hehn, M. Mattes, H.P. Friedlein, Nuclear data requirements for the calculation of absorbed dose and simulation of tissue response in neutron therapy, Proc.Int.Conf. on Neutron Physics and Nuclear Data for Reactors and other applied Purposes, Harwell (September 1978) p.

INSTITUT FUR KERNCHEMIE
PHILIPPS-UNIVERSITÄT MARBURG

1. Gamma-Ray Catalog

U. Reus, W. Westmeier, I. Warnecke*

The evaluation of cross sections for products of nuclear reactions requires comprehensive and reliable data compilations. As most of the available tables are out of date, we have put together a new compilation of properties of all known radionuclides with main emphasis on energies and absolute intensities of gamma rays which are emitted in the radioactive decay. References through June 1978 have been used.

The catalog covers data on 2311 nuclides and isomers with a total of more than 35,000 gamma energies. It is presented in two parts:
PART I is a listing of gamma rays in order of increasing energy. For reasons of practicability, only energies with absolute intensities of $\geq$ 0.5 percent are listed, except for nuclides where only very weak transitions are known.
PART II is a listing of properties of stable and radioactive nuclides ordered by mass number A and nuclear charge Z. Information on references, nuclear spin, decay modes, precursors in the radioactive decay, thermal neutron cross sections (for stable nuclides) and comments about the reliability of the data are also given in this part.

Copies of the catalog are available on request.

2. Alpha-Energy Table

W. Westmeier, R.A. Esterlund

A compilation of alpha-decay properties of all alpha-emitting nuclides, which includes data on alpha energies, intensities and the abundance of the alpha branch, is permanently being updated. The table is ordered by increasing energy and covers data on 502 alpha emitters with a total of 1518 energies at present.

Computer printout copies of the table are available on request.

---

* Gesellschaft für Schwerionenforschung mbH (GSI), Darmstadt

FACHINFORMATIONSZENTRUM ENERGIE PHYSIK MATHEMATIK

Status Report

H. Behrens, J.W. Tepel

1. Information System for Physics Data in the Federal Republic of Germany

This project has been described in the last Progress Reports NEANDC (E) - 172 U Vol. V, NEANDC (E) - 182 U Vol. V and NEANDC (E) - 192 U Vol. V. No details are therefore given here.

2. New Data Compilations

The following issues in the series Physics Data were published in the meantime:

3-3 (1978) : Datensammlungen in der Physik. Data Compilations in Physics. H. Behrens, G. Ebel. 74 pages. Supplement to No. 3-1 and 3-2 containing about 350 further references to tables and compilations.

4-2 (1979) : Compilations of Coupling Constants and Low-energy Parameters. M.M. Nagels, Th.A. Rijken, J.J. de Swart, G.C. Oades, J.L. Petersen, A.C. Irving, C. Jarlskog, W. Pfeil, H. Pilkuhn, H.P. Jakob

5-4 (1978) : Gases and Carbon in Metals (Thermodynamics, Kinetics and Properties). Part IV: Actinines (U, Th, Pu, Pa, Np, Am, Cm, Bk, Cf). H. Jehn, E. Fromm, G. Hörz

10-1 (1978) : Graphs of Neutron Cross Sections of Fission Product Isotopes from FPLIB 65/ENDF/B-IV. M. Mattes

11-1 (1979) : Nucleon-Nucleon Scattering Data. J. Bystricky, F. Lehar

12-1 (1979) : Handbook of Pion-Nucleon Scattering. G. Höhler, F. Kaiser, R. Koch, E. Pietarinen

13-1 (1979) : Evaluation of the Cross Sections for the Reactions $^{24}Mg(n,p)^{24}Na$, $^{64}Zn(n,p)^{64}Cu$, $^{63}Cu(n,2n)^{62}Cu$ and $^{90}Zr(n,2n)^{89}Zr$. S. Tagesen, H. Vonach, B. Strohmaier

14-1 (1979) : Compilation of Data from Hadronic Atoms.
H. Poth

Further data compilations on internal conversion coefficients and on charged particle reaction data are in preparation.

3. Bibliography of Existing Data Compilations

As mentioned under 2 a supplement has been issued to this worldwide survey of all existing physics data compilations, and another supplement is planned.

4. The Evaluated Nuclear Structure Data File (ENSDF)

The contribution of the Fachinformationszentrum Energie, Physik, Mathematik GmbH to the national collaboration in the evaluation of nuclear structure data (ENSDF) was reported in detail in the 1978 Progress Report. In the meantime the data on mass chain A = 86 have been published (J.W. Tepel, Nuclear Data Sheets 25 (1978) 553) and on two further chains, viz. A = 84 and 87, have been completed and are to appear in Nuclear Data Sheets. Data on three further mass chains, viz. A = 85, 91, and 92 are in preparation.

The bibliographic data file associated with ENSDF, the "Nuclear Structure References" of NSR, is implemented on our computer and enables us to decode references appearing in the ENSDF-file. The programmes needed for this operation were developed. Regular updates of NSR are provided via the Brookhaven National Laboratory.

Several data analysis programmes (ADINF, LEVINF, OLGA) were developed at the Fachinformationszentrum Energie, Physik, Mathematik and programmes from Oak Ridge (MEDLIST, ANCOR, ADOPFIT, COMPARE, DATACK, GBRANCH, TRANLOC) were adapted to our Siemens 7.755 installation. An application of the data bank was reported at the International Conference on the Dynamical Properties of Heavy-ion Reactions held at Johannesburg in August 1978. The title of the report was: "Dynamical properties of deformed nuclei deduced from the Evaluated Nuclear Structure Data File".

APPENDIX I

Addresses of Contributing Laboratories

Institut für Angewandte Kernphysik II
Director: Prof.Dr. G. Schatz
Senior reporters: Dr. S.W. Cierjacks
Dr. F. Käppeler
Kernforschungszentrum Karlsruhe
Postfach 3640
7500 Karlsruhe

Institut für Kernphysik I
Director: Prof.Dr. B. Zeitnitz
Senior reporter: Dr. H.O. Klages
Kernforschungszentrum Karlsruhe
Postfach 3640
7500 Karlsruhe

Institut für Neutronenphysik und Reaktortechnik
Director: Dr. G. Keßler
Senior reporter: Dr. F.H. Fröhner
Kernforschungszentrum Karlsruhe
Postfach 3640
7500 Karlsruhe

Institut für Chemie (1): Nuklearchemie
Director: Prof.Dr. G. Stöcklin
Senior reporter: Dr. S.M. Qaim
Kernforschungsanlage Jülich
Postfach 1913
5170 Jülich

Institut für Kernphysik:
Experimentelle Kernphysik II
Director: Prof.Dr. O. Schult
Senior reporter: Dr. H. Seyfarth
Kernforschungsanlage Jülich
Postfach 1913
5170 Jülich

Zentralabteilung für Chemische Analysen
Head: Prof.Dr. B. Sansoni
Senior reporter: Dr. G. Erdtmann
Kernforschungsanlage Jülich
Postfach 1913
5170 Jülich

I. Institut für Experimentalphysik
Director: Prof.Dr. H. Neuert
Senior reporter: Prof.Dr. W. Scobel
Universität Hamburg
Luruper Chaussee 149
2000 Hamburg 50

Institut für Kernchemie
Director: Prof.Dr. W. Herr
Senior reporter: Dr. R. Michel
Universität zu Köln
Zülpicher Str. 47
5000 Köln

Institut für Kernchemie
Director: Prof.Dr. G. Herrmann
Senior reporters: Prof.Dr. H.O. Denschlag
Dr. K.L. Kratz
Johannes Gutenberg-Universität Mainz
Friedrich von Pfeiffer Weg 14
6500 Mainz

Fachbereich Physik der
Technischen Universität München
Abteilung E14, Forschungsreaktor
Head and senior reporter: Prof.Dr. L. Köster
8046 Garching/München

Physikalisch-Technische Bundesanstalt
Abteilung 6, Atomphysik
Director: Prof.Dr. S. Wagner
Senior reporter: Dr. W. Mannhart
Bundesallee 100
3300 Braunschweig

Institut für Kernenergetik und Energiesysteme
Director: Prof.Dr. K.-H. Höcker
Senior reporter: G. Pfister
Universität Stuttgart
Pfaffenwaldring 31
7000 Stuttgart 80

Institut für Kernchemie
Senior reporter: Prof.Dr. P. Patzelt
Philipps-Universität Marburg
Lahnberge
3550 Marburg/Lahn

Fachinformationszentrum Energie, Physik und Mathematik
Director: Dr. W. Rittberger
Senior reporter: Dr. H. Behrens
Kernforschungszentrum
7514 Eggenstein-Leopoldshafen 2

APPENDIX II

CINDA Type Index

ELEMENT S	A	QUANTITY	TYPE	ENERGY MIN	ENERGY MAX	DOCUMENTATION REF	VOL	PAGE	DATE	LAB	COMMENTS
NN	001	DIFF ELASTIC	COMP-PROG	30+8	59+8	NEANDC(E)-202U	679			IKA	VOL.5.P.99.BYSTRICKY+PHYS DATA SERIE
NN	001	TOTAL	COMP-PROG	88+7	83+9	NEANDC(E)-202U	679			IKA	VOL.5.P.99.BYSTRICKY+PHYS DATA SERIE
H	001	N,PROTON	COMP-PROG	10+0	+9	NEANDC(E)-202U	679			IKA	VOL.5.P.99.BYSTRICKY+PHYS DATA SERIE
H	001	THERMAL SCAT	EXPT-PROG	ZERO		NEANDC(E)-202U	679			MUN	VOL.5.P.82.KOESTER+ SCAT SIG
H	001	TOTAL	EXPT-PROG	20+6	40+7	NEANDC(E)-202U	679			KFK	VOL.5.P.27.BENTE+ TRANS TOF, NDG
D	002	TOTAL	EXPT-PROG	20+6	40+7	NEANDC(E)-202U	679			KFK	VOL.5.P.27.BENTE+ TRANS TOF, NDG
HE	003	TOTAL	EXPT-PROG	10+6	40+7	NEANDC(E)-202U	679			KFK	VOL.5.P.26.HAESNER+ TRANS TOF
HE	004	TOTAL	EXPT-PROG	10+6	40+7	NEANDC(E)-202U	679			KFK	VOL.5.P.26.HAESNER+ TRANS TOF
B	010	TOTAL	EXPT-PROG	90+4	42+5	NEANDC(E)-202U	679			KFK	VOL.5.P.24.BEER. RES ANAL
C		THERMAL SCAT	EXPT-PROG	ZERO		NEANDC(E)-202U	679			MUN	VOL.5.P.82.KOESTER+ SCAT SIG
C		RESON PARAMS	EXPT-PROG	30+6	30+7	NEANDC(E)-202U	679			KFK	VOL.5.P.1.CIERJACKS+TRANS TOF,RES EN
C	012	THERMAL SCAT	EXPT-PROG	NDG		NEANDC(E)-202U	679			MUN	VOL.5.P.81.KOESTER+ COH SCAT LENGTH
C	013	THERMAL SCAT	EXPT-PROG	NDG		NEANDC(E)-202U	679			MUN	VOL.5.P.81.KOESTER+ COH SCAT LENGTH
C	013	THERMAL SCAT	EXPT-PROG	ZERO		NEANDC(E)-202U	679			MUN	VOL.5.P.82.KOESTER+ SPIN SCAT LENGTH
N	014	THERMAL SCAT	EXPT-PROG	NDG		NEANDC(E)-202U	679			MUN	VOL.5.P.81.KOESTER+ COH SCAT LENGTH
N	014	THERMAL SCAT	EXPT-PROG	ZERO		NEANDC(E)-202U	679			MUN	VOL.5.P.82.KOESTER+ SPIN SCAT LENGTH
N	015	THERMAL SCAT	EXPT-PROG	ZERO		NEANDC(E)-202U	679			MUN	VOL.5.P.82.KOESTER+ SPIN SCAT LENGTH
N	015	THERMAL SCAT	EXPT-PROG	NDG		NEANDC(E)-202U	679			MUN	VOL.5.P.81.KOESTER+ COH SCAT LENGTH
O		RESON PARAMS	EXPT-PROG	30+6	30+7	NEANDC(E)-202U	679			KFK	VOL.5.P.1.CIERJACKS+TRANS TOF,RES EN
O		THERMAL SCAT	EXPT-PROG	ZERO		NEANDC(E)-202U	679			MUN	VOL.5.P.82.KOESTER+ SCAT SIG
O	016	N,GAMMA	EXPT-PROG	PILE		NEANDC(E)-202U	679			JUL	VOL.5.P.45.WUEST+ 187 MICROB
O	016	THERMAL SCAT	EXPT-PROG	NDG		NEANDC(E)-202U	679			MUN	VOL.5.P.81.KOESTER+ COH SCAT LENGTH
O	017	THERMAL SCAT	EXPT-PROG	NDG		NEANDC(E)-202U	679			MUN	VOL.5.P.81.KOESTER+ COH SCAT LENGTH
O	018	THERMAL SCAT	EXPT-PROG	NDG		NEANDC(E)-202U	679			MUN	VOL.5.P.81.KOESTER+ COH SCAT LENGTH
F	019	THERMAL SCAT	EXPT-PROG	NDG		NEANDC(E)-202U	679			MUN	VOL.5.P.81.KOESTER+ COH SCAT LENGTH
F	019	THERMAL SCAT	EXPT-PROG	ZERO		NEANDC(E)-202U	679			MUN	VOL.5.P.82.KOESTER+ SCAT SIG
F	019	THERMAL SCAT	EXPT-PROG	ZERO		NEANDC(E)-202U	679			MUN	VOL.5.P.82.KOESTER+ SPIN SCAT LENGTH
NE	020	TOTAL	EXPT-PROG	+6		NEANDC(E)-202U	679			KFK	VOL.5.P.27.ABDEL-WAHAB+ NDG
NA	023	THERMAL SCAT	EXPT-PROG	ZERO		NEANDC(E)-202U	679			MUN	VOL.5.P.82.KOESTER+ SCAT SIG

ELEMENT S	A	QUANTITY	TYPE	ENERGY MIN	ENERGY MAX	DOCUMENTATION REF	VOL	PAGE	DATE	LAB	COMMENTS
NA	023	THERMAL SCAT	EXPT-PROG	ZERO		NEANDC(E)-202U	679			MUN	VOL.5.P.82.KOESTER+ SPIN SCAT LENGTH
MG		THERMAL SCAT	EXPT-PROG	NDG		NEANDC(E)-202U	679			MUN	VOL.5.P.81.KOESTER+ COH SCAT LENGTH
MG		THERMAL SCAT	EXPT-PROG	ZERO		NEANDC(E)-202U	679			MUN	VOL.5.P.82.KOESTER+ SCAT SIG
MG	024	N,PROTON	EVAL-PROG	50+6	21+7	NEANDC(E)-202U	679			IKA	VOL.5.P.99.TAGESEN+ PHYS DATA SERIES
AL	027	THERMAL SCAT	EXPT-PROG	ZERO		NEANDC(E)-202U	679			MUN	VOL.5.P.82.KOESTER+ SCAT SIG
AL	027	THERMAL SCAT	EXPT-PROG	ZERO		NEANDC(E)-202U	679			MUN	VOL.5.P.82.KOESTER+ SPIN SCAT LENGTH
AL	027	N,ALPHA	EXPT-PROG	FISS		NEANDC(E)-202U	679			PTB	VOL.5.P.86.MANNHART.SENSITIVITY COEF
P	031	N,HELIUM3	EXPT-PROG	15+4		NEANDC(E)-202U	679			JUL	VOL.5.P.39.QAIM+SIG SYSTEMATICS,GRPH
CL		THERMAL SCAT	EXPT-PROG	ZERO		NEANDC(E)-202U	679			MUN	VOL.5.P.82.KOESTER+ SCAT SIG
K	041	N,HELIUM3	EXPT-PROG	15+4		NEANDC(E)-202U	679			JUL	VOL.5.P.39.QAIM+SIG SYSTEMATICS,GRPH
SC	045	N,HELIUM3	EXPT-PROG	15+4		NEANDC(E)-202U	679			JUL	VOL.5.P.39.QAIM+SIG SYSTEMATICS,GRPH
TI	046	N,PROTON	EXPT-PROG	FISS		NEANDC(E)-202U	679			PTB	VOL.5.P.86.MANNHART.SENSITIVITY COEF
TI	047	N,PROTON	EXPT-PROG	FISS		NEANDC(E)-202U	679			PTB	VOL.5.P.86.MANNHART.SENSITIVITY COEF
TI	048	N,PROTON	EXPT-PROG	FISS		NEANDC(E)-202U	679			PTB	VOL.5.P.86.MANNHART.SENSITIVITY COEF
CR	050	N,N PROTON	EXPT-PROG	FISS		NEANDC(E)-202U	679			JUL	VOL.5.P.39.QAIM+ NDG
CR	050	RESON PARAMS	THEO-PROG	56+3	13+5	NEANDC(E)-202U	679			KFK	VOL.5.P.8.BEER.WG VALENCE-MDL CALC
CR	052	RESON PARAMS	THEO-PROG	50+4	14+5	NEANDC(E)-202U	679			KFK	VOL.5.P.8.BEER.WG VALENCE-MDL CALC
CR	054	RESON PARAMS	THEO-PROG	23+4	27+5	NEANDC(E)-202U	679			KFK	VOL.5.P.8.BEER.WG VALENCE-MDL CALC
FE	054	N,PROTON	EXPT-PROG	FISS		NEANDC(E)-202U	679			PTB	VOL.5.P.86.MANNHART.SENSITIVITY COEF
FE	054	RESON PARAMS	THEO-PROG	77+3	17+5	NEANDC(E)-202U	679			KFK	VOL.5.P.8.BEER.WG VALENCE-MDL CALC
FE	056	N,PROTON	EXPT-PROG	FISS		NEANDC(E)-202U	679			PTB	VOL.5.P.86.MANNHART.SENSITIVITY COEF
FE	056	RESON PARAMS	EXPT-PROG	10+4	60+4	NEANDC(E)-202U	679			KFK	VOL.5.P.3.WISSHAK+27.7KEV WN S-WAVE
FE	056	RESON PARAMS	THEO-PROG	27+4	14+5	NEANDC(E)-202U	679			KFK	VOL.5.P.8.BEER.WG VALENCE-MDL CALC
FE	058	N,GAMMA	EXPT-PROG	50+3	40+5	NEANDC(E)-202U	679			KFK	VOL.5.P.6.KAEPPELER+ PRELIM GRPH,TBC
FE	058	RESON PARAMS	THEO-PROG	10+4	18+5	NEANDC(E)-202U	679			KFK	VOL.5.P.8.BEER.WG VALENCE-MDL CALC
CO	059	N,HELIUM3	EXPT-PROG	15+4		NEANDC(E)-202U	679			JUL	VOL.5.P.39.QAIM+SIG SYSTEMATICS,GRPH
NI	058	N,ALPHA	EXPT-PROG	FISS		NEANDC(E)-202U	679			JUL	VOL.5.P.39.QAIM+ NDG
NI	058	N,N PROTON	EXPT-PROG	FISS		NEANDC(E)-202U	679			JUL	VOL.5.P.39.QAIM+ NDG
NI	058	N,PROTON	EXPT-PROG	FISS		NEANDC(E)-202U	679			PTB	VOL.5.P.86.MANNHART.SENSITIVITY COEF

ELEMENT S	A	QUANTITY	TYPE	ENERGY MIN	ENERGY MAX	DOCUMENTATION REF	VOL	PAGE	DATE	LAB	COMMENTS
NI	058	RESON PARAMS	THEO-PROG	15+4	12+5	NEANDC(E)-202U	679			KFK	VOL.5.P.8.BEER.WG VALENCE-MDL CALC
NI	060	RESON PARAMS	THEO-PROG	13+4	16+5	NEANDC(E)-202U	679			KFK	VOL.5.P.8.BEER.WG VALENCE-MDL CALC
NI	062	N,ALPHA	EXPT-PROG	FISS		NEANDC(E)-202U	679			JUL	VOL.5.P.39.QAIM+ NDG
NI	062	RESON PARAMS	THEO-PROG	45+3	11+5	NEANDC(E)-202U	679			KFK	VOL.5.P.8.BEER.WG VALENCE-MDL CALC
NI	064	RESON PARAMS	THEO-PROG	14+4	34+4	NEANDC(E)-202U	679			KFK	VOL.5.P.8.BEER.WG VALENCE-MDL CALC
CU	063	N,HELIUM3	EXPT-PROG	15+4		NEANDC(E)-202U	679			JUL	VOL.5.P.39.QAIM+SIG SYSTEMATICS,GRPH
CU	063	N,2N	EVAL-PROG	12+7	20+7	NEANDC(E)-202U	679			IKA	VOL.5.P.99.TAGESEN+ PHYS DATA SERIES
ZN	064	N,PROTON	EXPT-PROG	FISS		NEANDC(E)-202U	679			PTB	VOL.5.P.86.MANNHART.SENSITIVITY COEF
ZN	064	N,PROTON	EVAL-PROG	10+6	20+7	NEANDC(E)-202U	679			IKA	VOL.5.P.99.TAGESEN+ PHYS DATA SERIES
GA	071	N,HELIUM3	EXPT-PROG	15+4		NEANDC(E)-202U	679			JUL	VOL.5.P.39.QAIM+SIG SYSTEMATICS,GRPH
AS	075	N,HELIUM3	EXPT-PROG	15+4		NEANDC(E)-202U	679			JUL	VOL.5.P.39.QAIM+SIG SYSTEMATICS,GRPH
BR	081	N,HELIUM3	EXPT-PROG	15+4		NEANDC(E)-202U	679			JUL	VOL.5.P.39.QAIM+SIG SYSTEMATICS,GRPH
KR		N,GAMMA	EXPT-PROG	20+3	25+5	NEANDC(E)-202U	679			KFK	VOL.5.P.10.LEUGERS+ PRELIM GRPH
RB		THERMAL SCAT	EXPT-PROG	NDG		NEANDC(E)-202U	679			MUN	VOL.5.P.81.KOESTER+ COH SCAT LENGTH
RB	085	THERMAL SCAT	EXPT-PROG	NDG		NEANDC(E)-202U	679			MUN	VOL.5.P.81.KOESTER+ COH SCAT LENGTH
RB	087	THERMAL SCAT	EXPT-PROG	NDG		NEANDC(E)-202U	679			MUN	VOL.5.P.81.KOESTER+ COH SCAT LENGTH
ZR	090	N,2N	EVAL-PROG	12+7	20+7	NEANDC(E)-202U	679			IKA	VOL.5.P.99.TAGESEN+ PHYS DATA SERIES
NB	093	N,HELIUM3	EXPT-PROG	15+4		NEANDC(E)-202U	679			JUL	VOL.5.P.39.QAIM+SIG SYSTEMATICS,GRPH
TC	099	N,HELIUM3	EXPT-PROG	15+4		NEANDC(E)-202U	679			JUL	VOL.5.P.39.QAIM+SIG SYSTEMATICS,GRPH
RH	103	N,HELIUM3	EXPT-PROG	15+4		NEANDC(E)-202U	679			JUL	VOL.5.P.39.QAIM+SIG SYSTEMATICS,GRPH
IN	113	TOTAL	EXPT-PROG	FISS		NEANDC(E)-202U	679			PTB	VOL.5.P.86.MANNHART.SENSITIVITY COEF
IN	115	N,GAMMA	EXPT-PROG	FISS		NEANDC(E)-202U	679			PTB	VOL.5.P.86.MANNHART.SENTITIVITY COEF
IN	115	TOTAL	EXPT-PROG	FISS		NEANDC(E)-202U	679			PTB	VOL.5.P.86.MANNHART.SENSITIVITY COEF
IN	115	N,HELIUM3	EXPT-PROG	15+4		NEANDC(E)-202U	679			JUL	VOL.5.P.39.QAIM+SIG SYSTEMATICS,GRPH
SN		THERMAL SCAT	EXPT-PROG	NDG		NEANDC(E)-202U	679			MUN	VOL.5.P.81.KOESTER+ COH SCAT LENGTH
TE	123	N,ALPHA	EXPT-PROG	PILE		NEANDC(E)-202U	679			JUL	VOL.5.P.45.ALDEA+ PARTIAL SIG
CS	133	N,HELIUM3	EXPT-PROG	15+4		NEANDC(E)-202U	679			JUL	VOL.5.P.39.QAIM+SIG SYSTEMATICS,GRPH
BA	138	N,GAMMA	EXPT-PROG	18+4		NEANDC(E)-202U	679			KFK	VOL.5.P.12.BEER. VDG ACT,TBL
CE	140	N,GAMMA	EXPT-PROG	21+4		NEANDC(E)-202U	679			KFK	VOL.5.P.12.BEER. VDG ACT,TBL

ELEMENT S	A	QUANTITY	TYPE	ENERGY MIN	ENERGY MAX	DOCUMENTATION REF	VOL	PAGE	DATE	LAB	COMMENTS
CE	142	N,GAMMA	EXPT-PROG	21+4		NEANDC(E)-202U	679			KFK	VOL.5.P.12.BEER. VDG ACT,TBL
CE	142	N,HELIUM3	EXPT-PROG	15+4		NEANDC(E)-202U	679			JUL	VOL.5.P.39.QAIM+SIG SYSTEMATICS,GRPH
ND	143	N,ALPHA	EXPT-PROG	PILE		NEANDC(E)-202U	679			JUL	VOL.5.P.45.ALDEA+ PARTIAL SIG
TB	159	N,HELIUM3	EXPT-PROG	15+4		NEANDC(E)-202U	679			JUL	VOL.5.P.39.QAIM+SIG SYSTEMATICS,GRPH
TM	169	N,HELIUM3	EXPT-PROG	15+4		NEANDC(E)-202U	679			JUL	VOL.5.P.39.QAIM+SIG SYSTEMATICS,GRPH
LU	175	N,GAMMA	EXPT-PROG	20+4		NEANDC(E)-202U	679			KFK	VOL.5.P.12.BEER. VDG ACT,TBL
LU	176	N,GAMMA	EXPT-PROG	18+4		NEANDC(E)-202U	679			KFK	VOL.5.P.12.BEER. VDG ACT,TBL
TA	181	N,HELIUM3	EXPT-PROG	15+4		NEANDC(E)-202U	679			JUL	VOL.5.P.39.QAIM+SIG SYSTEMATICS,GRPH
TA	181	N,GAMMA	EXPT-PROG	18+4		NEANDC(E)-202U	679			KFK	VOL.5.P.12.BEER. VDG ACT,TBL
RE	187	N,HELIUM3	EXPT-PROG	15+4		NEANDC(E)-202U	679			JUL	VOL.5.P.39.QAIM+SIG SYSTEMATICS,GRPH
AU	197	N,GAMMA	EXPT-PROG	FISS		NEANDC(E)-202U	679			PTB	VOL.5.P.86.MANNHART.SENSITIVITY COEF
AU	197	N,2N	EXPT-PROG	FISS		NEANDC(E)-202U	679			PTB	VOL.5.P.86.MANNHART.SENSITITITY COEF
PB		THERMAL SCAT	EXPT-PROG	NDG		NEANDC(E)-202U	679			MUN	VOL.5.P.81.KOESTER+ COH SCAT LENGTH
BI		THERMAL SCAT	EXPT-PROG	NDG		NEANDC(E)-202U	679			MUN	VOL.5.P.81.KOESTER+ COH SCAT LENGTH
TH	232	STRNTH FNCTN	EXTH-PROG	50+4	10+7	NEANDC(E)-202U	679			KFK	VOL.5.P.31.FROEHNER+ S-WAVE,173 LVL
TH	233	STRNTH FNCTN	EXTH-PROG	50+4	10+7	NEANDC(E)-202U	679			KFK	VOL.5.P.31.FROEHNER+ S-WAVE, 57 LVL
U	235	STRNTH FNCTN	EXTH-PROG	50+4	10+7	NEANDC(E)-202U	679			KFK	VOL.5.P.31.FROEHNER+ S-WAVE,196 LVL
U	235	FISS PROD G	EXPT-PROG	PILE		NEANDC(E)-202U	679			MNZ	VOL.5.P.74.BRAUN+ CHAINS 133,135
U	235	FISS YIELD	EXPT-PROG	PILE		NEANDC(E)-202U	679			MNZ	VOL.5.P.74.BRAUN+CUMULATIV TE131,133
U	235	DELAYD NEUTS	EXPT-PROG	PILE		NEANDC(E)-202U	679			MNZ	VOL.5.P.76.OHM+RB94-97 NG-COINC SPEC
U	235	N,FISSION	EXPT-PROG	50+5	20+7	NEANDC(E)-202U	679			KFK	VOL.5.P.2.CIERJACKS+ ABSOL SIG
U	238	STRNTH FNCTN	EXTH-PROG	50+4	10+7	NEANDC(E)-202U	679			KFK	VOL.5.P.31.FROEHNER+ S-WAVE,191 LVL
U	238	FISS YIELD	EXPT-PROG	FISS		NEANDC(E)-202U	679			PTB	VOL.5.P.86.DEBERTIN. A=88TO151
NP	237	FRAG SPECTRA	EXPT-PROG	80+5	55+6	NEANDC(E)-202U	679			KFK	VOL.5.P.18.NAQVI+ FRAG KIN EN
NP	237	FISS YIELD	EXPT-PROG	80+5	55+6	NEANDC(E)-202U	679			KFK	VOL.5.P.18.NAQVI+ PROMPT FRAG MASS
PU	239	STRNTH FNCTN	EXTH-PROG	50+4	10+7	NEANDC(E)-202U	679			KFK	VOL.5.P.31.FROEHNER+ S-WAVE,257 LVL
PU	239	N,FISSION	EXPT-PROG	50+5	20+7	NEANDC(E)-202U	679			KFK	VOL.5.P.2.KARI+ TOF REL TO U235
PU	239	N,FISSION	EXPT-PROG	50+5	20+7	NEANDC(E)-202U	679			KFK	VOL.5.P.2.CIERJACKS+ ABSOL SIG
PU	240	TOTAL	EXPT-PROG	10+4	38+5	NEANDC(E)-202U	679			KFK	VOL.5.P.21.KAEPPELER+ GRPHS

ELEMENT S A	QUANTITY	TYPE	ENERGY MIN	ENERGY MAX	DOCUMENTATION REF	VOL	PAGE	DATE	LAB	COMMENTS
PU 240	STRNTH FNCTN	EXTH-PROG	50+4	10+7	NEANDC(E)-202U	679			KFK	VOL.5.P.31.FROEHNER+ S-WAVE,172 LVL
PU 240	N,FISSION	EXPT-PROG	50+5	20+7	NEANDC(E)-202U	679			KFK	VOL.5.P.2.KARI+ TOF REL TO U235
PU 240	N,FISSION	EXPT-PROG	50+5	20+7	NEANDC(E)-202U	679			KFK	VOL.5.P.2.CIERJACKS+ ABSOL SIG
PU 241	STRNTH FNCTN	EXTH-PROG	50+4	10+7	NEANDC(E)-202U	679			KFK	VOL.5.P.31.FROEHNER+ S-WAVE,123 LVL
PU 242	STRNTH FNCTN	EXTH-PROG	50+4	10+7	NEANDC(E)-202U	679			KFK	VOL.5.P.31.FROEHNER+ S-WAVE, 37 LVL
PU 242	TOTAL	EXPT-PROG	10+4	38+5	NEANDC(E)-202U	679			KFK	VOL.5.P.21.KAEPPELER+ GRPHS
AM 241	STRNTH FNCTN	EXTH-PROG	50+4	10+7	NEANDC(E)-202U	679			KFK	VOL.5.P.31.FROEHNER+ S-WAVE,189 LVL
AM 241	N,FISSION	EXPT-PROG	10+4	25+5	NEANDC(E)-202U	679			KFK	VOL.5.P.17.HAGE+ SUB-THRESH SIG
AM 241	N,GAMMA	EVAL-PROG	25-2		NEANDC(E)-202U	679			KFK	VOL.5.P.29.GOEL. 625+-20MB
AM 241	N,GAMMA	EXPT-PROG	10+4	25+5	NEANDC(E)-202U	679			KFK	VOL.5.P.15.WISSHAK+ GRPH
AM 242	STRNTH FNCTN	EXTH-PROG	50+4	10+7	NEANDC(E)-202U	679			KFK	VOL.5.P.31.FROEHNER+ S-WAVE, 6 LVL
AM 243	STRNTH FNCTN	EXTH-PROG	50+4	10+7	NEANDC(E)-202U	679			KFK	VOL.5.P.31.FROEHNER+ S-WAVE,219 LVL
CM 243	STRNTH FNCTN	EXTH-PROG	50+4	10+7	NEANDC(E)-202U	679			KFK	VOL.5.P.31.FROEHNER+ S-WAVE, 15 LVL
CM 244	STRNTH FNCTN	EXTH-PROG	50+4	10+7	NEANDC(E)-202U	679			KFK	VOL.5.P.31.FROEHNER+ S-WAVE, 34 LVL
MA NY	N,HELIUM3	EXPT-PROG	15+4		NEANDC(E)-202U	679			JUL	VOL.5.P.39.QAIM+SIG SYSTEMATICS,GRPH
MA NY	N,PROTON	THEO-PROG	15+7		NEANDC(E)-202U	679			JUL	VOL.5.P.41.QAIM. STATMDL, A=27TO5O
MA NY	N,ALPHA	THEO-PROG	15+7		NEANDC(E)-202U	679			JUL	VOL.5.P.41.QAIM. STATMDL, A=27TO5O
MA NY	N,TRITON	THEO-PROG	15+7		NEANDC(E)-202U	679			JUL	VOL.5.P.41.QAIM. STATMDL, A=27TO5O
MA NY	N,HELIUM3	THEO-PROG	15+7		NEANDC(E)-202U	679			JUL	VOL.5.P.41.QAIM. STATMDL, A=27TO5O
MA NY	N,GAMMA	EVAL-PROG	-3	+7	NEANDC(E)-202U	679			IKA	VOL.5.P.99.MATTES.PHYS DATA SERIES